12-31-2018

High-speed data communications for vehicular networks using free-space optical communications

Yagiz Kaymak
New Jersey Institute of Technology

Copyright Warning & Restrictions

The copyright law of the United States (Title 17, United States Code) governs the making of photocopies or other reproductions of copyrighted material.

Under certain conditions specified in the law, libraries and archives are authorized to furnish a photocopy or other reproduction. One of these specified conditions is that the photocopy or reproduction is not to be "used for any purpose other than private study, scholarship, or research." If a, user makes a request for, or later uses, a photocopy or reproduction for purposes in excess of "fair use" that user may be liable for copyright infringement,

This institution reserves the right to refuse to accept a copying order if, in its judgment, fulfillment of the order would involve violation of copyright law.

Please Note: The author retains the copyright while the New Jersey Institute of Technology reserves the right to distribute this thesis or dissertation

Printing note: If you do not wish to print this page, then select "Pages from: first page # to: last page #" on the print dialog screen

ABSTRACT

HIGH-SPEED DATA COMMUNICATIONS FOR VEHICULAR NETWORKS USING FREE-SPACE OPTICAL COMMUNICATIONS

by
Yagiz Kaymak

The demand for high-speed Internet access for vehicles, such as high-speed trains (HSTs) and cars, is on the rise. Several Internet access technologies that use radio frequency are being considered for vehicular networking. Radio-frequency communications technologies cannot provide high data rates due to interference, bandwidth limitations, and the inherent limited data rates of radio technology. Free-space optical communications (FSOC) is an alternative approach and a line-of-sight (LOS) technology that uses modulated light to transfer data between two free-space optical (FSO) transceivers. FSOC systems for vehicular networks are expected to provide data rates in the range of Gbps for stationary and mobile stations. They also have additional benefits over radio frequency technologies including immunity to electromagnetic interference, high security owing it to the use of directed light, and the use of an unregulated range of the spectrum or license-free.

An introduction and mobility-specific challenges to FSOC are presented in the first chapter of this dissertation. A geometrical model for a ground-to-train FSOC system is presented and its performance is analyzed in the second chapter. Two beam modalities (i.e., narrow and wide) are compared using this geometrical model. A wide-beam modality that lowers the complexity of an FSOC system is proposed. In addition, a range of beam divergence angles, which are selected according to practical constraints, such as the maximum speed of a fast steering mirror to track an HST traveling at 300 km/h and the connection time between the train and a base station are proposed. All divergence angles in the proposed range mitigate the impairing

effect of train-induced vibration without resorting to a feedback-control mechanism while guaranteeing high data rates (i.e., $\geq$ 1 Gbps).

An adaptive beam that adapts its divergence angle according to the receiver aperture diameter and the communication distance is proposed for a ground-to-train FSOC system in the third chapter of the dissertation. The proposed adaptive beam improves the received power and eases the alignment between the communicating parties in an FSOC system for HSTs. The received power, signal-to-noise ratio, bit error rate, and the maximum communication distance of the proposed adaptive beam technique are compared with those of the communications system that uses a beam with a fixed divergence angle of 1 mrad. The results indicate that the proposed adaptive beam technique yields a received power gain of 33 dB and extends the communication distance of an FSOC system for HSTs to about three times under different visibility conditions as compared to that of a fixed divergence beam. A new model on ground transceiver placement of ground transceivers of an FSOC system to increase connection efficiency is also proposed.

A novel diffused-light (DL) non-line-of-sight (NLOS) FSOC system for providing 1-Gbps Internet access to vehicles is proposed as the fourth chapter of this dissertation. This approach extends FSOC to locations that have no direct line-of-sight (LOS) between the transmitter and receiver. The amount of received power is shown for a receiving vehicle moving. Furthermore, the possible operation modes of the proposed diffused-light system is discussed to realize full-duplex communications.

HIGH-SPEED DATA COMMUNICATIONS FOR VEHICULAR NETWORKS USING FREE-SPACE OPTICAL COMMUNICATIONS

by
Yagiz Kaymak

A Dissertation
Submitted to the Faculty of
New Jersey Institute of Technology
in Partial Fulfillment of the Requirements for the Degree of
Doctor of Philosophy in Computer Engineering

Helen and John C. Hartmann Department of
Electrical and Computer Engineering

December 2018

APPROVAL PAGE

HIGH-SPEED DATA COMMUNICATIONS FOR VEHICULAR NETWORKS USING FREE-SPACE OPTICAL COMMUNICATIONS

Yagiz Kaymak

Dr. Roberto Rojas-Cessa, Dissertation Advisor — Date
Professor of Electrical and Computer Engineering, NJIT

Dr. MengChu Zhou, Committee Member — Date
Distinguished Professor of Electrical and Computer Engineering, NJIT

Dr. Nirwan Ansari, Committee Member — Date
Distinguished Professor of Electrical and Computer Engineering, NJIT

Dr. Abdallah Khreishah, Committee Member — Date
Associate Professor of Electrical and Computer Engineering, NJIT

Dr. Nicholas Madamopoulos, Committee Member — Date
Associate Professor of Electrical Engineering, CCNY, CUNY

BIOGRAPHICAL SKETCH

Author: Yagiz Kaymak

Degree: Doctor of Philosophy

Date: December 2018

Undergraduate and Graduate Education:

- Doctor of Philosophy in Computer Engineering,
  New Jersey Institute of Technology, Newark, NJ, 2018
- Master of Science in Computer Science,
  Ege University, Izmir, Turkey, 2011
- Bachelor of Science in Mathematics,
  Celal Bayar University, Manisa, Turkey, 2003

Major: Computer Engineering

Presentations and Publications:

Y. Kaymak, S. Fathi-Kazerooni, and R. Rojas-Cessa, "Non-Line-of-Sight Free-Space Optical Communications for Vehicular Networks," (under review).

A. Agnihotri, S. F. Kazerooni, Y. Kaymak, and R. Rojas-Cessa, "Evacuating Routes in Indoor-Fire Scenarios with Selection of Safe Exits on Known and Unknown Buildings using Machine Learning," (accepted in *the 39th IEEE Sarnoff Symposium*).

Y. Kaymak, S. Fathi-Kazerooni, R. Rojas-Cessa, J. Feng, N. Ansari, M. Zhou, and T. Zhang, "Beam with Adaptive Divergence Angle in Free-Space Optical Communications for High-Speed Trains," (under review).

Y. Kaymak, R. Rojas-Cessa, J. Feng, N. Ansari, M. Zhou, and T. Zhang, "A Survey on Acquisition, Tracking, and Pointing Mechanisms for Mobile Free-Space Optical Communications," *IEEE Communications Surveys and Tutorials*, vol. 20, no. 2, pp. 1104-1123, Secondquarter 2018.

S.F. Kazerooni, Y. Kaymak, R. Rojas-Cessa, J. Feng, N. Ansari, M. Zhou, and T. Zhang, "Optimal Positioning of Ground Base Stations in Free-Space Optical Communications for High-Speed Trains," *IEEE Transactions on Intelligent Transportation Systems*, vol. 19, no. 6, pp. 1940-1949, June 2018.

Y. Kaymak, R. Rojas-Cessa, J. Feng, N. Ansari, M. Zhou, and T. Zhang, "On Divergence-Angle Efficiency of a Laser Beam in Free-Space Optical Communications for High-Speed Trains," *IEEE Transactions on Vehicular Technology*, vol.66, Issue: 9, pp.7677-7687, March 2017.

Y. Kaymak and R. Rojas-Cessa, "Packet-Based Load Balancing in Data Center Networks," *Journal of Cyber Security and Mobility*, vol.5, Issue: 1, pp.1-18, 2016.

Y. Kaymak and R. Rojas-Cessa, "Per-Packet Load Balancing in Data Center Networks," in *Proc. of the 36th IEEE Sarnoff Symposium*, Newark, NJ, 2015, pp. 140-144.

R. Rojas-Cessa, Y. Kaymak, and Z. Dong, "Schemes for Fast Transmission of Flows in Data Center Networks," *IEEE Communications Surveys and Tutorials*, vol. 17, no. 3, pp. 1391-1422, thirdquarter 2015.

M. Sayit, S. Demirci, Y. Kaymak, and E.T. Tunali, "Adaptive, incentive and scalable dynamic tree overlay for P2P live video streaming," *Peer-to-Peer Networking and Applications*, vol.9, Issue: 6, pp.1074-1088, 2016.

M. Sayit, E. Karayer, K. D. Teket, Y. Kaymak, C. Cetinkaya, S. Demirci, and G. Kardas, "A Score-Based Packet Retransmission Approach For Push-Pull P2P Streaming Systems," in *Proc. of the 6th International Symposium on Multimedia Applications and Processing (MMAP'13)*, Kraków, Poland, September 8-11, 2013.

K. D. Teket, Y. Kaymak, and G. Kardas, "Engineering a Multi-agent System for Peer-to-Peer Video Streaming," in *Proc. of the IEEE International Symposium on INnovations in Intelligent SysTems and Applications (INISTA'13)*, Albena, Bulgaria, 19-21 June 2013.

Y. Kaymak, K. D. Teket, and M. Sayit, "A Study on ALTO-assisted P2P Live Video Streaming Systems," in *Proc. of the 4th International Workshop on Modeling and Simulation of Peer-to-Peer and Autonomic Systems (MOSPAS'13)*, Helsinki, Finland, 1-5 July 2013.

Y. Kaymak, K. D. Teket, and M. Fesci-Sayit "Parameter Analysis for a Push/Pull-based P2P Live Video Streaming Application," in *Proc. of the 21th IEEE Signal Processing and Communications Applications Conference (SIU'13)*, North Cyprus, 24-26 April 2013 (in Turkish).

M. Sayit, E. Karayer, Y. Kaymak, K. D. Teket, C. Cetinkaya, S. Demirci, and G. Kardas, "Parent Selection via Reinforcement Learning in Mesh Based P2P Video Streaming," in *Proc. of the 10th International Conference on Information Technology: New Generations*, Las Vegas, Nevada, USA April 15-17, 2013.

Y. Kaymak, K. D. Teket, S. Demirci, S. Getir, R. C. Erdur, and G. Kardas, "A Library Management System Implementation with Prometheus Methodology and JACK Agent Framework," in *Proc. of the National Software Engineering Symposium* 2012, pp. 121-128 (in Turkish).

O. Yilmaz, S. Demirci, Y. Kaymak, S. Ergun, and A. Yildirim "Shortest Hop Multipath Algorithm for Wireless Sensor Networks," *Computers and Mathematics with Applications*, vol. 63, Issue 1, January 2012, pp. 48-59.

M. Sayit, S. Demirci, Y. Kaymak, H. Bulut, and E. T. Tunali, "Multicast Tree Based Video Streaming Application Over Planetlab", in *Proc. of the IEEE Signal Processing and Communications Applications Conference (SIU'11)*, pp. 331-334 (in Turkish).

H. Bulut, A. Yardimci, S. Demirci, Y. Kaymak, M. Fesci-Sayit, and E. Turhan Tunali "An Efficient JSD-Based Search on Interest-Based Hierarchical Clustering of Overlay Networks," in *Proc. of the 2nd International Conference on Advances in P2P Systems*, Florence, Italy, October 25-30, 2010, pp. 63.

O. Yilmaz, S. Demirci, Y. Kaymak, and K. Erciyes, "Synchronous Distributed Spanning Tree Algorithm for Wireless Sensor Networks," in *Proc. of the First International Symposium on Computing in Science and Engineering*, June 3-5, 2010, Kusadasi-Turkey.

Y. Kaymak, O. Yilmaz, and S. Demirci, "The Chang Roberts Distributed Spanning Tree Algorithm Simulation on TinyOS Simulator in Wireless Sensor Networks," in *Proc. of the International Student Conference on Advanced Science and Technology (ICAST'10)*, Izmir-Turkey, 2010, pp. 229-230.

Sevgili annem, babam,
ve
canım sevgilim, Gokce'ye

To my dear mom, dad,
and
my beloved girlfriend, Gokce

ACKNOWLEDGMENT

As a PhD student in New Jersey Institute of Technology (NJIT), I enjoyed the time I spent and the experiences I gained, despite the stressful and hard times. I learned how to be patient and strong, and how to overcome the difficulties no matter what the circumstances are. I deeply appreciate the support of many people because this dissertation would not have been possible without them.

First, I would like to thank my advisor, Prof. Roberto Rojas-Cessa, for his immense support, guidance, and patience during my doctoral study. He guided me through the treacherous paths of research. I will always be grateful to him for letting me study in his lab.

I am also grateful to Distinguished Prof. MengChu Zhou, and Distinguished Prof. Nirwan Ansari of the ECE Department of NJIT for letting me a part of the "Free-Space Optical Communications for High-Speed Trains" project. I am thankful to Prof. Edip Niver and Prof. Haim Grebel for allowing me to use their laboratories and optical equipment. I also would like to thank Prof. Ziqian Dong of ECE Department of NYIT for her precious comments through my Ph.D. Last but not least, I would like to thank Prof. Nicholas Madamopoulos of the EE Department of CCNY, CUNY and all the committee members for serving on my dissertation committee and for their continued support.

I would like to thank NJIT and CRRC Corporation Limited for the teaching and research assistantship financial supports, respectively, which made this study possible.

I always feel lucky to have companionship of Sina Fathi-Kazerooni and Onur Yilmaz. I am thankful for their help and support.

Last, and not least, I would like to thank my dear mom and dad, Gungor Kaymak and Ahsen Kaymak, for their priceless support and patience. Words fall

short to express my feelings and gratitude to them. I would also like to thank my lovely girlfriend, Gokce Askan. If she were not with me, this work would not be possible.

TABLE OF CONTENTS

TABLE OF CONTENTS
(Continued)

Chapter **Page**

LIST OF TABLES

LIST OF FIGURES

Figure **Page**

LIST OF FIGURES
(Continued)

Figure **Page**

LIST OF FIGURES
(Continued)

Figure **Page**

CHAPTER 1

INTRODUCTION

Vehicular networking is an enabling communications technology for traffic safety, traffic efficiency, and vehicle infotainment applications. It will most likely pivotal for creating intelligent transportation systems [36]. The National Highway Traffic Safety Administration of United States has proposed a rule on vehicle safety standards that requires all new vehicles to be equipped with vehicle-to-vehicle (V2V) and vehicle-to-infrastructure communications capabilities, starting from 2019 [29]. As a part of the intelligent transportation system, high-speed trains (HSTs), which travel at speeds of 300 km/h or faster, play an increasing role in public transportation as the number of passengers traveling in them increases. For example, the number of HST passengers in China has increased from 128 million in 2008 to 672 million in 2013, representing an annual growth of approximately 39% [110].

Several technologies are being considered for vehicular networking. Radio frequency (RF) wireless technologies are currently being used to provide Internet access to vehicles [36]. Wireless fidelity (Wi-Fi), worldwide interoperability for microwave access (WiMAX), leaky coaxial cables, and 5G are employed or proposed to provide Internet access to vehicles, but they cannot provide high data rates due to interference, bandwidth limitations, and the inherent limited data rates of RF technology [131, 31, 50, 57, 122]. Long-term evolution (LTE) can provide a peak throughput of 31 Mbps to a mobile LTE receiver traveling at 200 km/h, it may not meet the demand for high-speed Internet access for vehicular networking [118]. Wi-Fi and WiMAX can potentially deliver peak data rates of up to 75 Mbps, but the actual data rates are lower than 10 Mbps [32]. The upcoming 5G communications technology, using millimeter wave, may be also employed for vehicular networking

[128]. It is expected that 5G will provide a peak data rate of 10 Gigabit per second (Gbps) in low mobility scenarios, such as for local wireless access, and 1 Gbps in high mobility scenarios in the near feature [128]. However, 5G is not yet deployed and requires spectrum licensing. Moreover, these existing communication technologies suffer from frequent and unreliable handovers affected by Doppler frequency shifts and penetration losses in vehicles [57, 95, 116, 135].

This dissertation has been motivated by the lack of a reliable and high-bandwidth communications technology that can provide high-speed Internet access (i.e., $\geq$ 1 Gbps) to vehicles, especially to HSTs and cars.

Free-space optical communications (FSOC), which is also known as optical wireless communications (OWC), is a line-of-sight (LOS) technology that propagates modulated light to transmit data between two stations in stationary or mobile conditions [35]. Recently, FSOC technology has attracted considerable attention because it has the potential to transmit at very-high data rates between two terminals separated over a distance of a few meters to thousands of kilometers. Free-space optics (FSO) finds its applicability in stationary and mobile scenarios including building-to-building communications, HSTs, unmanned aerial vehicles (UAVs), satellites, indoor and outdoor local- and wide-area networks, and deep-space communications [80]. FSOC possess multiple advantages, such as high bandwidth, license-free band use, long operational range, spatial reusability, security, and immunity to electromagnetic interference as compared to existing RF communications systems [82]. Frequencies used by FSOC are much higher than those used by RF communications. Therefore, high data rates can be achieved while using antennas that occupy a small footprint [53].

In the reminder of this chapter, the fundamentals of FSOC and its working mechanism, challenges, and applications are introduced. Mobile FSOC systems and their mobility-specific challenges are also presented in this chapter.

1.1 Free-Space Optical Communications

FSOC finds its applicability in many use cases, such as in HSTs, cars, UAVs, building-to-building, indoor LAN,satellites, and deep-space communications [48]. Figure 1.1 shows some FSOC applications with their communication ranges. FSOC is a technology that may be used as a stand-alone communications system or in combination with RF systems. As compared to existing RF-based wireless systems, FSOC possesses multiple advantages, which are listed as follows [82]:

- High bandwidth
- License-free band use
- Long operational range
- Spatial reusability
- Immunity to electromagnetic interference
- Security

Optical beams for FSOC can be categorized into narrow and wide beams. An optical beam with a divergence angle smaller than or equal to 0.1 milliradian (mrad) or 0.0057° is considered to be a narrow beam, and, therefore, a beam with a larger divergence angle is considered to be a wide one [84, 40, 60, 61]. In FSOC systems, narrow beams are usually preferred to increase the light intensity at the receiver and to decrease the geometric path loss, which depends on the beam divergence, as the beam propagates.

Frequencies and bandwidth used in FSOC are much higher than those used in RF communications. Therefore, FSOC can provide proportionally much higher data rates than RF communications while using antennas that occupy less real estate [53]. Moreover, the coherence of laser light in FSO links may reduce geometrical path loss and therefore, enable the transmission of high data rates at long distances [85, 33, 98, 69]. FSOC technology usually uses low-power infrared lasers, which

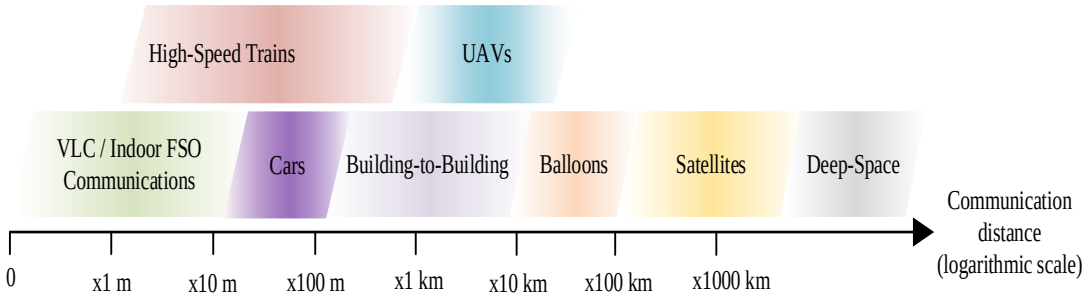

Figure 1.1 Comparative representation of FSOC systems by distance.

operate in an unlicensed electromagnetic-frequency band either are eye-safe or can be made to operate in an eye-safe manner [98]. The narrow and directional characteristics of laser beams employed in FSOC systems enable spatial reuse and make them hard to be eavesdropped, thus setting apart the level of security of an FSO link. Moreover, the use of light as carrier of FSOC provides immunity to electromagnetic interference [82].

Despite its advantages, terrestrial FSOC systems, where the beam travels through the Earth's atmosphere, are susceptible to some weather conditions, such as fog, rain, sleet, and snow [97], and atmospheric turbulence [94]. Atmospheric conditions may impair the propagation of an optical signal because the propagation of light may undergo a variety of atmospheric attenuations, such as absorption, scattering, and scintillation. The atmosphere is composed of gas molecules, water vapor, aerosols, dust, and pollutants whose sizes are comparable to the wavelength of a typical optical carrier [98]. Absorption occurs when suspended water molecules and aerosols in the Earth's atmosphere absorb the energy of photons as the light propagates through the atmosphere. Absorption is a wavelength-dependent phenomena. Certain wavelengths (or wavelength bands) in the visible and near-infrared wavelengths can experience severe absorption. Figure 1.2 shows the absorption of the atmosphere under clear weather conditions (visibility $>$ 10 miles) for various transmission wavelengths in the near-infrared spectral range (between 0.7

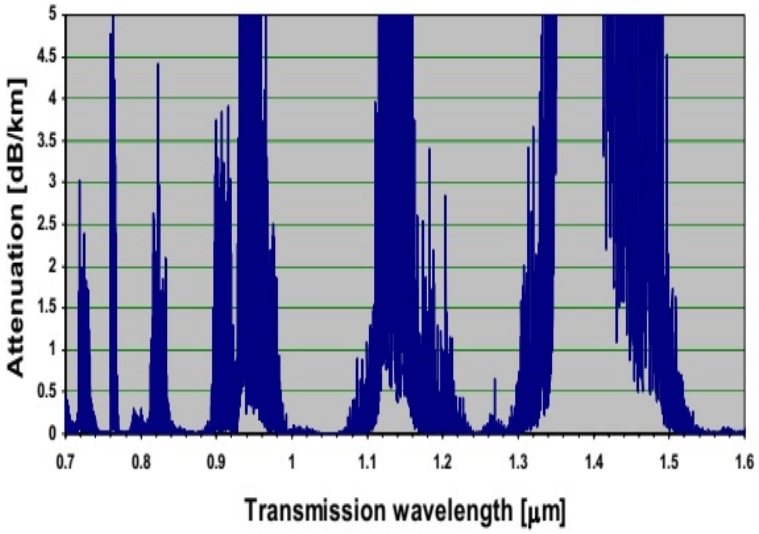

Figure 1.2 MODTRAN transmission calculation under clear weather conditions. *Source:* [20].

and 1.6 μm). This graph was created with MODTRAN [20], a software program that was developed to facilitate the study of transmission properties of the atmosphere [40].

Scattering, or light scattering, is another type of atmospheric attenuation for terrestrial FSOC, in which the propagating light is deflected from its straight path because of particles suspended in the atmosphere, such as air molecules, haze particles, and fog droplets [35, 56]. These particles have different scattering strengths on a propagating beam that uses a particular wavelength because the radius of each type of particle is different. There three types of scattering: Rayleigh, Mie, and non-selective [35]. Rayleigh scattering refers to scattering by molecular and atmospheric gases formed by molecules of sizes much smaller than the wavelength (i.e., between 0.5 and 2 μm) used by FSOC systems. Mie scattering is used to describe aerosol scattering and it occurs when the aerosol particle radius, which is in the range of 10^{-2} and 1 μm, is equal to or larger than one tenth of the wavelength of interest [35]. This phenomenon makes fog and haze a keys contributor to optical power/irradiance attenuation. The

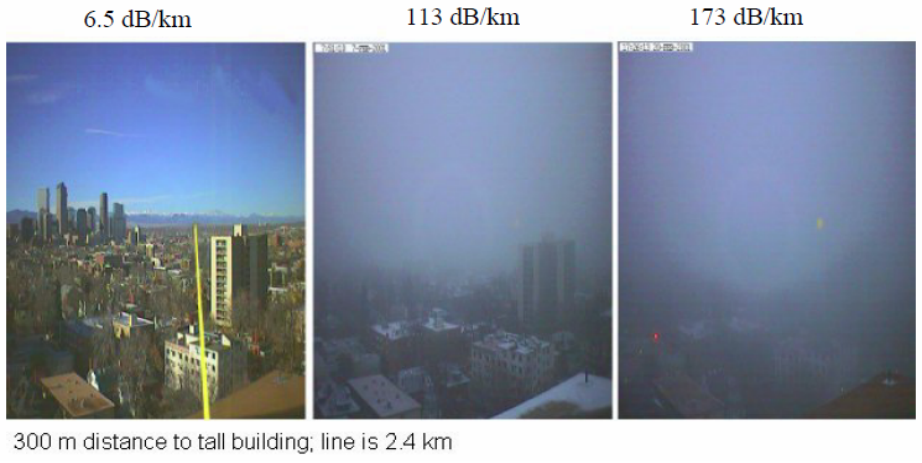

Figure 1.3 A fog event captured in Denver, Colorado. *Source:* [40].

attenuation due to Mie scattering can reach values of hundreds of dB/km. Figure 1.3 shows the attenuation levels during a fog event occurred in Denver, Colorado. The first picture on the left side of this figure shows clear atmospheric conditions with a visibility range of more than 2 km. For a clear sky, the attenuation level is measured as 6.5 dB/km. In the same figure, the picture in the middle shows the onset of a fog event, where the visibility dropped to 113 m and the attenuation level increased to 113 dB/km. The picture on the right side of the same figure depicts the time the visibility dropped to 75 m, corresponding to an attenuation of 173 dB/km. If the size of the particles in the atmosphere are much larger than the wavelength of the beam used by FSOC, non-selective scattering occurs. For example, rain droplets and snow flakes cause non-selective scattering. Rain droplets and snow flakes do not affect FSOC because laser light is able to pass through them easily. Another type of atmospheric attenuation is scintillation, which may be defined as the changing of light intensities in time and space on the plane of a receiver detecting a signal from a transmitter [40].

A pointing error caused by misalignment of the transceivers is another major challenge in FSOC [42]. This error is defined as the Euclidean distance between the centers of the photodetector and the beam footprint at the receiver [55]. Pointing error

may result in degradation or even total loss of the received signal. This error may arise because of transmitter/receiver sway, platform vibration, motion of mobile stations, error and uncertainties in the tracking system, or any kind of stress in electronic or mechanical devices used by FSOC systems. Another type of pointing error is beam wander caused by the inhomogeneities of large-scale eddies in the atmosphere (i.e., atmospheric turbulence), where the transmitted beam may deviate from its intended path [82].

Figure 1.4 shows a simplified half-duplex terrestrial FSOC system that consists of a transmitter and a receiver. In this figure, the laser light emitted from a laser diode is modulated to send the intended data. The transmitted beam is collimated by a collimating lens to minimize the beam spread as the light propagates. The propagating light goes through the atmosphere because the FSOC system shown in this figure is a terrestrial FSOC system. Note that there also are space and underwater FSOC systems. On the other end of an FSO link, the incident light on the surface of the FSO receiver is focused by a focusing lens to concentrate all the incident light to a small-sized (i.e., in mm or μm) photodiode. An FSO receiver is also equipped with some electronics, such as a trans-impedance amplifier to amplify the converted electrical signal, a low-pass filter to limit the thermal and background noise, and a symbol detector to recover the received data. A block diagram of such an FSO receiver is shown in Figure 1.5.

Each party (i.e., the transmitter and receiver) in an FSOC system is usually equipped with a *transceiver* that functions as both a transmitter and a receiver to provide full-duplex FSOC capability. In such an FSOC system, two optical links, one for downlink, one for uplink, are established between a pair of communicating parties. Figure 1.6 shows a full-duplex FSO transceiver. In this figure, two apertures next to each other work as a receiver and transmitter, respectively. In a different FSO configuration, the transmitted and received beams of a transceiver may share

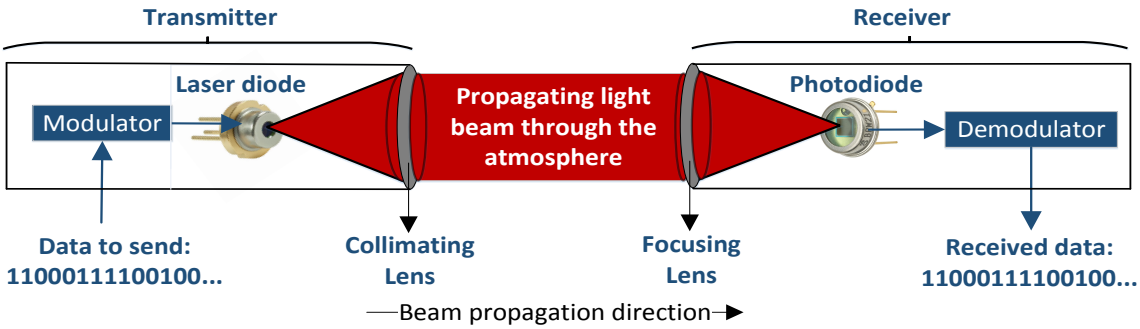

Figure 1.4 A half-duplex FSOC system.

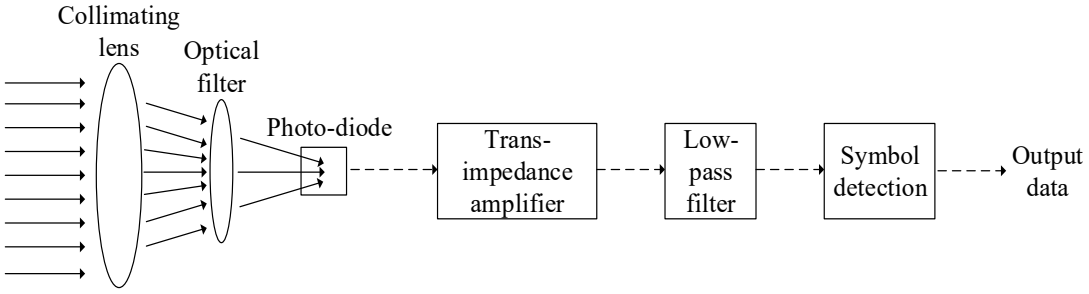

Figure 1.5 Block diagram of an FSO receiver.

the same optical path if the opposite FSO transceivers use two different transmission wavelengths (e.g., 1310 and 1550 nm). In such a configuration, the transmitting and receiving module of a transceiver does not have to be spatially diverse. One common aperture is used to both transmit and receive the beams and these beams are splitted by using beam splitters in the enclosing [126]. In the remainder of this dissertation, we assume that each FSO terminal is equipped with a transceiver.

Laser diodes operating at wavelengths between 780 and 1600 nm are usually preferred as light sources for FSOC systems because they may provide high data rates over long distances. Many FSOC systems use the laser diodes transmitting at the wavelength-windows of 780-850 and 1520-1600 nm [40]. These wavelengths may experience low atmospheric attenuation. Reliable, high-performance, and inexpensive transmitter and receiving components are available in the 780-850-nm window.

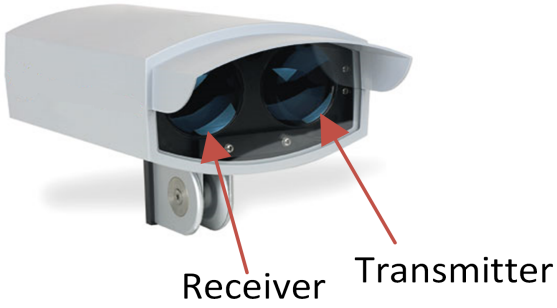

Figure 1.6 A full-duplex FSO transceiver. *Source:* [3].

Silicon (Si) avalanche photodiodes (APDs) and vertical-cavity surface-emitting lasers (VCSEL) use this wavelength window. The wavelengths in the 1520-1600-nm window are compatible with erbium-doped fiber amplifier (EDFA) technology, which is important for FSOC systems that require high transmission powers (i.e., $>$ 500 mW) and high data-rates (i.e., $>$ 2.5 Gbps) [40]. Moreover, lasers that use a wavelength in this window can transmit up to 50 to 65 times the transmission power of lasers transmitting at 780 to 850 nm in the same eye-safety classification. The solar spectral irradiance may be a deteriorating factor for outdoor FSOC systems. The power per unit area of the solar irradiance is smaller for the wavelengths in the 1520-1600-nm range than the wavelengths in the 780-850-nm range [124].

Both parties in an FSOC system must be aligned carefully to point the transmitting laser beam to the receiver [40]. Alignment is even needed for stationary transceivers. For example, building-to-building FSOC systems use alignment and tracking mechanisms to handle the motion of transceivers generated by thermal expansion, wind sway, and vibration [40]. This alignment mechanism is usually called acquisition-tracking-pointing (ATP) [81]. The beam alignment becomes more challenging when the transmitter, receiver, or both parties are in motion. The extent of impairing effects, such as vibration, is expected to be severe in mobile FSOC. In this context, an ATP mechanism is used to acquire the exact location of the

Figure 1.7 An FSOC system for HSTs.

transmitter/receiver (in both parties), point the transmitter to the receiver, and correct the pointing/tracking errors while the mobile station is in motion [68].

1.1.1 Free-Space Optical Communications for Vehicular Networks

A mobile FSOC system is capable of tracking a vehicle, like a car or HST. A mobile FSOC system requires additional features and capabilities, such high-speed tracking, vibration mitigation, and seamless handover over a stationary one. An illustration of a mobile FSOC system for HSTs is depicted in Figure 1.7. In this figure, an FSO base station (BS) and a mobile FSO terminal on an HST communicate using a full-duplex link that establishes two parallel beams; a downlink and an uplink.

As all other communication technologies proposed for providing Internet access to vehicles, mobile transceivers must be able to perform a handover for continuous communication as the vehicle travels. Handover is defined as the process of transferring an ongoing call/data session from one (i.e., source) base station to another

(i.e., target) BS when a mobile node travels from the coverage area of the source BS to the coverage area of the target BS [127]. Handover in RF communications systems, such as LTE, IEEE 802.11p, WiMAX, and Radio-over-fiber (RoF) is performed based on measurements of the channel quality, such as received signal strength (RSS), signal to interface ratio (SIR), and bit error rate (BER), over an overlapping region covered by two or more adjacent BSes [135, 95, 136]. When the channel quality indicator of the link between the mobile node and a BS drops below a pre-determined threshold, handover is carried out.

Handover in mobile FSOC may be handled in a different way from a handover in RF communications systems because the light beam characteristics is different from the omnidirectional transmission of RF. A part of the handover process in FSOC involves the alignment of a steering mechanism, such as a fast steering mirror (FSM), gimbal, or both, which are used to align the beam for communication between a pair of communicating parties. The alignment mechanism steers the transceivers from source BS to target BS as the mobile station enters the coverage area of the target BS [126, 104]. For HSTs, handover is performed frequently and it may shorten the connection time, which is the time when the train's transceiver transmits and receives user data [126]. Another handover-related challenge for mobile FSOC systems is the steering speed of the ATP mechanism used in FSO transceivers. The angular steering speed of the steering mechanism for a train moving at high speed may not be satisfied by off-the-shelf steering mechanisms [6, 5, 1].

The narrow-divergence and highly collimated characteristics of a laser beam make mobile FSOC challenging. Specifically, a narrow beam is prone to larger pointing/tracking errors than a wide beam because of motion-related disturbances, such as the vibration induced by a vehicle's motion, road/track irregularities, and the turbulence effect generated by a vehicle moving through the atmosphere. Vibrations can cause a significant reduction in the amount of received power at the receiver,

resulting in transmission errors [69]. The vehicle vibrations may exacerbate the extent of detector-decoupling loss, which is defined as the ratio of the optical power in the receiver's focal plane to the power incident on the active area of the optical detector [40]. As the received beam spot wanders off the center of the optical detector, the detector-coupling loss increases and the received power decreases. Among the types of train vibrations (i.e., vertical, lateral, and longitudinal) vertical vibrations generate the largest displacement of a vehicle (and the transceivers) [133]. Therefore, we focus on vertical vibrations and their impact on the received power. The use of a narrow beam requires a precise alignment if this beam operates over a long distance, such as 1 km [72, 121]. Such a precise alignment may jeopardize the connectivity between the two parties [41]. Therefore, it is clear that an ATP mechanism is required to track the moving vehicle and ensure alignment of the FSO beam.

Feedback control mechanisms may be used in FSOC systems as a part of an ATP system to mitigate the effects of vibration and pointing errors [106, 46, 115, 126, 104]. Measurements from position-sensing detectors, quadrant photodiodes (QPDs), or complementary metal-oxide-semiconductor (CMOS) sensors may be used to control and align the transceiver. Moreover, wide-angle beacon lights might be employed as a part of an ATP mechanism to align the transceivers [126, 104].

An alternative to a narrow beam is the use of a wide beam for FSOC. A wide beam may generate a large spot size at the receiver location to cover the transceiver or even the complete vehicle. The use of a wide beam may relax the constraints on an ATP mechanism, such as the steering speed of the FSM, or completely eliminate the need for an ATP [88].

The contributions of this dissertation are listed as follows:

1. It compares different beam modalities and reveals a viable range of divergence angles to realize an FSOC system for HSTs, for the first time. The revealed range of divergence angles mitigates the impairing effect of train-induced vibration while guaranteeing high data rates (i.e., $\geq$ 1 Gbps) for an HST. The

divergence angles in the proposed range meet the theoretical maximum steering speed of an FSM, and lowers the complexity of an FSOC system.

2. It proposes an adaptive-divergence beam in an FSOC system for HSTs, which improves the received power, signal-to-noise ratio, and the bit error rate as compared to a

   fixed-divergence beam. The proposed adaptive-divergence approach adapts the beam divergence angle of the transmitted beam to achieve a footprint of the diameter of the receiver aperture and minimize the geometric loss of the optical link for a given communication distance between a transmitter-receiver pair.

3. It proposes a new ground station placement in an FSOC system for HSTs to place the ground stations right above the passage of an HST to achieve an efficient alignment between the ground stations and the mobile FSO stations on the train. This new placement improve the received power by decreasing the lateral distance between the train and the ground transceivers, and makes the ground transceivers parallel to the track.

4. It proposes a novel outdoor diffused-light non-line-of-sight FSOC (DL-NLOS-FSOC) system that does not require a direct LOS between the communicating parties for vehicular networks. The proposed communications system allows the receivers to receive a transmitted beam regardless of the angle of view, which eliminates the fine alignment requirement in mobile FSOC systems.

Further details on above points are given next. An outline of the dissertation is presented at the end of this chapter.

1.2 Divergence-Angle Efficiency of a Laser Beam in Free-Space Optical Communications for High-Speed Trains

Two different laser beam modalities, narrow and wide beam, in an FSOC system for ground-to-train HST communications are compared, where the trade-offs among receiving power, coverage area and the complexity of an ATP mechanism are analyzed. A divergence angle of a wide beam in the range of [0.07°, 2.002°] is proposed to relax the steering speed of a FSM, which is one of the major components of the ATP mechanisms in mobile FSOC systems. A beam using a divergence angle in the proposed range allows to overcome the negative effects of vertical vibrations induced by the train's motion. The proposed divergence angles provide a large link range,

effective coverage length, and long contact time as compared to a narrow divergence angle.

1.3 Beam with Adaptive Divergence Angle in Free-Space Optical Communications for High-Speed Trains

Adaptive beam that adapts its divergence angle according to the receiver aperture diameter and the communication distance is proposed to improve the received power and ease the alignment between the communicating terminals as compared to a fixed-divergence-angle beam in an FSOC system for HSTs. The proposed adaptive beam outperforms a fixed-divergence-angle beam that uses a divergence angle of 1 mrad by an average received-power difference of approximately 33 dB. Moreover, the adaptive divergence beam increases the maximum communication distance of an FSOC system for HSTs by an average distance of 742 m over a fixed-divergence beam by guaranteeing a BER of 10^{-9} for different visibility values. A new placement of ground transceivers above the track (above the train passage) is also proposed for an FSOC system for HSTs, for an optimum alignment with the train movement. The proposed transceiver placement decreases the lateral distance between the transceiver on the train and a base station, and in turn increases the received power of 3.8 dB, in average, over a layout that places base stations next to the track.

1.4 Diffused-Light Non-Line-of-Sight Free-Space Optical Communications for Vehicular Networks

A novel DL-NLOS-FSOC system is proposed for providing high-speed (i.e., ≥ 1 Gbps) Internet access to vehicles. This approach extends FSOC to locations that have no direct LOS between the transmitter and receiver. We analyze the amount of received power by a moving vehicle and show the received power for a receiving vehicle moving. Furthermore, we introduce possible operation modes for realizing full-duplex communications with DL-NLOS-FSOC. Our results show that a 1-Gbps optical link

between a transmitter-receiver pair can be achieved with an average DR-to-receiver distance of 220 meters for varying transmission powers of 50 to 200 mW.

1.5 Dissertation Outline

This dissertation is organized as follows. In Chapter 2, a ground-to-train FSOC system that lowers the complexity and mitigates the train-induced vibration is presented. In Chapter 3, an adaptive divergence beam that adapts the divergence angle of a transmitted beam to improve the received power, signal-to-noise ratio, and the bit error rate is presented. In Chapter 4, a diffused-light non-line-of-sight FSOC system that eliminates the direct LOS requirement of an FSOC system is proposed for vehicular networks. In Chapter 5, discussions, concluding remarks, and future research plans are presented.

CHAPTER 2

DIVERGENCE-ANGLE EFFICIENCY OF A LASER BEAM IN FREE-SPACE OPTICAL COMMUNICATIONS FOR HIGH-SPEED TRAINS

In this chapter, we employ a geometrical model to represent a ground-to-train FSOC system and to analyze its performance. Using this geometrical model, we present a comparison between narrow or wide beam modalities. This chapter aims to reveal which of the beam modalities lowers the complexity of an FSOC system. In addition, we propose a range of beam divergence angles, [0.07°, 2.002°], that is selected according to practical constraints, such as the maximum speed of a FSM to track a high-speed train at 300 km/h, the connection time between the train and a BS, and the train's vertical displacements of up to 50 mm. The smallest divergence angle in the proposed range, 0.07°, is selected to keep the needed angular speed of a commercial FSM [6]. This maximum angular speed dictates the minimum divergence angle of the proposed range when the tilt angle of the beam is 45° or larger. The largest divergence angle in the proposed range, 2.002°, is selected to allow a connection time of at least twice the largest handover time, which is reported as 1 second for an FSO communications systems for HSTs [38]. Moreover, all divergence angles in the proposed range mitigate the impairing effect of the vibration induced by the motion of the train without resorting to a feedback-control mechanism while guaranteeing high data rates ($\geq$ 1 Gbps). To the best of our knowledge, this is the first work that compares the narrow and wide beam modalities used in FSOC for HSTs.

The remainder of this chapter is organized as follows. Section 2.1 presents our system model. Section 2.2 compares narrow and wide beam modalities and lists their advantages and disadvantages. Section 2.3 presents our numerical results. Section 2.4 summarizes the chapter.

2.1 System Model

A geometrical model [112] is adopted to compare and analyze the different beam modalities. The beam propagation model of the laser light considered in this chapter is characterized as a Gaussian distribution [62, 34]. The Gaussian beam model is adopted in our analysis because it is a natural consequence of the laser resonant cavity, and it has been widely adopted in the literature [40, 62].

In a typical ground-to-train FSOC model, a train car has an FSO transceiver installed on the roof, and each BS on the ground has an FSO transceiver. Section 2.3 discusses the separation distance between two consecutive BSes. For the sake of description, we focus on ground-to-train communications in this chapter. Note that the establishment of a ground-to-train communications link also guarantees a train-to-ground link because the transmitter and receiver of a transceiver are aligned with the same orientation [126]. Therefore, our analysis actually applies to both links.

We consider that the transceiver on the train and the BSes along the track use a wavelength of 850 nm. This wavelength is selected because of its availability, reliability, high-performance capabilities, and the lower cost of the transmitter and detector [35]. We also consider that the transceiver of each BS might be connected to the fiber-optic backbone where a wavelength between 1530 and 1565 nm (i.e., C-band) is usually employed [8, 15, 58]. Owing to the different wavelengths that the proposed FSOC system and a fiber-optic backbone operate, a fiber-to-fiber media converter [9, 7, 18] may be needed for wavelength conversion.

Figure 2.1 shows the geometrical model of the ground-to-train FSOC system from a superior view (i.e., as seen from the top). In this figure, we assume that the train travels along line segment $[DB]$ from D to B. d_1 denotes the distance between the BS and the track and is set to 1 m [112]. d_2 is the horizontal distance between the BS and the track and it designates the location of the shortest coverage point (represented by C) of the beam on the track. θ is the divergence angle of the

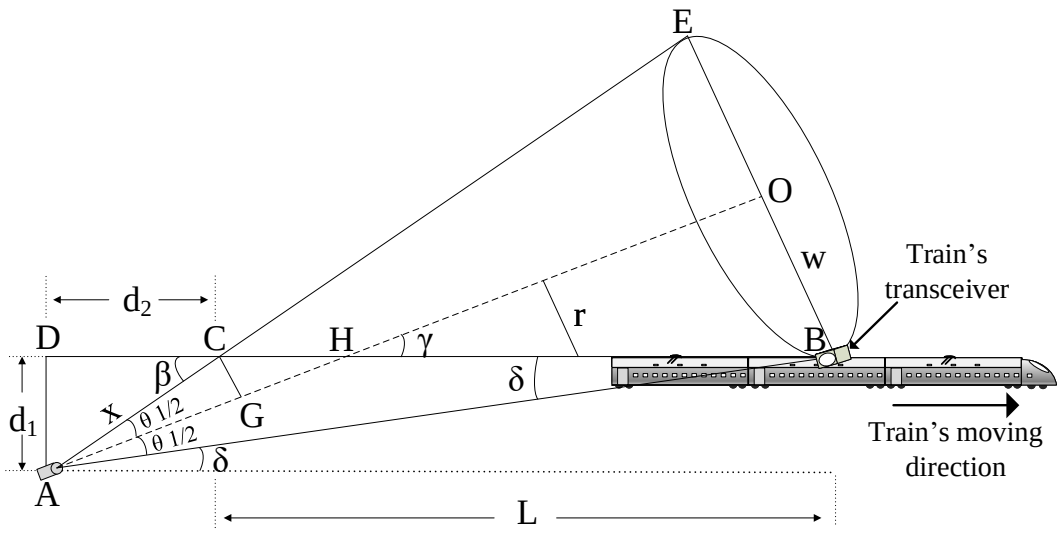

Figure 2.1 Top view of the geometrical model of the ground-to-train FSOC system along a straight track [DB].

laser beam. This angle impacts the beam radius, w, and the coverage length, L, along the track. In Figure 2.1, $tan\,\beta$ and $tan\,\delta$ are calculated as $tan\,\beta = d_1/d_2$ and $tan\,\delta = d_1/(d_2 + L)$ using the triangles ACD and ABD, respectively. Furthermore, because $\theta = \beta - \delta$, the coverage length of the light beam, L, in terms of d_1, d_2, and, θ can be represented as:

$$L = \frac{x^2\,tan\,\theta}{d_1 - d_2\,tan\,\theta} \tag{2.1}$$

where x is the hypotenuse of the triangle ACD in Figure 2.1, and $x = \sqrt{{d_1}^2 + {d_2}^2}$. Denote $\theta_{1/2}$ as half of the divergence angle (i.e., $\theta_{1/2} = \frac{\theta}{2}$) and $\gamma = \theta_{1/2} + \delta$ as the tilt angle of the beam. The tilt angle is the angle between the optical axis of the beam and the horizontal axis, which is parallel to the track. This angle affects L because γ is a function of δ and θ. Note that d_2 affects the tilt angle of the transceiver on the ground. If d_1 is kept constant, the tilt angle of the laser beam decreases as d_2 increases. The height of the BS is the same as the height of the train, which is

approximately about four meters above the ground level. $\vec{AO}$ in Figure 2.1 is the optical axis of propagation, and z is the distance from the light source along the optical axis. The beam radius at distance z is denoted by $w(z)$ and, is calculated by [62]:

$$w(z) = w_0 \sqrt{1 + (\frac{\lambda z}{\pi {w_0}^2})^2}, \tag{2.2}$$

where $w_0 = \frac{\lambda}{\pi \theta_{1/2}}$ is the beam waist of the laser source at the transmitter. Here, $z = |AH| + |HO|$ and $|AH| = |AG| + |GH|$. In addition, the length of the line segment $[HO]$ can be written as $|HO| = (L - |CH|)\, cos\, \gamma$. Thus, z can be given as $z = |AG| + |GH| + (L - |CH|)\, cos\, \gamma$. Therefore, z can be written as:

$$z = L\, cos\, \gamma + x\, cos\, \theta_{1/2}, \tag{2.3}$$

where r is the orthogonal offset from the optical axis of propagation of the light beam, which corresponds to the shortest distance between the $[GO]$ and $[CB]$ segments at distance z. For instance, r is equal to $|CG|$ at the shortest coverage point C, and it is equal to $w(z)$ when z is equal to $|\vec{AO}|$. Considering triangle OHB, we obtain $r = (L - |CH|) sin\, \gamma$. Using a calculation similar to that in equation (2.3), r is given as:

$$r = L\, sin\, \gamma - x\, sin\, \theta_{1/2} \tag{2.4}$$

The received power at distance z along the track for a Gaussian beam is [62]

$$P_{rx} = \frac{2\, P_{tx}\, A_c}{\pi\, (w(z))^2} e^{-(2r^2/(w(z))^2)} \tag{2.5}$$

where P_{tx} is the transmission power, and A_c is the effective light collection area of the receiver. A_c is given by [107]:

$$A_c = \frac{n^2 \, A_d}{sin^2 \, \psi_c} \tag{2.6}$$

where n is the refractive index of an optical concentrator that focuses the incoming light on the photo diode, in the receiver, A_d is the photosensitive area of the photo diode in m^2, and ψ_c is the half-angle field-of-view (FOV) of the receiver after the lens. For the analysis in Section 2.3, we use $A_d = 7mm^2$, $\psi_c = 5.15°$, and $n = 1.5$ [112].

2.2 Comparison of Narrow and Wide Beams

In this section, we compare the narrow and wide beam modalities of laser light transmission for high-speed ground-to-train FSOC in HSTs. We discuss their strengths and weaknesses for HST communications.

FSOC are susceptible to weather conditions such as fog, haze, rain, snow, and combinations of them [40]. In free space, these weather conditions may cause the atmospheric attenuation of the transmitted optical beam. Fog and haze cause the most severe attenuation because of the occurrence of Mie scattering in the wavelength band of interest (between 500 and 2000 nm) [35, 45]. A narrow beam has an advantage over a wide beam under the weather conditions where the visibility decreases because of fog or haze. Because decreasing the beam divergence decreases the spreading of the transmitted beam between the transmitter and the receiver, which in turn improves the link margin [40, 112]. Moreover, a higher link margin leads to an increase in the link range (i.e., the maximum achievable distance) for a given sensitivity of the receiver and makes a narrow beam preferred over a wide beam when the link range is long [40]. As a consequence of the increase in the link range of a narrow beam, the separation distance between two consecutive BSes may be increased. Therefore,

the total number of BSes along the track and their total cost may be smaller for a narrow-beam system than for a wide-beam system.

The light intensity of a narrow beam is greater than that of a wide beam at a given distance for sources with the same transmission power [69]. On the other hand, a narrow beam provides a shorter coverage length than a wide beam for a given tilt angle as equation (2.1) shows. Moreover, it is easier to block the light of a narrow beam than that of a wide beam. Therefore, some FSO products use multiple parallel beams to increase the reliability of the link. If any of the parallel beams is blocked the unblocked beams can continue to communicate. For instance, a commercial FSO product uses four parallel beams that start overlapping at 100 meters [3]. If these parallel beams have large divergence angles, the combined coverage area of them is larger than that generated by multiple narrow beams, which may increase the reliability of FSOC system.

Train vibrations generate larger pointing and tracking errors for a narrow beam than for a wide beam. Because the size of the receiver aperture of an FSO transceiver is usually small, train vibrations may cause the transmitting light to fall off of the receiver's aperture and this loss of line-of-sight disrupts the connectivity between the BS and the train. Therefore, an ATP mechanism for a narrow beam is required to maintain the transmitter and the receiver of the FSO link aligned at all times, even in the occurrence of vibration induced by the motion of the train. The employment of such an ATP mechanism increases the cost of the FSOC system [68].

Regarding security, it is harder to intercept a narrow beam than a wide beam because the narrow beam has a smaller spatial footprint. Furthermore, regardless of whether the beam is narrow or wide, laser light employed in FSOC cannot penetrate walls or opaque obstacles, thus making eavesdropping difficult. Table 2.1 presents a comparison of the the properties, advantages and disadvantages of two beam modalities for high-speed ground-to-train FSOC.

Table 2.1 Comparison of Narrow and Wide Beam

Condition/Scenario	**Preferred Beam**	**Reason**
Weather effect	Narrow	A narrow beam is less susceptible to fog, rain, and snow [40].
Range	Narrow	A narrow beam has larger link margin, achieving greater distances [40].
BS cost	Narrow	The narrow-beam achievable distance allows longer separation of BSes, thus needing fewer BSes.
Light intensity	Narrow	A narrow beam achieves high light intensity [69].
Coverage length	Wide	The coverage area of a wide beam is larger than that of a narrow beam.
Blocking laser light	Wide	A wide beam is more difficult to block at the receiver side.
Parallel beams	Wide	Wider beams may attain increased coverage and reliability.
Vibration	Wide	Wide beams may allow stronger vibrations than a narrow beam to keep the receiver in the covered area.
ATP requirement	Wide	A wide beam may need less alignment than a narrow beam; relaxing the need for ATP.
Transceiver cost	Wide	A wide beam without ATP may be more cost effective.
Security	Narrow	A narrow beam offers increased link security as the spatial footprint is small [99].

2.3 Results and Discussion

In this section, we analyze and compare narrow- and wide- beam modalities in terms of the impact of the divergence angle of a laser beam on the maximum achievable distance (i.e., link range), coverage length, and contact time. We present the received power over different tilt angles and d_2 values. We analyze the angular speed of the FSM for various divergence angles and present the impact of train vibrations on the received power. We also report a laser experiment performed in a laboratory environment that shows the theoretical received power values given by equation (2.5) match actual power values. The experimental results are provided at the end of this section.

Based on the results given in this section, we propose to employ a divergence angle of a wide beam in the range [0.07°, 2.002°] to drastically reduce the steering speed of the FSM, to accommodate vertical displacements of the train of up to 50 mm while guaranteeing a 1-Gbps data rate, and to provide connection time to the train that is larger than or equal to the handover time.

We use MATLAB® [101] to perform numerical evaluations of the models described by equations (2.1) - (2.6). We consider on–off keying (OOK) as the adopted modulation scheme, which is widely used in FSOC [40, 69]. A BER of 10^{-9} is adopted to guarantee an error-free data transmission for 1 Gbps at the receiver sensitivity threshold and no forward error coding scheme is used. We summarize the system model parameters used in the analysis of our FSOC system in Table 2.2.

According to equation (2.5), Figure 2.2 shows the maximum achievable distance along the track when θ varies from 0.002 to 3.002° in 0.1° steps; the maximum achievable distance for each θ is calculated according to the receiver sensitivity threshold, which is -36 dBm at 1 Gbps. The maximum achievable distance corresponds to the maximum distance at which the received light signal can be decoded and converted back to an electrical signal. We adopt -36 dBm as the receiver

Table 2.2 System Model Parameters for Divergence Angle Efficiency

Symbol	**Parameter**	**Value**	**Unit**
θ	Beam divergence angle	variable	degree
λ	Laser operating wavelength	850	nm
γ	Tilt angle of the BS	variable	degree
d_1	Vertical distance of the BS from the track	1	m
d_2	Horizontal distance of the BS from the track	variable	m
L	Coverage length of the beam	variable	m
P_{tx}	Transmission power of the laser	100	mW
S	Receiver sensitivity (at 1 Gbps)	-36	dBm
n	Refractive index of the optical concentrator	1.5	-
ψ_c	Receiver half-angle field-of-view	5.15	degree
A_d	Photodetector area	7	mm^2
f	Frequency of the vibration	80	Hz
a	Amplitude of the vibration	[0, 60]	mm
v	Speed of the train	300	km/h

sensitivity threshold because silicon positive-intrinsic-negative (PIN) photodiodes with a transimpedance amplifier can provide data rates up to 1 Gbps at that sensitivity threshold by using an 850-nm laser [40, 60]. Also note that there are some FSOC systems that provide a data rate of 1 Gbps or higher [130, 107, 103, 102, 108, 109, 40] but for stationary communications for fixed transceivers. For instance, a fabricated indoor optical wireless communication system capable of transmitting at a data rate of 1.25 Gbps using an 825-nm-wavelength with a transmission power of 25 mW has

been demonstrated [107]. This transmission power is lower than the one used in our analysis [107, 103]. The same study shows that the measured sensitivity of the employed avalanche photodiode is -35 dBm at 1.25 Gbps for a BER below 10^{-9}. Moreover, commercial full-duplex FSOC products are reported to achieve data rates of up to 1.25 Gbps with a range of up to 4 km in clear weather conditions [60]. Besides, 850-nm vertical-cavity surface-emitting lasers (VCSELs), usually employed in FSOC systems, can be easily modulated at 2.5 GHz to provide a data rate of 2.5 Gbps, with a potential transmission capability of up to 10 Gbps [40, 130].

According to the results in Figure 2.2, the narrow beam reaches up to 181,696 m from the BS while still providing larger power than the minimum receiver threshold. This result is expected because the highly collimated characteristics of the narrow laser beam lead to a significant increase in the intensity of the light at the receiver for a given transmitted power, which in turn results in a link range longer than that of a wide beam [69].

Based on the selected divergence angle, the maximum achievable distance of the beam determines the largest separation distance between two consecutive BSes. Therefore, each divergence angle in the proposed range is associated with a maximum achievable distance.

Coverage Length. According to equations (2.1), (2.5), and the receiver sensitivity threshold, Figure 2.2 shows the effective coverage length along the track when θ varies from 0.002 to 3.002° in 0.1° steps. As this figure shows, with the increase in the maximum achievable distance, the effective coverage length of the narrow beam along the track increases.

Contact Time. This metric is defined as the time the transceivers are within the coverage area and eligible for establishing communication. The contact time includes the connection time and the time to perform handover. Figure 2.2 shows the contact time as θ varies from 0.002 to 3.002° in 0.1° steps for an HST moving at 300 km/h (or

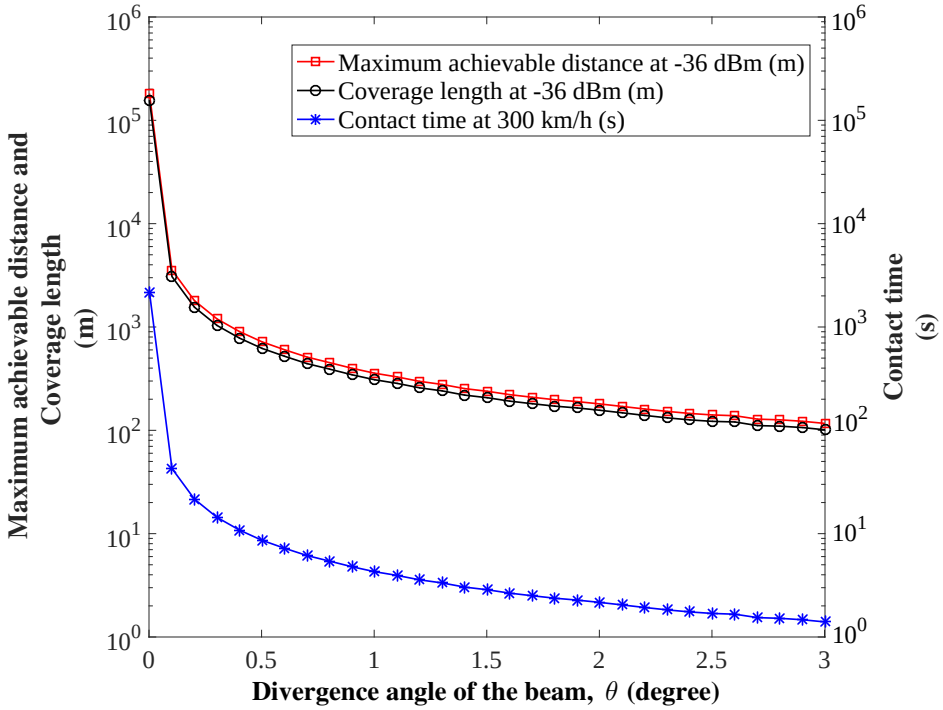

Figure 2.2 Maximum achievable distance at -36 dBm (m), the coverage length at -36 dBm (m), and contact time at 300 km/h (s) for θ from 0.002 to 3.002° in 0.1° steps.

$83\frac{1}{3}$ m/s). As expected, the narrow beam provides the longest contact time because it attains the longest link range among the considered divergence angles. Table 2.3 summarizes the maximum achievable distances, effective coverage lengths along the track and contact times for the sampled θ values.

We use the largest divergence angle that allows a connection time of at least twice the handover time [38]. The largest reported handover time for FSOC systems in HSTs is 1 second [38]. Considering that, a wide beam with a divergence angle smaller than or equal to 2.002° yields a contact time larger than 2 seconds, allowing a connection time of 1 second or longer (see Table 2.3).

Received Power. We graph the received power considering the receiver sensitivity threshold, tilt angle, and equation (2.5), as Figure 2.3 shows, when γ decreases from 0.1 to 45.1°. The results in this figure reveal that for a tilt angle around 0°, the

Table 2.3 Maximum Achievable Distance, Effective Coverage Length and Contact Time at 300 km/h for Sampled θ Values

θ	**Max Achievable Distance (m)**	**Effective Coverage Length (m)**	**Contact Time at 300 km/h (s)**
0.002	181,696	156,951	2,180
0.07	5,190	4,487	53.80
0.502	718.22	620.72	8.61
1.002	357.03	308.73	4.28
1.502	238.75	206.85	2.86
2.002	180.08	156.38	2.16
2.502	140.84	122.14	1.69
3.002	116.56	101.16	1.39

received power is not strong enough to allow the light be converted to an electrical signal for a data rate of 1 Gbps. On the other hand, the narrow beam provides a constant received power of approximately 20 dBm even the tilt angle is almost 0° (i.e., the BS becomes almost parallel to track). Note that a decrease in the tilt angle increases the achievable distance between the BS and the train, and the narrow beam has a considerably longer link range than a wide beam.

Figure 2.4 shows the received power when d_2 varies between 1 and 100 m. This figure also shows that d_2 can reach beyond 100 m without a significant decrease in power for the narrow beam. Moreover, these results indicate that a beam with a divergence angle in the proposed range may deliver enough power at the receiver to operate above the sensitivity threshold as d_2 approaches 100 m. Similar to the results shown in Figure 2.3, d_2 increases for a constant d_1 as the tilt angle decreases. Therefore, d_2 is longer for the narrow beam than that of the wide beam.

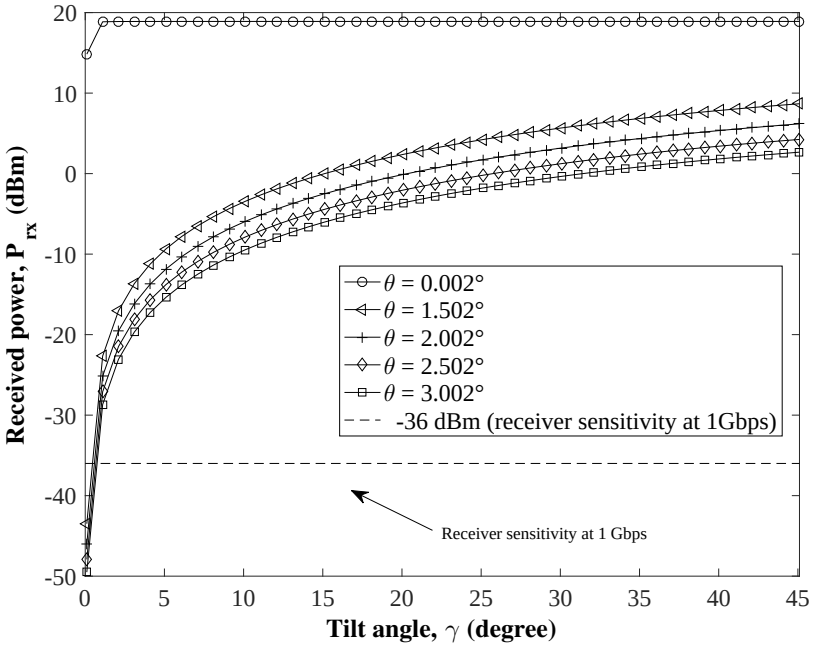

Figure 2.3 Received power as a function of γ.

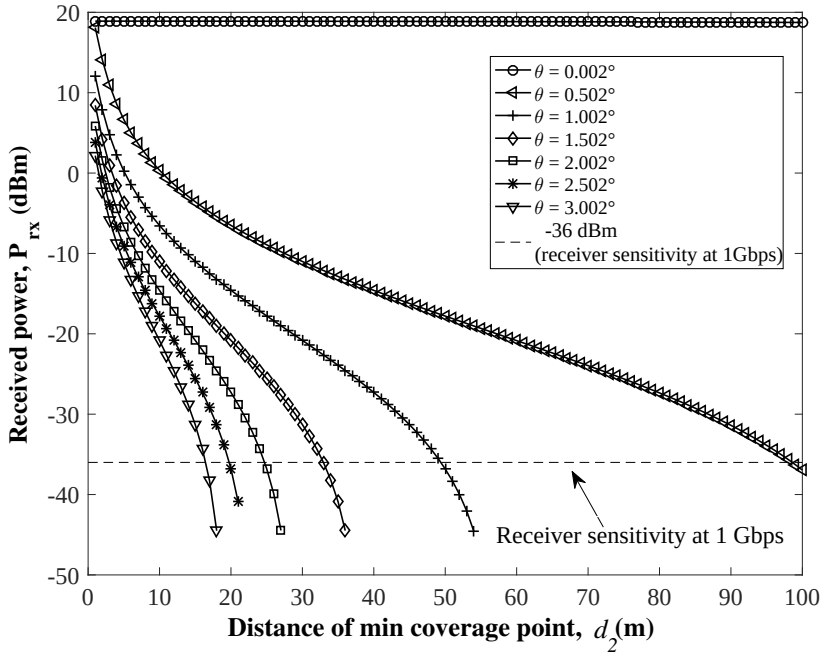

Figure 2.4 Received power as the distance of the minimum coverage point varies between 1 and 100 m.

An FSO transceiver is usually equipped with an optical concentrator, a photodiode, and receiver electronics. The optical concentrator focuses the incident light onto the photodiode, and the photodiode converts the received light into electrical signals, which are then recovered by the receiver electronics. According to equations (2.6) and (2.5), an increase in the photosensitive area of the photodiode (A_d) or a decrease in the FOV of the concentrator (half of FOV angle is denoted as ψ_c) results in an increase in the received power (P_{rx}). The impact of A_d on P_{rx} is a direct result of the constant radiance theorem, and that impacts the maximum collection area of an optical receiver for a given FOV, the reflective index of the optical concentrator, and the radiation collection area of the photodiode [111, 107]. Moreover, FOV has an adverse effect on the received power because the constant concentrator gain within the FOV of the optical concentrator (i.e., $\frac{n^2}{sin^2\,\psi_c}$) decreases as the FOV increases [75, 112, 47]. On the other hand, increasing the photosensitive area increases the capacitance of the photodiode and, therefore, decreases its response time [10]. Also, an increase of A_d leads to a decrease of the receiver bandwidth and to contribute to the dark current noise of the photodiode in the absence of light [75]. In addition, an increase in FOV increases background noise, and that degrades the SNR of the received signal [117].

Figure 2.5 shows the relationship among A_d, ψ_c, and P_{rx} for $\theta = 0.502°$. A_d in this figure is selected from a commercially-available range of [0.1, 10] mm^2 [17]. We select the range of ψ_c between 0.1 and 45° because the FOV of a concentrator is usually bound to 45° [75]. Figure 2.5 shows that a small FOV and large photosensitive area are beneficial to FSOC systems because they yield a greater received power. The shaded zone of the 3D graph in this figure represents the A_d-ψ_c pairs forming a region where the received power is at least -36 dBm for a data rate of 1 Gbps.

There are commercial large-area photodetectors operating at 10 Gbps or higher speeds [4, 13, 12, 14]. For instance, a receiver-optical subassembly (ROSA) InGaAs

PIN photodiode with a preamplifier may provide a data rate of up to 11.3 Gbps with a photosensitive area of 1.25 mm [11]. Moreover, these ROSA modules may increase their received data rate up to 100 Gbps by employing WDM techniques [4]. These works show that photodiode areas larger than that considered in this dissertation may achieve larger data rates.

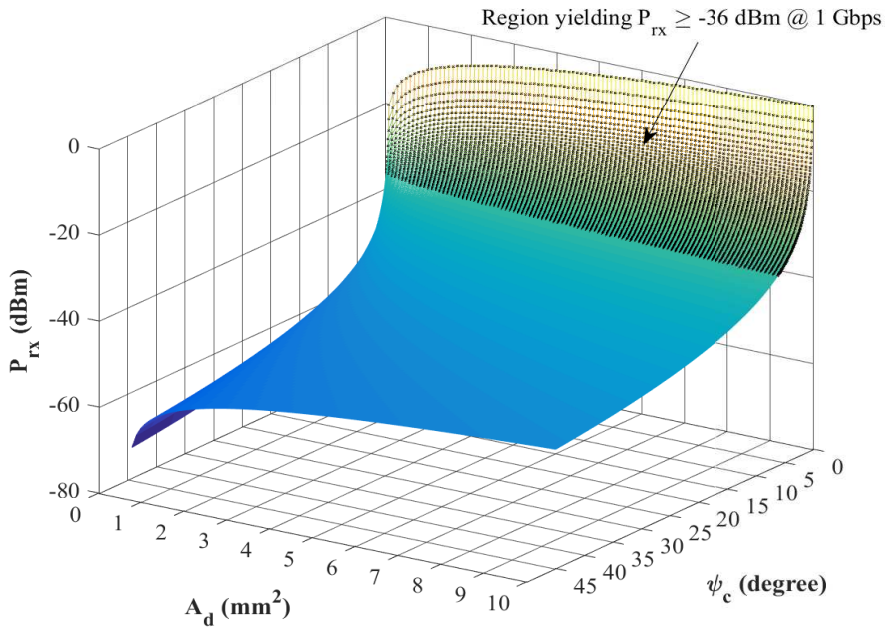

Figure 2.5 Received power as a function of half-angle field-of-view and the size of the photosensitive area of the photodiode when $\theta = 0.502°$.

Angular Speed of FSM. Figure 2.6 shows the angular speed of the FSM of a transceiver for a train moving at 300 km/h. The dashed line in this figure indicates the maximum angular speed that a commercial FSM can reach, which equals to 300 radian/s, or 17188°/s [6]. In this calculation, we steer the FSM from 0.1 to 45.1° in 1° steps. For each $\{\theta, \gamma\}$ pair, we calculate the effective coverage length, $L_{\theta,\gamma}$, where θ and γ are selected from the represented divergence and tilt angles, respectively. We obtain the required angular speed of the FSM by estimating the time it takes for the train to travel over each $L_{\theta,\gamma}$. Note that the speed of the FSM slows down as the beam divergence angle increases because the coverage length of a wide beam increases

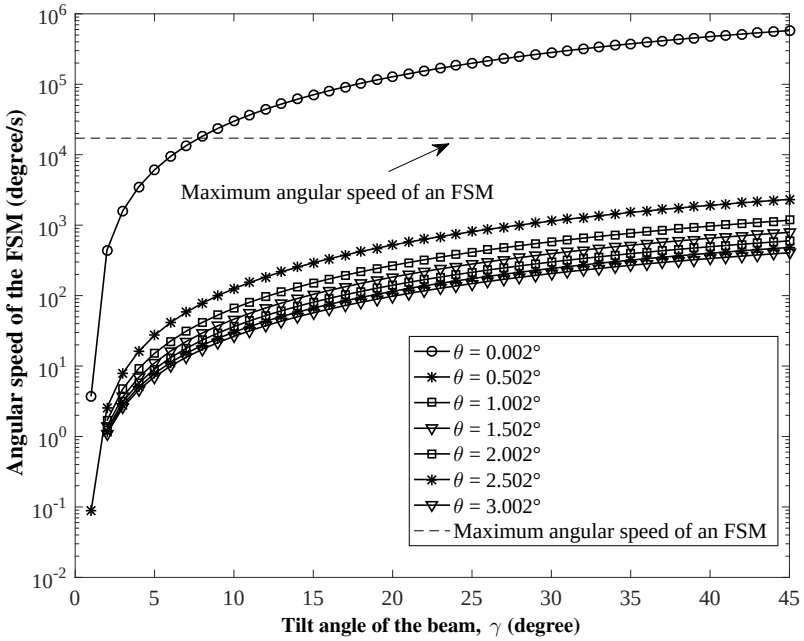

Figure 2.6 Angular speed of the FSM for γ from 0.1 to 45.1° in 1° steps.

as the divergence angle increases. Figure 2.6 shows that the maximum angular speed of the narrow beam is required to be approximately 598,935 degree/s. However, this speed is infeasible for commercially available FSMs [1, 5, 6].

We base the minimum value of the proposed range for the divergence angle on the maximum angular speed of a commercial FSM. This maximum angular speed dictates the minimum divergence angle of the proposed range when the tilt angle of the beam is 45° or larger [6]. Therefore, we propose to use the smallest divergence angle in the proposed range; 0.07°, to keep the needed angular speed within the range of a commercial FSM.

Vibration Effect. Possible movements of the train are modeled in three dimensions: longitudinal; along the direction in which the train moves, vertical, and lateral. Figure 2.7 shows these directions in reference to the train position. Because the

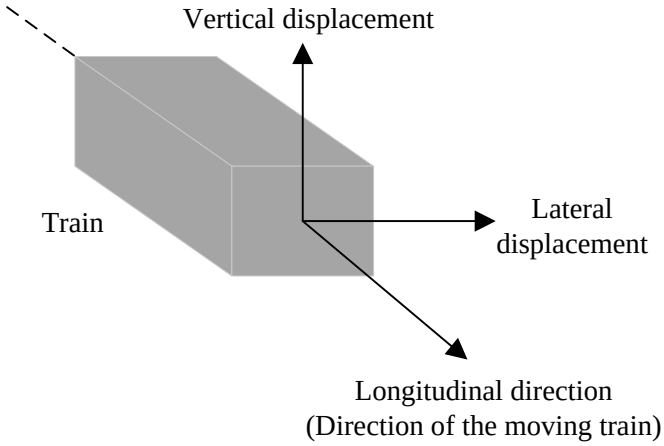

Figure 2.7 Three-dimensional view of the train and the vibration types.

train smoothly moves in the longitudinal direction, we analyze the vibration in the vertical and lateral directions.

Vertical Train Vibration. We first investigate the impact of the vertical displacement of the train on the received power to determine the maximum amplitude of the vertical displacement that may cause connectivity problems between a BS and the train. Figure 2.8 shows how the received power changes as the vertical displacement of the train varies between 0 and 60 mm. As the figure shows, there is a drastic reduction in the received power with the increase in the vertical displacement of the train for the narrow beam. Specifically, the narrow beam crosses the receiver sensitivity threshold when the amplitude of the vertical displacement of the train equals to 39 mm. The loss of received power in this figure occurs because the detector coupling loss of the narrow beam becomes severe. However, the changes in the received power of the considered wide beam modalities are too small to measure. Moreover, among the wide beams presented in Figure 2.8, the ones in the proposed divergence-angle range

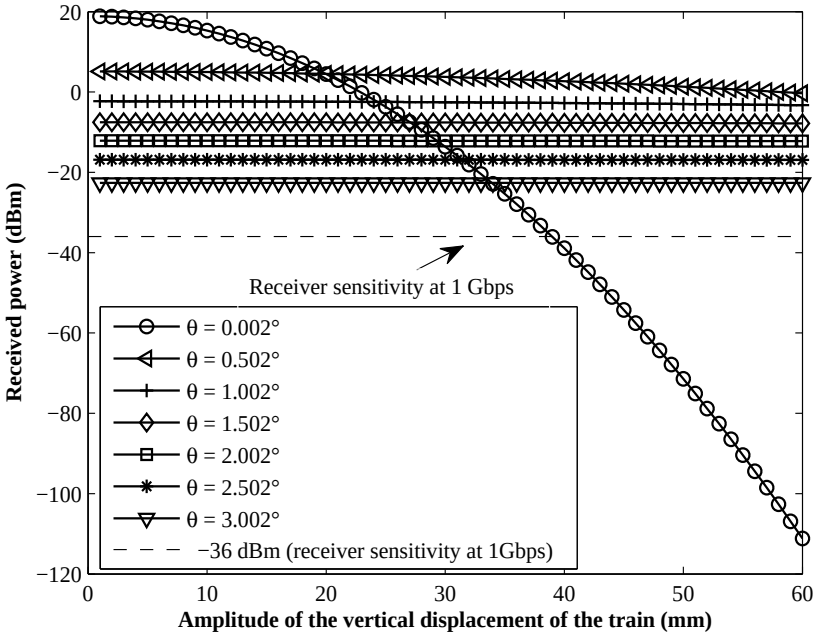

Figure 2.8 Received power in function of the amplitude of vertical displacement of the train.

provide a received power greater than the receiver sensitivity threshold when the extent of the maximum vertical displacement changes from 0 to 60 mm.

In the remainder of this chapter, we adopt 30 and 50 mm as amplitudes of vertical displacement that yield the received power values above and below the receiver sensitivity threshold for the narrow beam, respectively. The 30-mm vertical displacement that does not cause a disconnection and the 50-mm displacement causes a disconnection between the BS and the train.

We consider that the vertical displacement of the train can be positive (i.e., upwards) or negative (i.e., downwards). Figure 2.9 depicts the scenarios for positive or negative vertical displacement of the train. This vertical vibration is modeled as sinusoidal vibrations that can be generated by the unevenness of a wheel of an HST or the rail [123]. The vibrational frequency used in this analysis was set to 80 Hz, which is the upper frequency limit of the ground vibration measured when an HST travels at speeds up to 290 km/h [133].

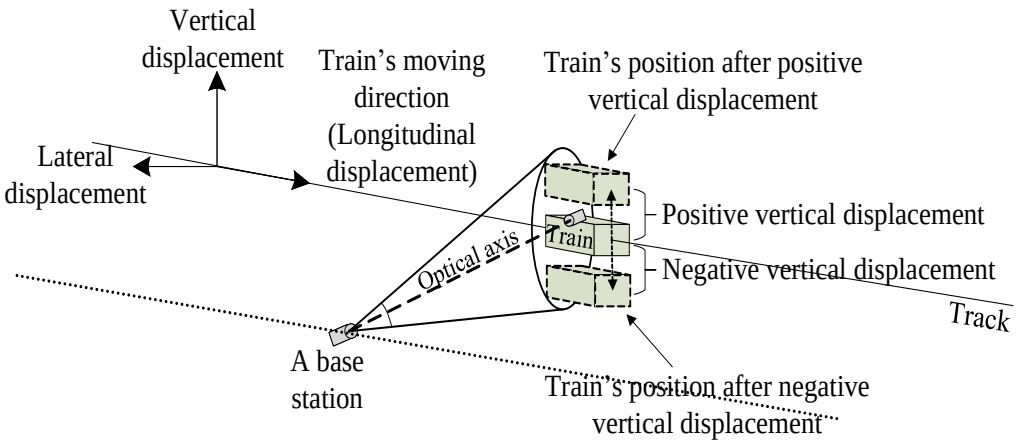

Figure 2.9 Scenario for positive or negative vertical displacement of the train.

Figures 2.10(a) and 2.10(b) show the corresponding impact of the train vibration on the received power for maximum vertical displacements of 30 and 50 mm, respectively. When the vertical displacement of the train fluctuates, the received power of the narrow beam also fluctuates. The 50 mm displacement causes the received power to decrease below the the receiver sensitivity threshold because the center of the beam moves far from the receiver, and the received power decreases in accordance with the gaussian distribution of the beam. Therefore, a vertical displacement of 50 mm may result in disconnections between the BS and the receiver on the train. These results show that a narrow beam may not be an appropriate beam modality for ground-to-train FSOC for HSTs undergoing vertical displacements of 50 mm and larger. Moreover, Figures 2.10(a) and 2.10(b) show that the divergence angles in the proposed range yield a received power above the receiver sensitivity threshold for a vertical displacement of the train of up to 50 mm.

Lateral Train Vibration. We calculate the coverage-distance safety margins that guarantee a BS to be covered by the transmitting beam from the train in case of a lateral displacement of the train. As the boundary of a covered distance is limited by the divergence angle, we consider that a reliable coverage distance is the largest

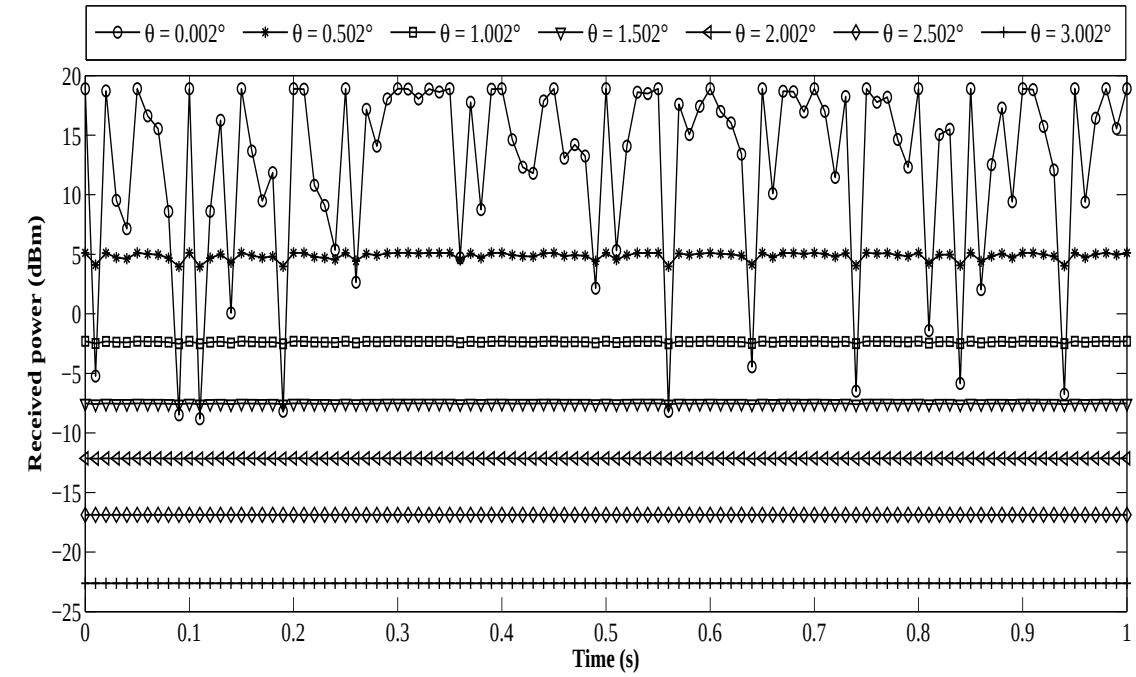

(a) Maximum displacement of 30 mm.

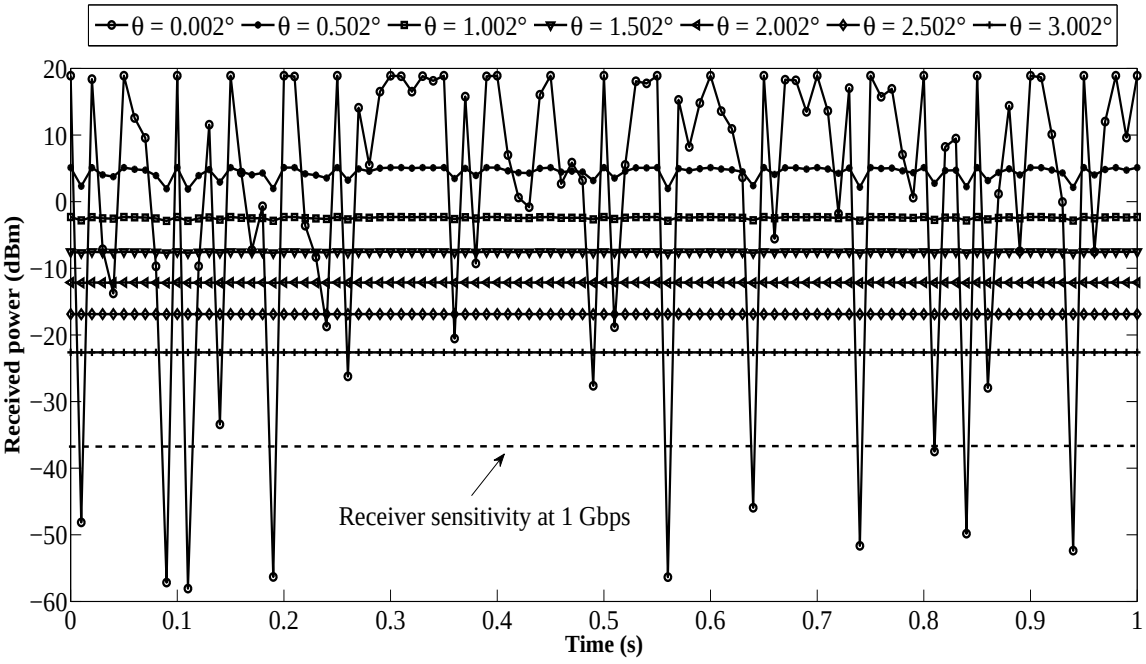

(b) Maximum displacement of 50 mm.

Figure 2.10 Impact of the vertical vibration of the train with a frequency of 80 Hz and a maximum displacement of 30 and 50 mm for 1 second on the received power.

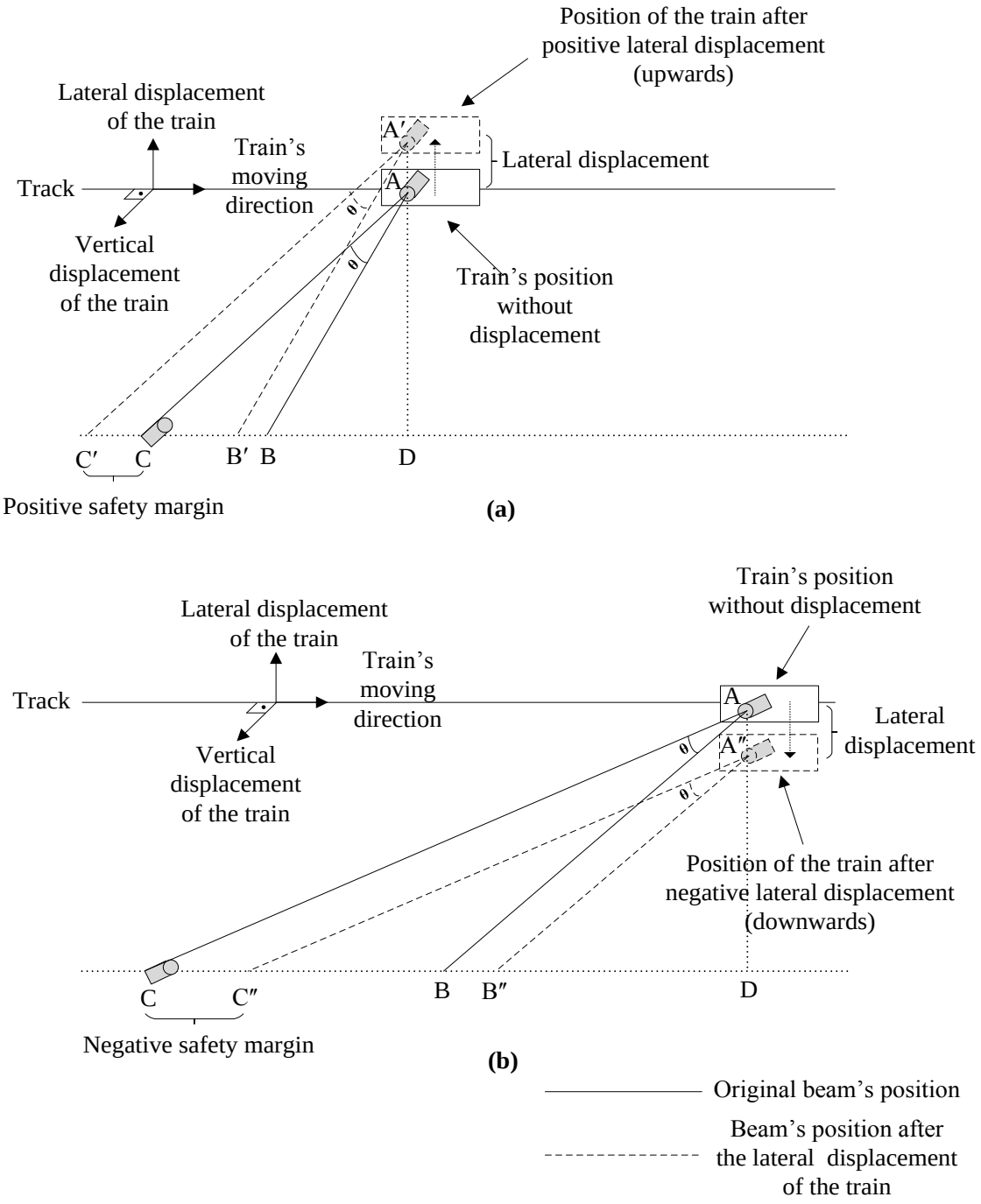

Figure 2.11 Top views of a **(a)** positive (updwards) lateral displacement of the train and the corresponding safety margin, $[C'C]$, and **(b)** negative (downwards) lateral displacement of the train and the corresponding safety margin, $[CC"]$.

one for each divergence angle minus the safety margins needed for compensating the largest lateral displacement caused by lateral vibration. These safety margins

might be required for the transmitting beam not to lose the line-of-sight between the train and a BS when a lateral displacement occurs on the train. We consider $d_2 = 15$ m as the starting position where the train and a BS make contact for the first time. This position is found at the leftmost position of the coverage distance of train's transmitter [112]. The rightmost position covered by the beam corresponds to the maximum achievable distance of the beam. Figure 2.11 depicts the two possible lateral displacements (i.e., upwards or downwards) of the train, and the corresponding safety margins, respectively. $[C'C]$ and $[CC'']$ in Figures 2.11(a) and 2.11(b) show the safety margins for positive and negative lateral displacement of the train, respectively. Table 2.4 shows these values for the sampled divergence angles. For the considered divergence angles, the positive safety margin at the leftmost coverage point is calculated by using triangle similarity between the $A'C'D$ and ACD triangles in Figure 2.11(a). The 50-mm positive lateral displacement of the train yields a 0.75 m displacement for the BS in Figure 2.11(a) according to $\frac{|A'A|}{|A'D|} = \frac{|C'C|}{|C'D|}$ triangle similarity, where $|A'A| = 0.05$ m.

Table 2.4 Sampled Safety Margins Required for Different Divergence Angles to Compensate for Lateral Train Vibration

θ **(degrees)**	**Safety Margin (m)**
0.002	9084.86
0.07	259
0.502	35.96
1.002	17.90
1.502	11.98
2.002	9.05
2.502	7.09
3.002	5.87

Similarly, the negative safety margin at the rightmost coverage point in Figure 2.11(b) is calculated by considering the maximum achievable distance and triangle similarity between the ACD and $A''C''D$ triangles. Furthermore, by considering the maximum achievable distance of a beam, a negative lateral displacement (in the downwards direction) of the train causes the maximum coverage point of the 0.07° beam to be adjusted to 4,931 m, which yields a 259-m safety margin. In other words, a 50-mm lateral displacement of the train would leave 259 m of the coverage length uncovered when the divergence angle is selected as 0.07°. Therefore, we exclude that length from the maximum achievable distance. Similarly, the same negative lateral displacement causes the beam with a divergence angle of 2.002° to displace about 9 meters. Therefore, a lateral displacement of 50 mm defines safety margins (i.e., 0.75 and [9, 259] m, respectively) for the beams in the proposed range such that the train and corresponding BS keep line-of-sight despite the occurrence of lateral vibrations.

2.3.1 Experimental Results

We performed a laser experiment in a laboratory environment to show that the theoretical received power values calculated by using equation (2.5) match actual power values. The experiment consists of measuring the received power at different distances using an optical power meter. The transmitter comprises of a collimated 532-nm laser diode with an output power of 70 mW and a biconvex lens with a focal length of 10 cm to diverge the beam. The receiver is a bolometer (Scientech 361) with an aperture size of 2.5 cm. We measured the received power and the beam diameter for different distances between the transmitter and the receiver. The considered distances are from 10 to 25 m. The longest considered distance is limited by the sensitivity of the bolometer. Figure 2.12(a) shows the bolomoter used in the experiment and the beam formation at the receiver when the light source is placed 20

m away from the receiver. The laser beam through the lens sets a divergence angle of 10.5 mrad or 0.6°, as defined by:

$$\theta = 2 \arctan \left| \frac{D_{i+1} - D_i}{l} \right| \tag{2.7}$$

where D_i and D_{i+1} are the beam diameters at two separate points, i and $i+1$, and l is the distance between these two measurement points. The theoretical received power for each distance in the experiments is calculated by using equations (2.2), (2.5), (2.6), and (2.7). Figure 2.12(b) shows the comparison of the theoretical and experimental received power of the wide beam with a divergence angle of 0.6°. The results show that the experimental received power closely follows the theoretical model. It is worth nothing that the small discrepancies in the comparison may be caused by some measurement errors as exact measurement of spot diameter and power are complex. The results are encouraging.

We calculated the SNR and the BER using the received power values collected from the conducted experiment. The SNR at the receiver is given by [75], as:

$$SNR = \frac{RP_{rx}}{\sigma^2_{total}} \tag{2.8}$$

where R is the responsivity of the photodiode in A/W, and σ^2_{total} is the total noise variance, which is equal to the sum of the variances of shot, thermal, and background noises [99, 100]. The BER is expressed as $BER = Q\left(\sqrt{SNR}\right)$, where the Q function is the tail probability of the standard normal distribution and it is given as:

$$Q(x) = \frac{1}{2\pi} \int_x^\infty e^{\left(-y^2/(2)\right)} dy \tag{2.9}$$

We assumed an Si APD with a responsivity of 0.5 A/W being used for a system operating at 850 nm [19]. We also assumed that the total noise power in the system is

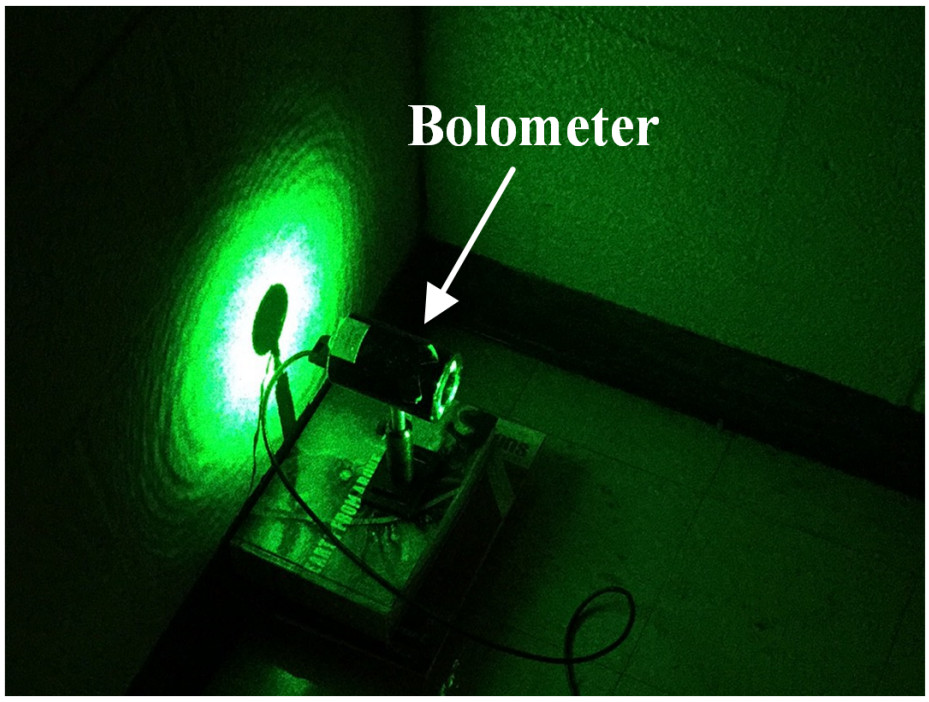

(a) The bolomoter used to measure the received power and the beam formation of the performed experiments.

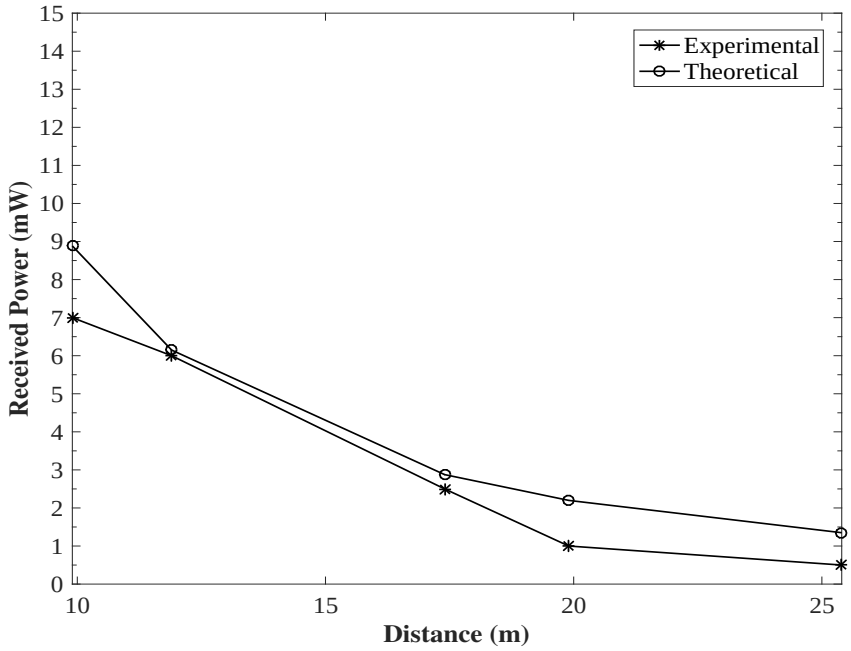

(b) Aggregated energy demands.

Figure 2.12 Comparison of the experimental and the theoretical received power for the wide beam with a divergence angle of 0.6°.

equal to 10 μW [49, 83, 112]. The calculated BER for the received power values given in Figure 2.12(b) are negligibly small to provide an error-free transmission at 1 Gbps. This is an expected result because of the high transmission power the employed laser in the experiment. According to the calculated BER, a high-speed FSOC system with a received power of greater than or equal to 77.5 μW can support an error-free transmission at 1 Gbps for the parameters used in this experiment. This result may be verified by using an optical simulation environment, such as OptiSystem [16].

Some other laboratory experiments for ground-to-train FSOC, which use the same propagation model as equation (2.5), have been reported [114, 113]. These experiments achieved successful FSOC between a toy train and a BS. By using a light source with an output power of 10 mW, a BER of 10^{-12} at 10 Mbps [113] and a data rate of 155 Mbps [114] are achieved, respectively. In another experiment, a diverged beam is used to show how the received power changes when the distance between the light source and the diverging lens varies [134]. The experimental results in [134] show that a data rate of 622.08 Mbps is achieved when the minimum received power is -36 dBm. These experimental results support that the propagation model used in this chapter is valid and experimental results match the theoretical analysis.

2.4 Chapter Summary

Two different laser beam modalities, narrow and wide beams, for FSOC have been investigated in the context of ground-to-HST communications. These two beam modalities are compared and their advantages and disadvantages are revealed. The covered distance, steering speed, steering arc, covered area, and the impact of vibration for each angle are also estimated. Considering the results presented in this chapter, we propose to use a divergence-angle range to enable a contact time larger than or equal to the worst-case handover time. The impact of vibration is also examined and our results show that the proposed range of divergence angles

guarantees that the received power is larger than the receiver sensitivity threshold with the maximum vertical vibration amplitude smaller than or equal to 50 mm.

The findings in this chapter motivate us to propose an adaptive-divergence beam in the next chapter to further improve the received power, SNR, and BER of a mobile FSOC system for HSTs. A laser beam that adopts its divergence angle according to the communication distance between a transmitter-receiver pair and the aperture diameter of the receiver may take advantage of minimizing the geometric loss of the optical link while facilitating the transmitter-receiver alignment.

CHAPTER 3

BEAM WITH ADAPTIVE DIVERGENCE ANGLE IN FREE-SPACE OPTICAL COMMUNICATIONS FOR HIGH-SPEED TRAINS

In this chapter, an adaptive beam that adapts its divergence angle according to the receiver aperture diameter and the communication distance is proposed. The proposed adaptive beam improves the received power and eases the alignment between the communicating optical transceivers in an FSOC system for HSTs. The received power, SNR, BER, and the maximum communication distance of the proposed adaptive beam are compared with a beam that uses a fixed divergence angle of 1 mrad. The results indicate that the proposed adaptive beam yields a higher received power with an increase of 33 dB in average over that achieved by the fixed-divergence beam under varying visibility conditions and distances. Moreover, the proposed adaptive divergence-angle approach extends the communication distance of an FSOC system for HSTs to about three times as compared to that of a fixed divergence beam. A new ground transceiver placement that places the ground transceivers of an FSOC system on gantries placed above the train passage is also proposed. The proposed transceiver placement provides a received-power increase of 3.8 dB in average over the conventional placement of ground-station transceivers next to the track.

The remainder of this chapter is organized as follows. Section 3.1 presents our system model. Section 3.2 presents numerical results of our adaptive divergence angle model. Section 3.3 concludes the chapter.

3.1 System Model

Several recently proposed geometric models of FSOC systems for HSTs [112, 79, 56] place the base stations next to track. Among these studies, the results in [56] show that minimizing the vertical distance between a base station and the train improves the received power and increases the coverage area of the base station. These results

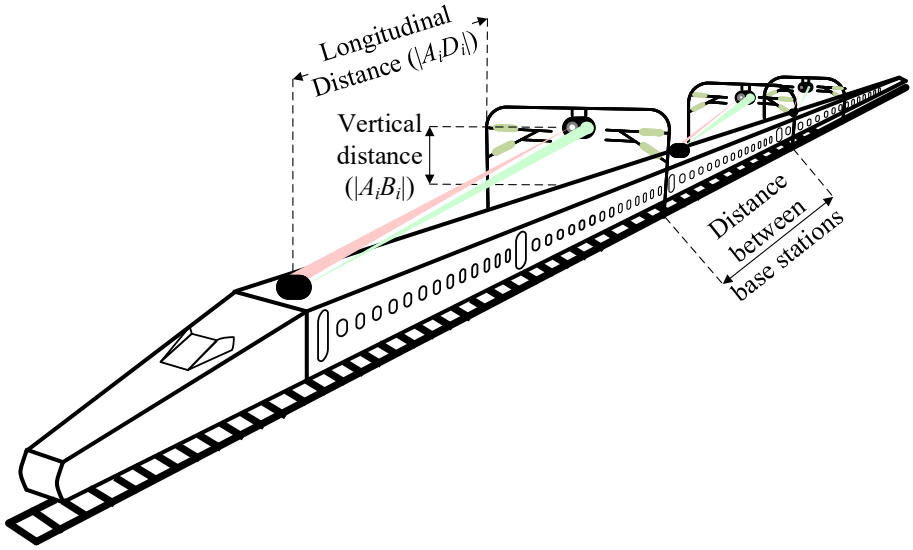

Figure 3.1 3D view of the proposed FSOC system for HSTs.

provide a motivation to propose an FSOC system for HSTs, where the base stations are placed above the track (and above the train passage), as shown in Figure 3.1. In this model, gantries may be used as supporting structure for ground transceivers. An FSOC system having the base stations attached to the gantries instead of placing them next to the track decreases the distance between the base stations and the center of the track or the path followed by the train, thus, improving the received power, SNR, and BER. Figure 3.2 compares the received power of an FSOC model that places the base stations next to the track [79] and our proposed ground transceiver placement where the base stations are attached to gantries. Both models in Figure 3.2 use an adaptive beam that adjusts its divergence angle according to the diameter of the receiver aperture and the communication distance. According to the results in this figure, the proposed placement achieves a higher received power with an increase of 3.8 dB on average.

Each base station in the proposed ground transceiver placement is attached to a gantry that may be used in the power network along the track. Therefore, this

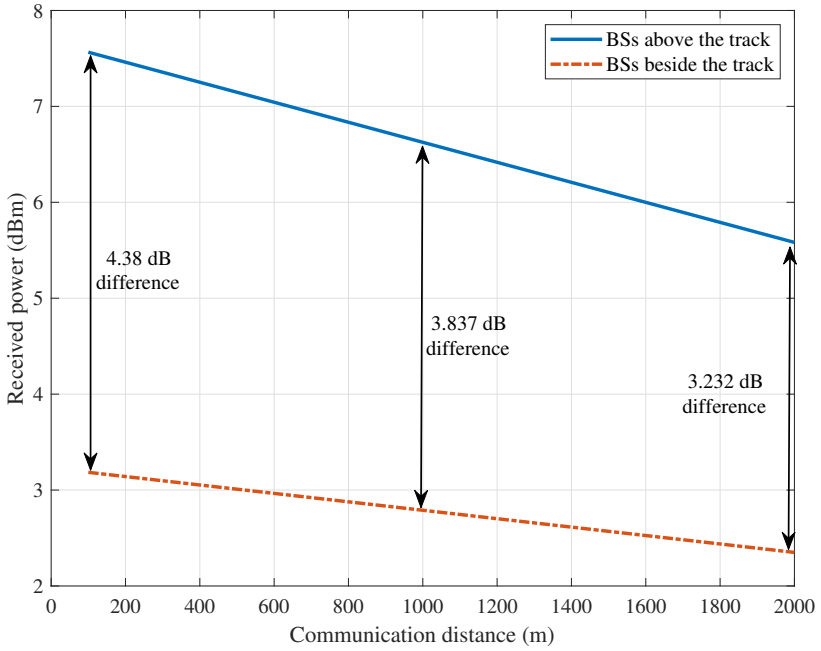

Figure 3.2 Comparison of received power for a system that places base stations on the track's side and another above the track, both using adaptive divergence angle. The visibility is 5 km and transmission power is 10 dBm.

placement may not only increase the data rates or inter-station distance but also it may decrease deployment costs. Moreover, at least two transceivers are placed on an HST in the proposed model, as they allow establishing multiple optical connections between the train's transceivers and multiple consecutive base stations. Establishing multiple simultaneous optical connections between the train and the consecutive base stations may improve reliability and increase the aggregated data rate of the proposed FSOC system for a train passing through an area covered by multiple base stations. For instance, the three transceivers on the train in Figure 3.1 are connected to three consecutive base stations, and this multi-link connection may improve the reliability of the proposed FSOC system.

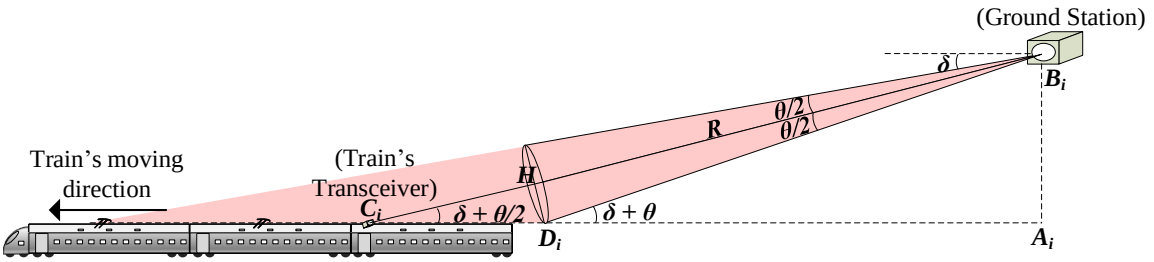

Figure 3.3 Geometric representation (lateral view) of the transmitted beam from a base station located at B_i.

3.1.1 Geometric Model

The geometric model of the proposed FSOC system presented in this section enables the calculation of the received power. Figure 3.3 shows the lateral view of a beam transmitted from a base station located at B_i. The transmitted beam is received by a transceiver on the train located at H.

The longitudinal distance between the train's transceiver at H and a base station at B_i is denoted as $|A_iD_i|$. The vertical distance between the train and the base station is $|A_iB_i|$. Therefore, $|B_iD_i|$ can be calculated as

$$|B_iD_i| = \sqrt{|A_iB_i|^2 + |A_iD_i|^2} \tag{3.1}$$

The radius of the receiver aperture, r_{rx}, is equal to $\sqrt{S_{rx}/\pi}$ for a given receiver aperture area, S_{rx}. Therefore, the divergence angle of the transmitted beam is calculated as

$$\theta_{1/2} = \arcsin\left(\frac{r_{rx}}{|B_iD_i|}\right) \tag{3.2}$$

The communication distance between the transmitter and receiver, R, (in Figure 3.3) is calculated as

$$R = \cos(\theta_{1/2})|B_i D_i| \tag{3.3}$$

3.1.2 Calculation of Received Power and Impact of Fog

The received power of the optical radiation along the axis of propagation is calculated according to Friis formula [99]:

$$P_{rx} = P_{tx} G_{tx} G_{rx} \Big(\frac{\lambda}{4\pi R}\Big)^2 L_{geo} L_{tx} L_{rx} \eta_{tx} \eta_{rx} \tag{3.4}$$

where P_{rx}, P_{tx}, G_{tx}, G_{rx}, λ, R, L_{geo}, L_{tx}, L_{rx}, η_{tx}, and η_{rx} are the received power, transmission power, transmitter antenna gain, receiver antenna gain, wavelength of the beam, communication distance between the transmitter and receiver, geometric loss, transmitter pointing loss, receiver pointing loss, transmitter optical efficiency, and the receiver optical efficiency, respectively.

In general, laser-beam propagation can be approximated by assuming that the lasers emit beams with a Gaussian profile, where the laser is said to be operating on the fundamental transverse mode, or TEM00 mode of the laser's optical resonator [37]. Therefore, we follow this approximation and assume that the laser beam considered in this dissertation has a Gaussian profile. The approximation of the transmitter antenna gain for a Gaussian beam is given by [92]:

$$G_{tx} = \frac{32}{\theta^2} \tag{3.5}$$

where θ is the divergence angle of the transmitted beam, in radians. The receiver antenna gain is given by [99, 71]:

$$G_{rx} = \Big(\frac{\pi D_{rx}}{\lambda}\Big)^2 \tag{3.6}$$

where D_{rx} is the telescope aperture diameter, in meters. The laser beam disperses conically upon exiting the transmitter lens. This dispersion increases as the distance from the laser source increases according to the geometrical loss, L_{geo}, which is given by [40]:

$$L_{geo} = \Big(\frac{D_{rx}}{D_{tx} + \theta R}\Big)^2 \tag{3.7}$$

where D_{tx} is the diameter of the transmitter, in meters.

L_{tx} and L_{rx} in equation (3.4) are the transmitter and receiver pointing loss [93], respectively, which are given by

$$\begin{aligned} L_{tx} &= e^{-G_{tx}\gamma^2}, \\ L_{rx} &= e^{-G_{rx}\zeta^2} \end{aligned} \tag{3.8}$$

where γ and ζ denote the radial pointing errors of the transmitter and receiver in radians, respectively.

Fog and rain attenuate the propagating beam as the water molecules/droplets of fog and rain absorb and scatter the optical signal [35]. Fog is the most dominant atmospheric attenuating factor for FSOC systems among all weather conditions as the radius of water molecules of fog is in the range of the wavelength of the communicating beam [35]. Therefore, we take the impact of fog into consideration in calculating the received power. Some empirical fog models, such as Kruse [90], Kim [85], and Ijaz [73] have been proposed to express the fog-induced power loss in dB/km [73]. These fog models represent the received power as a function of the transmission wavelength, meteorological visibility, and the coefficient related to the particle size distribution in the atmosphere. The Kruse model is considered to be not accurate enough for visibilities less than 0.5 km because it is originally proposed for haze particles [73]. Moreover, the Kim model neglects the relationship between visibility and wavelength

for visibilities smaller than 0.5 km. Therefore, we adopt The Ijaz fog model for visibilities in the range of [0.015, 1) km. The Kim model is adopted for visibilities greater than 1 km. The Ijaz and Kim fog models share a common loss function that is given by [73, 85]:

$$L_a = \frac{17}{V}\Big(\frac{\lambda}{0.55\mu m}\Big)^{-q(\lambda)} \tag{3.9}$$

where L_a is in dB/km, V is the meteorological visibility in km, λ is the transmission wavelength of the laser, in μm, and q is the size distribution of the scattering particles. According to the meteorological visibility, q values are given by [73, 85]:

$$q = \begin{cases} 1.6, & V \geq 50\ km \\ 1.3, & 6 \leq V < 50\ km \\ 0.16V + 0.34, & 1 \leq V < 6\ km \\ 0.1428\lambda - 0.0947, & 0.015 < V < 1\ km \\ 0, & V \leq 0.015\ km \end{cases} \tag{3.10}$$

The received power after the impact of fog is calculated by subtracting the fog-induced power loss, equation (3.9), from the received power calculated in (3.4), which is given by

$$P_{rx_{fog,dBm}} = 10\log_{10} P_{rx} - L_a \tag{3.11}$$

3.1.3 Detection of Optical Radiation

The optical radiation transmitted from a base station is received by a direct detection receiver on the train. A direct-detection FSO receiver in the proposed communications system consists of a collimating lens that collects and focuses the incident light

radiated by the transmitter, an optical filter to filter out the undesirable background radiations such as direct, reflected, or scattered sunlight, a photodiode that converts the optical signal to electrical signal, a trans-impedance amplifier to amplify the electrical signal, a low-pass filter to limit the thermal and background noise, and a symbol detector to recover the received data. The mentioned receiver equipment may induce some noise that degrades SNR at the receiver. The total noise for a direct detection receiver that employs an APD is a combination of the photo-current shot, thermal (i.e., Johnson noise), dark current, and background illumination noises [75, 125]. The thermal noise, also called Johnson or Nyquist noise, is the electronic noise induced by the thermal agitation of the electrons passing through an electrical conductor [125]. The dark current is the current that flows through the bias circuit of a photodiode even without the incident light [125]. The dark current noise arises from electrons and/or holes that are thermally generated in the p-n junction of a photodiode. The background noise is the result of the undesirable background radiation collected by the photodetector, which may arise from the intense and visible background light, such as sunlight and artificial lights [75, 100]. The shot noise, which is also known as the quantum noise in optical communications, originates from the random occurrence of photon absorption events in a photodetector [100]. The number of photons of the incident light fluctuates by following a Poisson distribution at the receiver and the random occurrences of the incident photons on the receiving surface causes the shot noise. If all noise sources have zero mean and are statistically independent of each other, then the total noise power at the receiver can be calculated by

$$\sigma^2_{total} = \sigma^2_{dark} + \sigma^2_{background} + \sigma^2_{shot} + \sigma^2_{thermal} \tag{3.12}$$

The average received power is typically larger than the signal current, which makes dark current and background noises negligible in practice [125]. Therefore, the total variance of the receiver-related noise of a receiver that employs an APD is denoted by

$$\sigma^2_{total_{APD}} = \sigma^2_{shot} + \sigma^2_{thermal} \tag{3.13}$$

where σ^2_{shot} of an APD is given by

$$\sigma^2_{shot} = 2q_e M i_M F(M) \Delta f \tag{3.14}$$

where q_e is the electron charge, M is the multiplication gain of the APD, i_M is the average value of total multiplied output current, $F(M)$ is the excess noise factor of the photodiode, and Δf is the system bandwidth. The multiplication gain of an APD, M, is a statistical process and defines the ratio between the multiplied output photocurrent, i_M, and the primary un-multiplied photocurrent, i_S [125]. $F(M)$ of an APD increases the statistical noise caused by the multiplication process. In other words, $F(M)$ is a multiplier indicating the increase in noise if all the photo-carriers of an APD are multiplied by M. Δf is the system bandwidth, which is typically selected as the data rate of the FSOC system.

Thermal noise, $\sigma^2_{thermal}$, of an APD is given by

$$\sigma^2_{thermal} = \frac{4kT\Delta f}{R_{load}} \tag{3.15}$$

where k is Boltzmann constant, T is the absolute temperature, and R_{load} is the load resistance of the trans-impedance amplifier.

The SNR, which is the ratio of the average signal power over the average noise power, at the receiver is given by [75]:

$$SNR = \frac{(SP_{rx_{fog,watt}})^2}{\sigma^2_{total_{APD}}} \tag{3.16}$$

where S is the photodiode sensitivity, in A/W, and $P_{rx_{fog,watt}}$ and $\sigma^2_{total_{APD}}$ are calculated as in equations (3.11) and (3.13), respectively. We adopt OOK -non-return-to-zero (OOK-NRZ) as modulation scheme [40, 69]. The BER of an FSOC system that uses an OOK-NRZ modulation is calculated by

$$BER = Q(\sqrt{SNR}) \tag{3.17}$$

where Q function is given by [76, 66]:

$$Q(x) = \frac{1}{\sqrt{2\pi}} \int_x^\infty e^{-u^2/2} du \tag{3.18}$$

3.1.4 Beam Divergence Adjusting Mechanisms

In this section, we introduce some beam divergence adjusting mechanisms to obtain a desired beam divergence for the proposed adaptive beam. A beam expander is an optical device that accepts a collimated beam as the input and expands the diameter of the beam as the beam leaves the expander [70]. A beam expander may also reduce the beam width if the expander is used in the reverse configuration. Note that the collimated beam diameter is proportional to the divergence angle of a beam. Therefore, a beam expander may alter the beam divergence of an input beam by changing its diameter. A simple beam expander, which is also referred to as a Keplerian telescope, consists of two lenses with different diameters and focal lengths. The magnification ratio of a Keplerian beam expander is equal to the ratio of the focal lengths of the employed lenses. For instance, the magnification ratio of a beam

expander with two lenses having the focal lengths of f_1 and f_2, respectively, is equal to $\frac{f_2}{f_1}$. Another implementation of beam expansion can be realized by using a Galilean telescope that also uses two lenses, one with positive and the other with negative focal length.

A motorized beam expander, which usually incorporates groups of moving lenses, adjusts the diameter and hence, the divergence angle of the output beam within its magnification range [23, 25]. Therefore, by using a motorized beam expander the divergence of a beam may be adjusted dynamically. Another method to adjust the beam divergence is to use a 1xN optical switch with one input and N output ports [70]. The input port of the optical switch is connected to a laser diode or a fiber optic cable that generates the input beam. Each output port of the optical switch is connected to a beam expander with a different magnification ratio. The desired divergence angle of the output beam is obtained by the selection of a specific output port that is connected to the beam expander. The motorized-beam-expander approach yields a continuously-variable divergence angle for the output beam. On the other hand, the approach that uses a 1xN optical switch may allow adjustment of the divergence angle of the output beam discretely because one beam expander with a fixed magnification ratio can be selected at a time by forwarding the inbound optical beam to only one output port of the optical switch. A third method to adjust the divergence angle of a beam is a combination of the first two approaches, where a 1xN optical switch with N motorized beam expanders connected to the switch's output ports is employed. This beam-divergence adjustment method is the most flexible one in terms of the magnification ratio owing to the various magnification ranges of the motorized beam expanders connected to the switch. A beam-divergence adjustment method that uses a motorized beam expander, however, may induce a delay called the expansion change time/delay, which is the time required to move the lenses of a beam expander to create the desired output beam. Some commercial beam expanders have expansion change

Table 3.1 Evaluation Parameters for Adaptive-Divergence Beam

Parameter	**Symbol**	**Value**	**Unit**
Wavelength	λ	1550	nm
Transmission power	P_{tx}	10	mW
Photodiode sensitivity	S	0.9	A/W
Electronic charge	q_e	$1.602\text{x}10^{-19}$	C
Boltzmann constant	k	$1.38\text{x}10^{-23}$	J/K
Absolute temperature	T	298	K
Multiplication gain of the APD	M	10	-
Excess noise factor	$f(M)$	3.2	-
System bandwidth	Δf	10^9	Hz
Resistance of the amplifier	R_{load}	50	Ohm
Surface area of the transmitter	S_{rx}	9	cm^2
Surface area of the receiver	S_{rx}	95	cm^2
System losses	L_{sys}	0.5	-

times of 5 seconds to adjust the output beam's divergence angle from the maximum to the minimum divergence angle of the beam expander [23]. Therefore, we prefer to use a 1xN optical switch with N beam expanders that have a fixed magnification ratio to avoid the expansion change delay in this chapter.

3.2 Results and Discussion

In this section, we provide the numerical analysis performed in MATLAB®, where the adaptive and fixed divergence angle approaches are compared in terms of the received power, communication distance, SNR, and BER. Table 3.1 shows the parameters used in the numerical analysis.

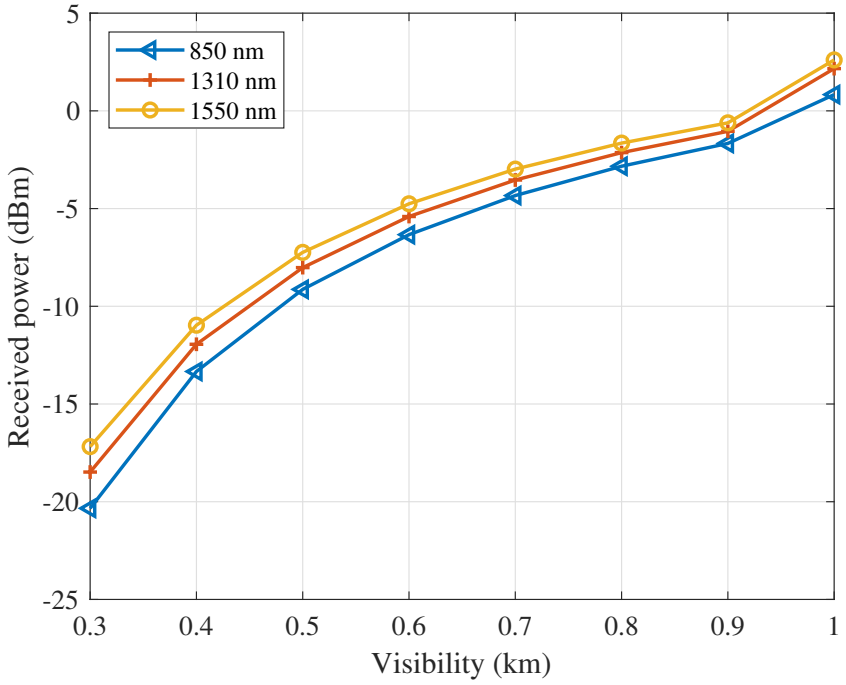

Figure 3.4 Impact of the wavelength on the received power as visibility varies.

We use a laser diode transmitting at the wavelength of 1550 nm as the light source. 1550 nm is a well-studied wavelength for FSOC with the following advantages: 1) The atmospheric attenuation of that wavelength range is low. 2) High quality transmitter and detector components that use 1550-nm wavelength are available in the market and they are capable of transmitting high power (i.e., more than 500 mW) and high data rates (i.e., more than 2.5 Gbps). 3) Lasers that use a wavelength of 1550 nm can transmit 50 to 65 times the transmission power of the lasers transmitting at 780 to 850 nm for the same eye safety classification [40, 85]. Figure 3.4 compares the impact of the transmission wavelength on the received power for the three most-common wavelengths, 850, 1310, and 1550 nm in FSOC. In Figure 3.4 the transmission power and the communication distance are 10 dBm and 500 m, respectively. The 1550-nm light (line with circular marks) yields the highest received power values among the represented wavelengths for the visibilities ranging from 0.3 to 1 km. These results support our wavelength selection for the proposed FSOC system.

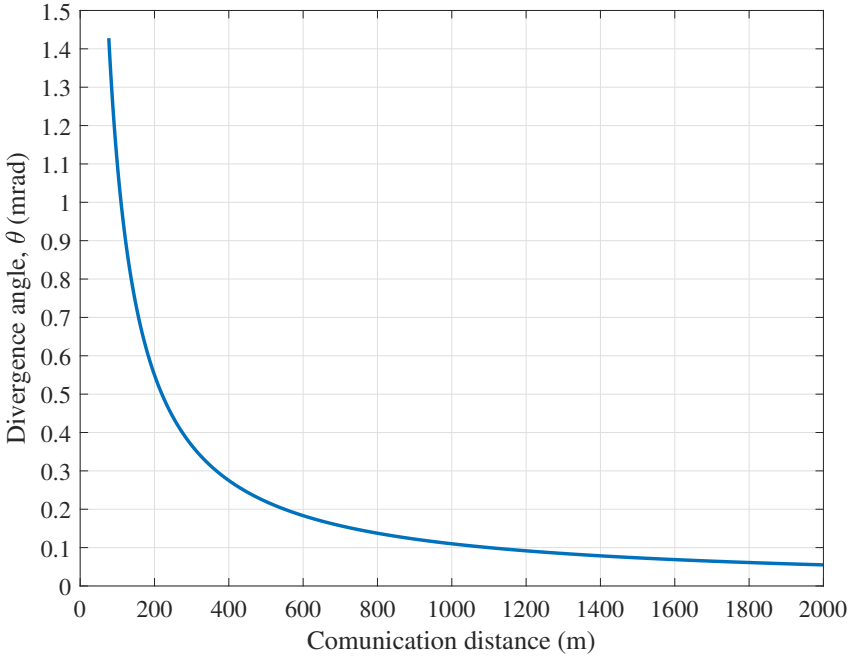

Figure 3.5 Divergence angle of the proposed adaptive beam as a function of the communication distance between a transceiver on the train and a base station.

The transmission power of the light source used in the evaluations is selected as 10 mW to make the light source eye safe. Specifically, a laser transmitting at 1550 nm with a transmission power of 10 mW is considered as a Class 1 laser, which is eye safe in an exposure of for up to 100 seconds [52]. The sensitivity, multiplication gain, and the excess noise factor of the selected photodiode, given in Table 3.1, are typical values for high-speed APDs [105]. The resistance of the load resistor of the trans-impedance circuit is selected as 50 Ω, which is suitable for high rate FSO links. The transmitter and receiver telescopes with the surface areas of 9 and 95 cm^2, respectively, are also available in the market [21]. We combine L_{tx}, L_{rx}, η_{tx}, and η_{rx} to derive the system loss, denoted by L_{sys} in Table 3.1. $L_{sys} = 0.5$ is used in the evaluations [56].

Figure 3.5 shows the divergence angle variation of the proposed adaptive beam for different communication distances between a transceiver on the train and a base station. The adaptive beam in this figure adapts its divergence angle to keep the beam

width equal to the diameter of the receiver aperture for each communication distance. Specifically, having a beam width equal to the diameter of the receiver aperture makes the alignment between the communicating terminals more effective than using a fixed-divergence-angle beam of 1 mrad. Because the fixed-divergence-angle beam creates a beam width smaller than the receiver aperture diameter for a communication distance of up to110 m, the adaptive beam is preferred for such a communication distance. Moreover, the width of the fixed beam becomes larger than the receiver aperture diameter as the communication distance goes beyond 110 m. Having a larger beam width than the receiver aperture diameter increases the geometric loss, which results in a decrease of the received power. The adaptive beam, on the other hand, reduces the geometric loss by constantly adapting the beam divergence and the beam width as the communication distance varies. Therefore, an adaptive beam is more effective than a fixed-divergence-angle beam in an FSOC system for HSTs. Such beam attains a higher received power for communications distances over 110 m for this specific scenario than a fixed-divergence-angle beam.

We use 75 m as the shortest communication distance between a train transceiver and a base station in our evaluations because L_{geo} becomes greater than 1.0 for a smaller distance, whereas its range should be in [0, 1] for a fixed divergence beam having a divergence angle of 1 mrad. Moreover, we use 2,000 m as the longest communication distance in our evaluations as δ for the fixed divergence beam becomes negative for larger distances.

We aim to provide an error-free optical link with a data rate of 1 Gbps between a high-speed train traveling at 400 km/h and the base stations along the track. Therefore, we target a BER equal to or smaller than 10^{-9} in our evaluations. Figure 3.6 shows the BER of an intensity-modulation/direct-detection (IM/DD) FSO link for different values of SNR according to equations (3.17) and (3.18). Figure 3.6 indicates that there is a non-linear relationship between the SNR and BER. Moreover, Figure

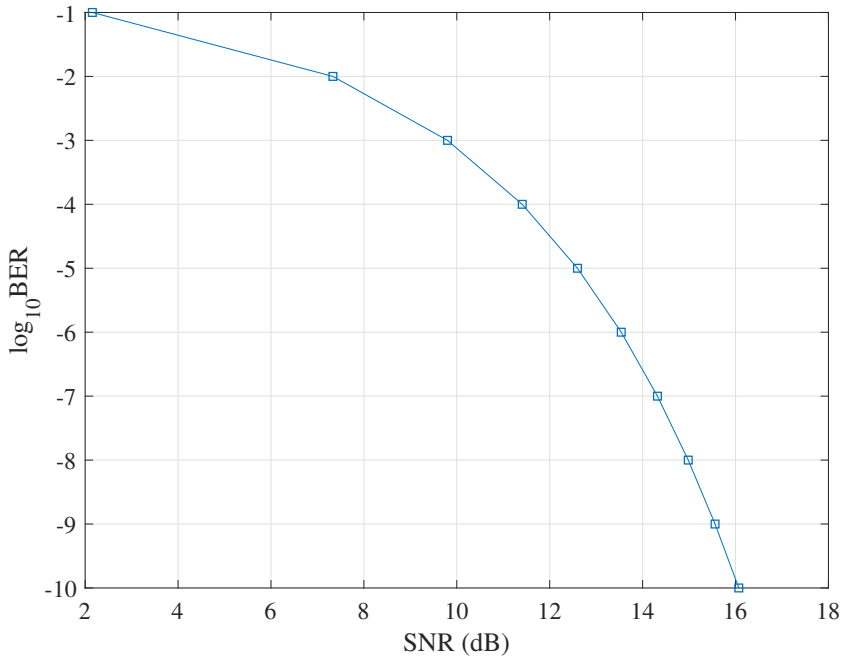

Figure 3.6 BER as a function of SNR.

3.6 reveals that a BER of 10^{-9} can be guaranteed if the SNR is greater than or equal to 15.56 dB. Therefore, we adopt such SNR as the reference value to calculate the required received power that satisfies our BER by using equations (3.11) and (3.13).

Figure 3.7 shows the SNR of an FSOC system, according to equation (3.16), for different received power values. The variance of the total noise used to calculate equation (3.16) follows equations (3.13), (3.14), and (3.15), and the parameters given in Table 3.1. The solid blue line in Figure 3.7 indicates the received power values and the corresponding SNR that provide a BER of 10^{-9} or lower. As the received power exceeds -21.94 dBm, the corresponsing SNR becomes greater than 15.56 dB, which yields a BER of up to 10^{-9}, as denoted by the solid blue line in Figure 3.7. Therefore, a received power of -21.94 dBm is used as the minimum required received power when the maximum communication distances of adaptive- and fixed-divergence beams are calculated and presented in Figure 3.8. This figure compares the maximum communication distances of adaptive and fixed divergence beams that

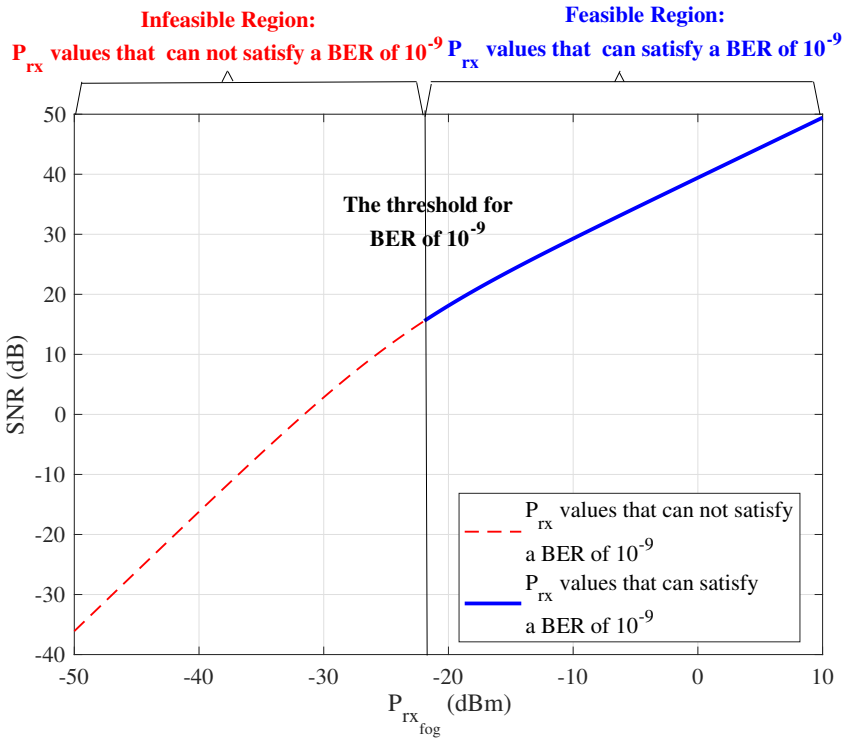

Figure 3.7 SNR as a function of the received power by a direct detection receiver with an APD. The variance of the noise is calculated according to equations (3.13), (3.14), and (3.15). The visibility is 500 m, or the presence of moderate fog.

satisfy a minimum BER of 10^{-9} as the visibility varies. The use of adaptive divergence angle extends the communication distance of an FSOC system about three times when compared to the use of a fixed divergence angle.

Figure 3.9 shows the impact of meteorological visibility and the communication distance on the received power, in dBm. In this figure, the power loss is a function of visibility and is calculated by following equations (3.9) and (3.10). The adaptive divergence beam yields higher received power than the fixed divergence beam. Moreover, the received power gap between the adaptive and fixed divergence beams increases as the communication distance increases. For instance, the adaptive divergence beam in this figure yields 33 dB higher received power for a visibility of 1 km than the fixed divergence beam.

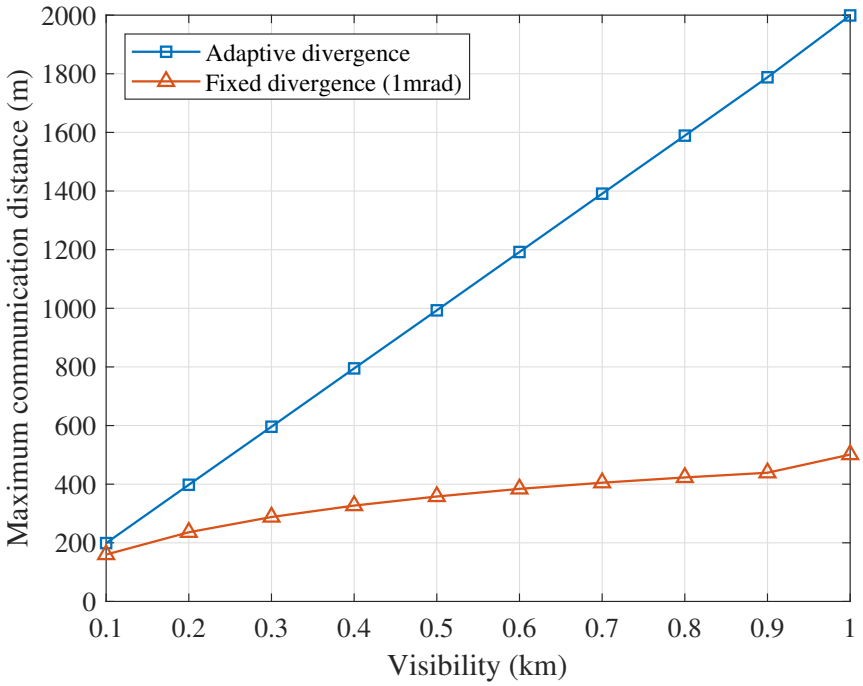

Figure 3.8 Maximum communication distance for adaptive and fixed divergence angle approaches for different visibilities. A received power of -21.94 dBm is used as the minimum required received power to satisfy a minimum BER of 10^{-9}.

Figure 3.10 shows a comparison of received power of the adaptive and fixed divergence beams for a visibility of 1 km. It is assumed that divergence adjustment for the adaptive beam is performed by a motorized beam expander that has an expansion change time of 5 seconds. Note that the expansion change time induces a delay on the divergence adjustment that may create a beam divergence difference between the expected and the actual divergence angles of the transmitted beam at time t. The location of the train is periodically sent to the source base station to have the divergence angle of the transmitted beam adjusted by the base station. The exact location of an HST can be detected by track circuits, such as Eurobalises that use the magnetic transponding technology [51]. The location information can then be disseminated to all base stations by using various communications technologies, such as global system for mobile communications in railway (GSM-R), universal

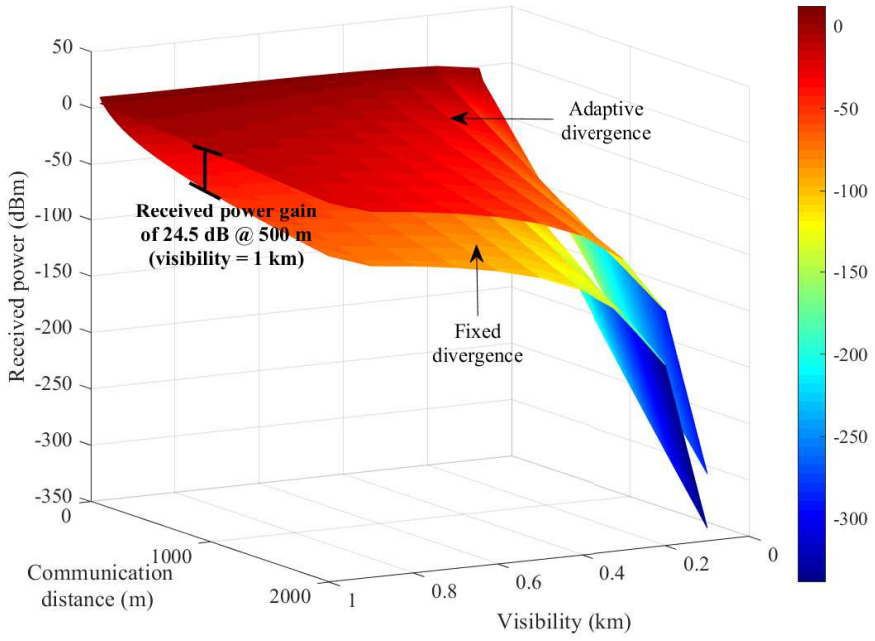

Figure 3.9 Comparison of the received power for fixed and adaptive divergence beams as a function of the communication distance and visibility.

mobile telecommunications system (UMTS), or satellite [65]. Assuming that the train's location is sent to a source base station at time t, the time that the control message carrying the train's location reaches the source base station is $t+t_{trans}+t_{prop}$, where t_{trans} and t_{prop} are the transmission and propagation delays for the control message, respectively. As the control message is received by the source base station at time $t + t_{trans} + t_{prop}$, the communication distance between the train and the base station is calculated based on the location information in the control message. The divergence angle of the transmitted beam is then adjusted according to the calculated communication distance between the train and the base station, and the diameter of the receiver aperture. The time it takes to adjust the divergence angle of the adaptive beam at the base station is t_{adjust}. Therefore, the new beam divergence angle for the transmitting beam becomes available at time $t + t_{trans} + t_{prop} + t_{adjust}$. Because of the small size of the control message (i.e., tens of bytes) and the short communication

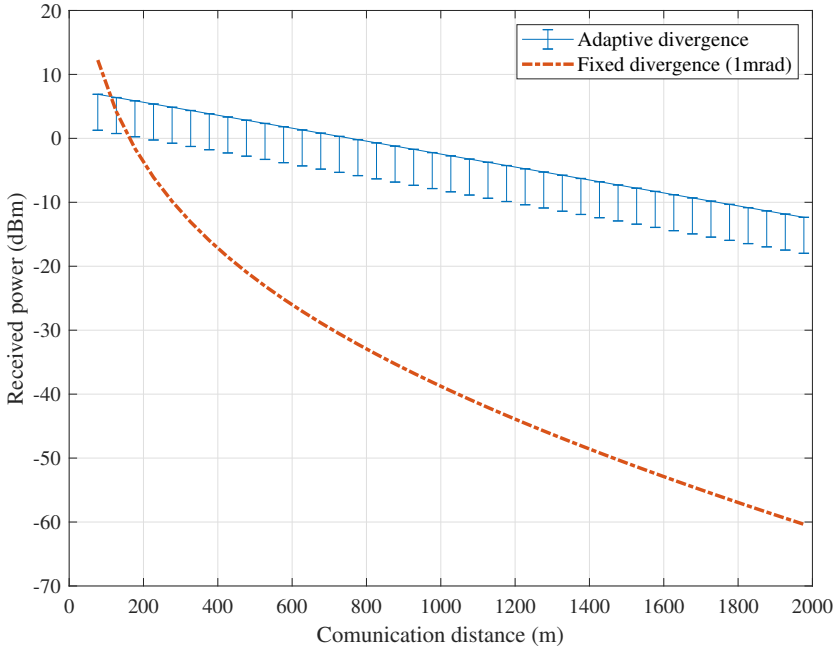

Figure 3.10 Comparison of the received power between the adaptive and fixed divergence angle approaches when a motorized beam expander is used.

distances (i.e., hundreds of meters) between the train and base station, $t_{trans} + t_{prop}$ may be considered negligible. The major contributor to the total beam adjustment delay is t_{adjust}, which is equal to 5 seconds in this calculation [23, 25]. Therefore, the beam adjustment is completed at $t + 5$ after the train's location is sent by an Eurobalise at time t. The received-power error bars for the adaptive beam in Figure 3.10 show the error induced by the total beam adjustment delay by a motorized beam expander. Note that the beam adjustment delay may be eliminated by using an 1xN optical switch, in which each output port is connected to a fixed-magnification beam expander.

Figure 3.11 shows the BER of the adaptive and fixed divergence beams as a function of the communication distance for visibility values of 0.5 and 1 km. The fixed divergence beam can guarantee a BER of 10^{-9} up to 190 and 224 m for visibility values of 0.5 and 1 km, respectively. The BER of an FSOC system that uses a

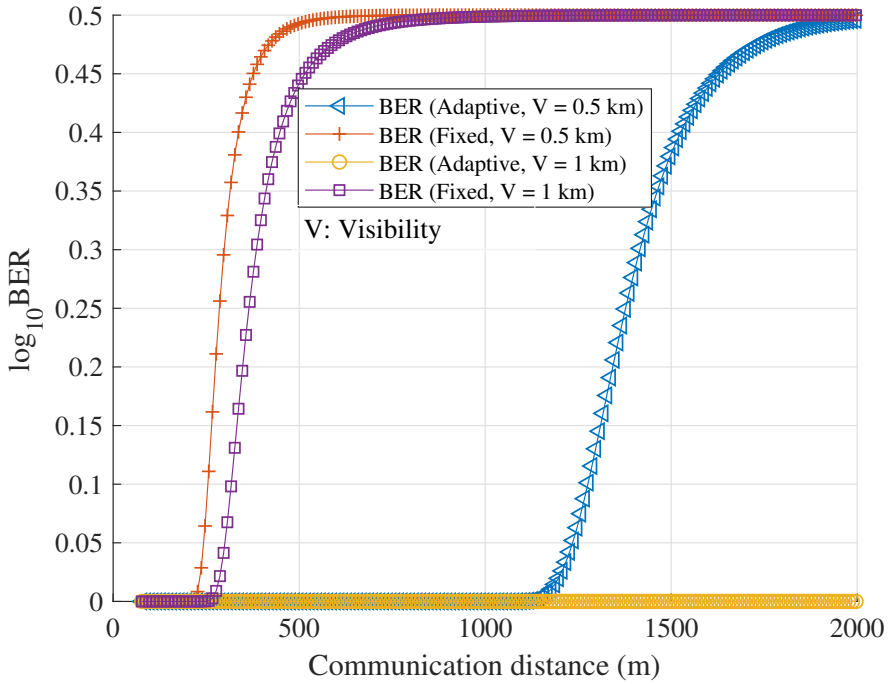

Figure 3.11 BER of adaptive and fixed divergence beams as a function of the communication distance for visibility values of 0.5 and 1 km.

fixed-divergence beam quickly increases and converges to 0.5 as the communication distances become longer than 190 and 224 m for visibility values of 0.5 and 1 km , respectively. The adaptive divergence beam, on the other hand, extends the communication distances up to 994 and 2,000 m while guaranteing a BER of 10^{-9} for the visibilities of 0.5 and 1 km, respectively. Note that the adaptive beam yields a BER smaller than or equal to 10^{-9} for distances longer than 2,000 m for a visibility of 1 km. Because of the limitations on δ for the fixed divergence beam, the results in Figure 3.11 do not show communication distances longer than 2,000 m.

3.3 Chapter Summary

An adaptive beam that adapts its divergence angle according to the receiver aperture diameter and the communication distance is proposed to improve the received power, SNR, and BER as compared to a fixed-divergence beam in an FSOC system for HSTs.

The results showed that the proposed adaptive beam outperforms a fixed-divergence beam that uses a divergence angle of 1 mrad by an average received-power difference of approximately 33 dB. Moreover, the adaptive beam approach increases the maximum communication distance of an FSOC system for HSTs with an average of 742 m over a fixed-beam approach while guaranteeing a BER of 10^{-9} for different visibility values ranging from 0.1 to 1 km. It is also proposed a new placement of ground transceivers above the track (above the train passage) of an FSOC system for HSTs; for an optimum alignment with the train movement. The proposed transceiver placement decreases the lateral distance between the transceiver on the train and a base station, which increases the received power of 3.8 dB in average over the base station layout that places the base stations next to track.

In the next chapter, we expand the application of mobile FSOC systems from HSTs to vehicles including cars. We tackle the LOS problem inherent to FSOC systems by proposing a novel diffused-light non-line-of-sight FSOC system that establishes high-speed optical links, one for downlink, one for uplink, between a pair of optical terminals with no LOS.

CHAPTER 4

DIFFUSED-LIGHT NON-LINE-OF-SIGHT FREE-SPACE OPTICAL COMMUNICATIONS FOR VEHICULAR NETWORKING

In this chapter, we tackle the LOS problem inherent to FSOC by proposing a novel approach that establishes high-speed optical links, one for downlink, one for uplink, between a pair of optical stations with no LOS in between. The proposed DL-NLOS-FSOC system consists of a transmitter, a receiver, and diffuse reflector (DR) that uniformly diffuses the incident light toward all directions except towards the DR, allowing the receiver to detect the diffusely reflected light regardless of the angle of view. Figure 4.1 shows an illustration of the proposed DL-NLOS-FSOC providing full-duplex optical communications between a ground station and a car. In Figure 4.1, DRs 1 and 2 are used for car-to-ground (i.e., uplink) and ground-to-car (i.e., downlink) communications. Here, an indirect path between a transmitter-receiver pair is established by selecting the closest DR within LOS by transmitter and receiver.

Our proposed communications system simplifies the complexity of an adopted ATP mechanism and can be used to establish full-duplex communications links. The transmitter of the DL-NLOS-FSOC system uses a laser diode (LD) that emits a narrow laser beam (i.e., with a divergence angle smaller than or equal to 1 mrad) as the light source. The transmitted laser beam is pointed towards a DR, creating a projection of the signal. The receiver points its aperture towards the DR to receive the diffusely reflected light. A high-speed optical link between the transmitter and receiver is then established. The DRs used in this proposal do not have any electric nor mechanical parts and they are made of inert materials, such as Teflon, ceramic, or even paint. DRs are not only inexpensive but easy to deploy. They may be easily attached to buildings, bridges, towers, walls of the tunnels, traffic signs, or traffic or street lights. They may be even carried by drones to form an infrastructure for the

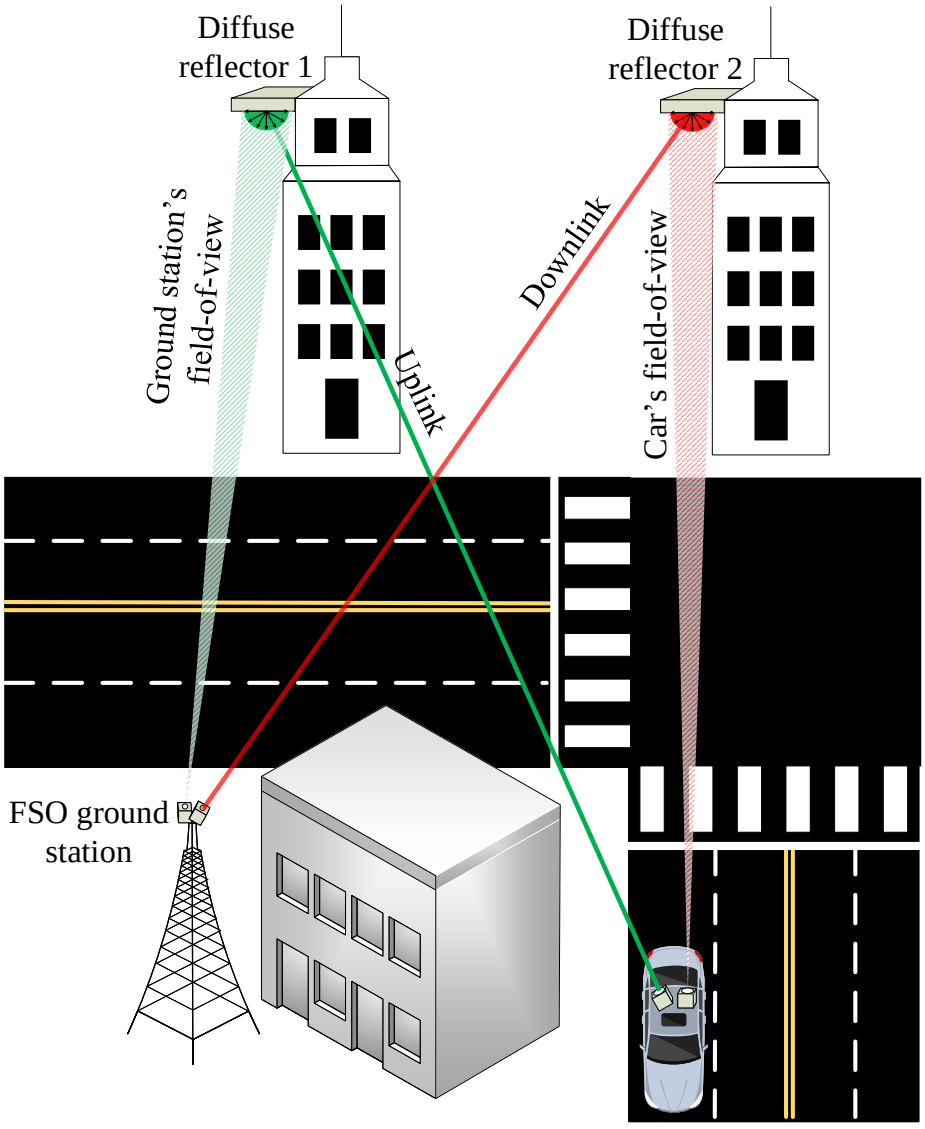

Figure 4.1 Full-duplex DL-NLOS-FSOC between a ground station and a car.

proposed DL-NLOS-FSOC system. Therefore, our proposed communications system may be easily used in urban or suburban areas. In the transmission of the beam, the geometric loss of the proposed communications system is minimum because the laser beam is narrow and collimated, and this feature considerably extends the distance between the transmitter and the DR. However, this is not the case for the receiver as diffused light beams have less intensity and larger divergence angles than direct light (i.e., light transmitted between transmitter and receiver with LOS), yet they remain coherent. We analyze the receiving power at a receiver in the proposed system and its bit-error rate (BER) to demonstrate feasibility of the proposed DL-NLOS-FSOC system.

Several indoor wireless data communications systems that use diffuse infrared radiation are proposed [59, 132, 75]. The first indoor wireless data communications system that uses diffuse infrared radiation interconnects a cluster of data stations placed in the same room [59]. A transmitter (i.e., satellite) with multiple LED-arrays facing different directions is placed on the floor of a room and diffusely scatters infrared radiation to be received by the data stations located in the same room. The transmitted beams are scattered from the surrounding walls, ceiling, and other objects in the room, thus filling the entire room with the optical signal carrier. This communications system does not require a direct LOS between the transmitter and receiver. The transmission wavelength and the average transmission power of the transmitter is 950 nm and 100 mW, respectively. Multiple transmitters (i.e., one transmitter per room) are interconnected by wire and controlled by a cluster controller to create a multi-room in-house network. Multipath signal dispersion limits the maximum data rate of this communications system to 260 Mbps because the transmitted optical signal may reach the receiver by following different optical paths which may differ in length and propagation time. Our D-NLOS-FSOC system differs from this indoor infrared data communications system as we propose an

outdoor D-NLOS-FSOC system that does not suffer from multipath signal dispersion because of the single optical path followed by the transmitted beam. Moreover, our D-NLOS-FSOC system uses a laser diode as the light source that allows us to emit a narrow beam [79], which minimizes the geometric loss between a transmitter and DR.

Another indoor wireless communications system is proposed to use a plaster wall (or ceiling) as an indoor DR to diffuse the projection of a transmitted beam on the wall. A receiver is faced towards a diffusing spot, which is nothing but a particular area of the plaster wall where the beam is projected on, to receive the reflected optical radiation [132]. Unlike a diffuse infrared radiation configuration where a wide-angle diverging beam is employed to illuminate the whole wall or ceiling, a narrow beam is employed to limit the geometric loss between the transmitter and the diffusing surface in this communications system. An optical-disc-drive laser that transmits a beam at a wavelength of 780 nm with an average transmission power of 0.8 mW is used as the light source. A fly-eye receiver design equipped with multiple lenses and corresponding photodiodes facing different directions is proposed to allow an one-to-many (i.e., multicast) communication pattern between a transmitter and multiple receivers. A diffusing spot enables the proposed one-to-many communications pattern by using a plaster wall with a reflectance of 0.718 to diffuse and reflect the projected spot on a wall to almost all directions. Therefore, any fly-eye receiver can receive the diffused beam if one of the receiver lenses faces towards a diffusing spot. These indoor wireless communications systems deviate from our work as we employ perfect Lambertian DRs, with a reflectance of 1 located at well-known locations to construct an outdoor D-NLOS-FSOC infrastructure for vehicular networking.

Several FSOC systems using a ultraviolet (UV) transmission-wavelength are proposed to collect scattered light of a transmitted beam as the photons of the beam collide with the particles in the atmosphere to establish a NLOS FSO link between a

transmitter-receiver pair [67, 54, 96]. In these UV-FSOC systems, the optical course of the transmitted beam and the FOV of the receiver intersect to allow the receiver to collect the scattered light . Note that the wavelengths (i.e., 10 to 400 nm) used in the UV-band of the spectrum are smaller than the wavelengths (i.e., $>$ 700 nm to 1 mm) used in the infrared-band of the electromagnetic spectrum. Therefore, the particle sizes creating particle scattering for the FSOC systems using a wavelegnth in the UV-band are smaller than the FSOC systems that use a wavelength in the infrared band. Moreover, an under-water NLOS FSOC system uses the wavy surface of the ocean to back-reflect a transmitted beam to establish a NLOS FSOC link between a transmitter and receiver that are both placed on the ocean floor [39]. This under-water FSOC system deviates from our work as the propagating light behaves differently under water and through the atmosphere.

The remainder of the chapter is organized as follows. Section 4.1 presents our system model. Section 4.2 presents the numerical results of our DL-NLOS-FSOC system and discusses associated technical details. Section 4.3 summarizes the chapter.

4.1 System Model

In this section, first, we briefly provide some background information about diffuse reflection. Then, we introduce our system model and provide the power budget calculations of the proposed DL-NLOS-FSOC system.

4.1.1 Diffuse Reflection

A diffuse reflection is the reflection of light or other waves or particles from a surface such that a ray incident on the surface is scattered at many angles rather than at just one angle, as in the case of specular reflection [64]. The ideal diffusely-reflecting surface is known as a perfect Lambertian surface [74]. A perfect Lambertian surface is a surface that reflects all the incident light toward all angles, absorbing none. The incident light on a perfect Lambertian surface is uniformly distributed over

a hemisphere and the intensity of the reflected light is the same regardless of the observer's angle of view [91]. Note that many commercial DRs with near-perfect Lambertian reflectance characteristics are available in the market [22, 28, 24]. Therefore, without loss of generality, we assume that the employed DR in the proposed DL-NLOS-FSOC system is a perfect Lambertian; with a reflectance of 1.

4.1.2 Geometric Model

Figure 4.2 shows our geometric system model based on a perfect Lambertian DR. This DR uniformly diffuses and reflects the incident laser light emitted by the laser diode (LD) of the transmitter to all directions in a hemisphere. The receiver projects the projection of the receiver's photodiode on the diffusing surface, which overlaps with the projection of the transmitted beam to establish an optical link. The notation used in Figure 4.2 is defined as follows: d_T is the distance from the LD to the collimating lens at the transmitter. D_T is the transmitter-DR distance. θ_T is the incident angle of the transmitted beam to the normal of the DR. D_R is the DR-receiver distance. d_R is the distance between the focusing lens and the photodiode at the receiver. θ_R is the reflectance angle of the receiver to the normal of the DR. Although they are not marked in Figure 4.2, f_T and f_R are the focal lengths of the transmitting and receiving lenses, respectively. Table 4.1 lists the geometric notation used throughout this chapter.

d_T is selected to be equal to f_T to minimize the geometric loss of the transmitted beam. d_R is selected to be equal to f_R for the sake of simplicity. However, d_R may vary and differ from f_R to control the radius of the receiver's projection on the diffusing surface. d_R may be adjusted according to the surface area of the DR and the receiver-DR distance. The adaptive control of the surface area of the receiver's projection on the DR is discussed in Section 4.2.

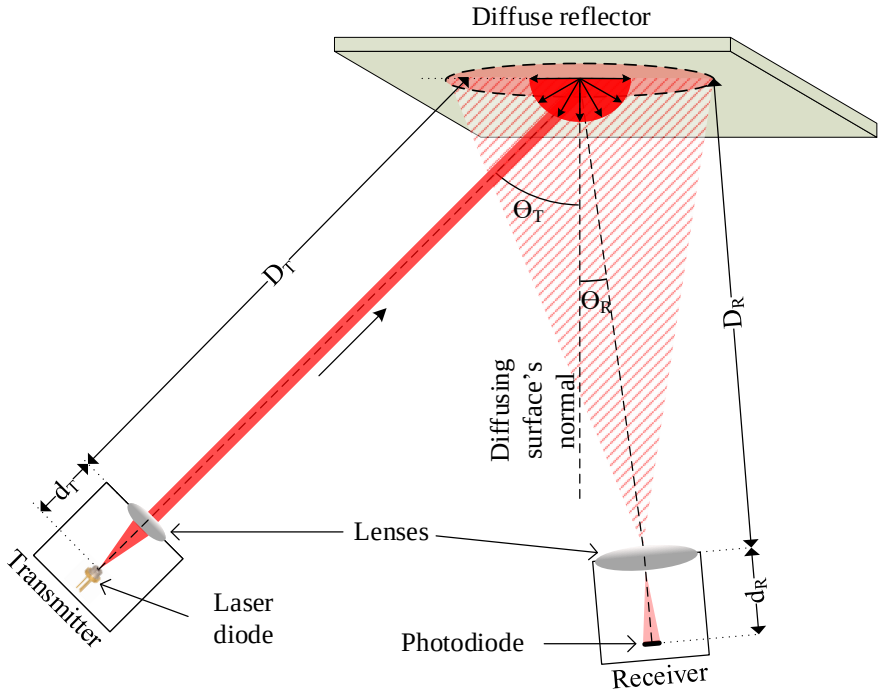

Figure 4.2 Geometric model of the DL-NLOS-FSOC system using a perfect Lambertian DR.

Table 4.1 Geometric Notation for DL-NLOS-FSOC System

Notation	**Definition**
D_T	Transmitter-diffuser distance
D_R	Diffuser-receiver distance
d_T	Transmitter-transmitting lens distance
d_R	Receiving lens-photodiode distance
θ_T	Incident angle
θ_R	Reflectance angle
A_{LD}	Surface area of the laser diode
A_{PD}	Surface area of the photodiode
A_T	Aperture area of the transmitting lens
A_R	Aperture area of the receiving lens
S_T	Surface area of the projected beam
S_R	Surface area of the projected FOV of the photodiode
f_T	The focal length of the transmitting lens
f_R	The focal length of the receiving lens

LDs are preferably used as light sources because of their higher modulation bandwidth, greater electrical/optical (E/O) conversion efficiency, smaller emitting surface area, and lower geometric loss than LEDs or other light sources [43]. The baseband modulation bandwidth of LEDs is limited to tens of kHz to tens of MHz, whereas LDs can be modulated at tens of GHz. The higher modulation bandwidth of LDs allows LDs to provide high-speed transmission data rates (i.e., $\geq$ 1 Gbps) if they are used as the light source of an FSOC system. E/O conversion rates of LEDs are in the range of 10-20%, whereas the E/O conversion rates of LDs are in the range of 30-70% [43]. The higher E/O conversion rates of LDs make LDs better candidates than LEDs for FSOC. Moreover, LEDs suffer from a rapid decline in quantum efficiency, a phenomenon called *droop*, as the operating currents increase [86]. An LD is considered as a perfect point-light source with a smaller emitting surface area than an LED. Therefore, the emitting surface area of an LED can not be neglected, whereas an LD may be considered as a geometric point on the diffusing surface, with an emitting surface area almost equal to zero [132]. The geometric loss of a laser beam is much smaller than that of a beam emitted by an LED for the same communication distance [132]. Because of the mentioned reasons, we decide to use an LD as the light source in our proposed DL-NLOS-FSOC system.

4.1.3 Calculation of Received Optical Radiation

The minimum area of a projected spot, which is emitted by a light source with non-negligible surface area, on a diffusing surface may be achieved if d_T equals to f_T. This minimum spot size is approximated as follows [132]:

$$S_T \approx \frac{D_T \ A_{LD}}{f_T \ cos\,\theta_T} \tag{4.1}$$

where A_{LD} is the surface area of the employed LD. In a case where an LD is used as the light source, the spot size of the laser beam on the diffusing surface may be as small as the diffraction limit of the laser, which makes the surface area of the laser beam's projection negligibly small.

The surface area of the projection of the receiver's photodiode on a surface can be similarly calculated as [132]:

$$S_R = \frac{D_R \; A_{PD}}{f_R \; cos\,\theta_R} \tag{4.2}$$

where A_{PD} is the surface area of the employed photodiode. The maximum received power can be achieved if $S_R \geq S_T$, and S_T completely overlaps with S_R. The received power is calculated by integrating the reflected light over the intersection of the surface areas of the projected laser beam and the projection of the receiver on a perfect Lambertian DR as [132]:

$$P_{rx} = \int_{S_T \cap S_R} \frac{P_{tx} \; R \; A_R \; cos\,\theta_R}{\pi \; S_T \; D_R^2} d\sigma \tag{4.3}$$

where P_{tx} is the total transmission power of the projected laser beam, A_R is the aperture area of the receiving lens, R is the reflectance of the DR and $d\sigma$ is the position of the intersected area of $S_T \cap S_R$ on the diffusing surface.

P_{rx} is calculated over the intersected area of $S_T \cap S_R$, equation (4.3) and simplified by taking $D_R^2 \gg A_R$ and $S_R \geq S_T$ into account as [132]:

$$P_{rx} = \frac{P_{tx} \; R \; A_R \; cos\,\theta_R}{\pi \; D_R^2} \tag{4.4}$$

4.1.4 SNR and BER Calculations

In the proposed DL-NLOS-FSOC system, the transmitted optical radiation is received by a direct detection receiver. We employ a direct detection receiver because of its

simplicity and common use in FSOC [69]. A direct-detection receiver in the proposed communications system consists of a collimating lens that collects and focuses the incident light, an optical filter to filter out the undesirable background radiations such as direct, reflected, or scattered sunlight, a photodiode that performs O/E signal conversion, an amplifier to amplify the converted electrical signal, and a symbol detector to recover the received data. We adopt a Mercury Cadmium Telluride (HgCdTe) avalanche photodiode (APD) that has a built-in low-noise transimpedance amplifier [129, 120, 119]. The reasons we choose an HgCdTe APD in our proposed communications system are as follows: 1) Photon-counting-level ultra-high sensitivity of HgCdTe APDs at 1550 nm allows to capture the optical radiation carrying tens of photons. 2) Internal amplification (i.e., avalanche) process of the optical receivers using APDs provides higher SNRs over the PIN photodiodes for the same incident optical power [78].

The mentioned components of a direct detection receiver may induce some noise that degrades SNR at the receiver. The total noise of a direct-detection receiver may be the aggregation of the photo-current shot (i.e, quantum noise), thermal (i.e., Johnson noise), dark current, and the background illumination noises [75, 125]. The shot noise, which is also known as the quantum noise in optical communications, originates from the random occurrence of photon absorption events in a photodetector [100]. The number of photons of the incident light fluctuates by following a Poisson distribution at the receiver causes the shot noise. The thermal noise, also called Johnson or Nyquist noise, is the electronic noise induced by the thermal agitation of the electrons passing through an electrical conductor [125]. The dark current is the current that flows through the bias circuit of a photodiode even without the incident light [125]. The dark current noise is the result of thermally generating electrons and/or holes by the p-n junction of the photodiode. The background noise is the result of the undesirable background radiation collected by the photodetector, which

may arise from the presence of intense and visible background light, such as sunlight and artificial lights [75, 100].

The average received power is typically larger than the signal current, which makes the dark current noise negligible in practice [125]. We employ a bandpass filter, centered at 1550 nm, to eliminate the solar-radiation-induced background noise [27, 77]. Bandpass filters are used to transmit a well-defined wavelength band of light, while rejecting other unwanted radiation [27]. Moreover, it is worth noting that solar-radiation-induced background noise is more likely to be effective at smaller wavelengths (e.g., 850 nm) than at the wavelength used in our proposed communications system [124]. In addition to the employed bandpass filter, a narrow FOV receiver that satisfies $S_R \geq S_T$ may further reduce the impact of the solar-radiation-induced noise at the receiver. Moreover, proper housing of a receiver, such as the ones used for commercial FSOC transceivers [2], may also reduce the solar background radiation by creating some shadowing at the aperture of the receiver. Therefore, we neglect the background radiation, which makes the receiver shot and/or thermal noise limited.

The shot noise is a more dominant factor than the thermal noise for a photon-counting direct-detection receiver [44]. This means that the variance of the shot noise is greater than the variance of the thermal noise, and that makes our proposed DL-NLOS-FSOC system shot-noise limited.

The sensitivity of a shot-noise limited receiver, which is the minimum required optical power to keep the BER below a given value, is estimated by [30] :

$$P_{min} = N_p \, h \, v \, B \tag{4.5}$$

where N_p is the average number of photons contained in a single bit, h is Planck's constant, v is the frequency of a photon, and B is the data rate of the FSOC system [30]. hv is also referred to as the energy of a photon at a given wavelength.

The relation between the SNR and the number of photons incident to the photodiode is given by [30]:

$$SNR = \eta\, N_p \tag{4.6}$$

where η is the quantum efficiency of the photodiode, given by [26]:

$$\eta = 1240\, \frac{S}{\lambda} \tag{4.7}$$

where S is the receiver responsivity and λ is the wavelength of the laser diode in use.

We consider the widely adopted OOK-NRZ as the modulation scheme [40, 69]. The BER of an FSOC system that uses an OOK-NRZ modulation is calculated by

$$BER = erfc(\sqrt{SNR/2}) \tag{4.8}$$

where *erfc* is the complementary error function given as [76, 66]:

$$erfc(z) = \frac{2}{\sqrt{\pi}} \int_z^\infty e^{-t^2}\, dt \tag{4.9}$$

4.1.5 Full-Duplex FSOC

Each party (e.g., car, ground station, or any optical station) in the proposed DL-NLOS-FSOC system is equipped with a transmitter and a receiver that can be independently pointed to any direction by using light-weight gimbals. A full-duplex FSOC between two communicating stations, $station\, i$ and $station\, i+1$, can be established by using two different DRs, DR 1 and 2, to establish one downlink and

one uplink, as shown in Figure 4.1. In this configuration, the transmitter of *station* i and the receiver of *station* $i+1$ point toward the DR 2 to establish a downlink from *station* i to *station* $i+1$. At the same time, the transmitter of the *station* $i+1$ and the receiver of *station* i point toward the DR 1 to establish an uplink from *station* $i+1$ to *station* i. Another possible configuration to achieve a full-duplex FSOC between a pair of communication stations is to project the laser beams of the stations onto the same DR with a spatial diversity between them. Figure 4.3 shows a full-duplex FSO link between a pair of communication stations, *station* i and *station* $i+1$. In this figure, two spatially diverse laser beams emitted by *station* i and *station* $i+1$ are projected on a DR to create two non-overlapping beam footprints. These beam footprints are then received by the intended receivers as the laser beam footprints are within the FOV of the corresponding receivers. Note that if two communicating stations employ different wavelengths (e.g., 1310 and 1550 nm, respectively) the laser beams of the communicating stations may be follow the same optical path and overlap on the diffusing surface [56]. In this case, the transmitter and receiver of each station is combined in an enclosure to form a transceiver. The transmitted and received beams sharing the same optical path may be splitted by using beam splitters at the transceivers [126].

A coordination may be needed between a transmitter-receiver pair to select a common DR for communication. The global positioning system (GPS) coordinates of both the transmitter and receiver may be used to select the closest DR for given coordinates of all DRs scattered around the transmitter and receiver at any time. If both transmitter and its intended receiver select the same DR at the same time, an optical link may be established.

In a ground-to-mobile communications scenario, we assume that there is at least one DR illuminated by the closest ground station. A receiver intended to communicate with its corresponding transmitter may face toward the closest DR

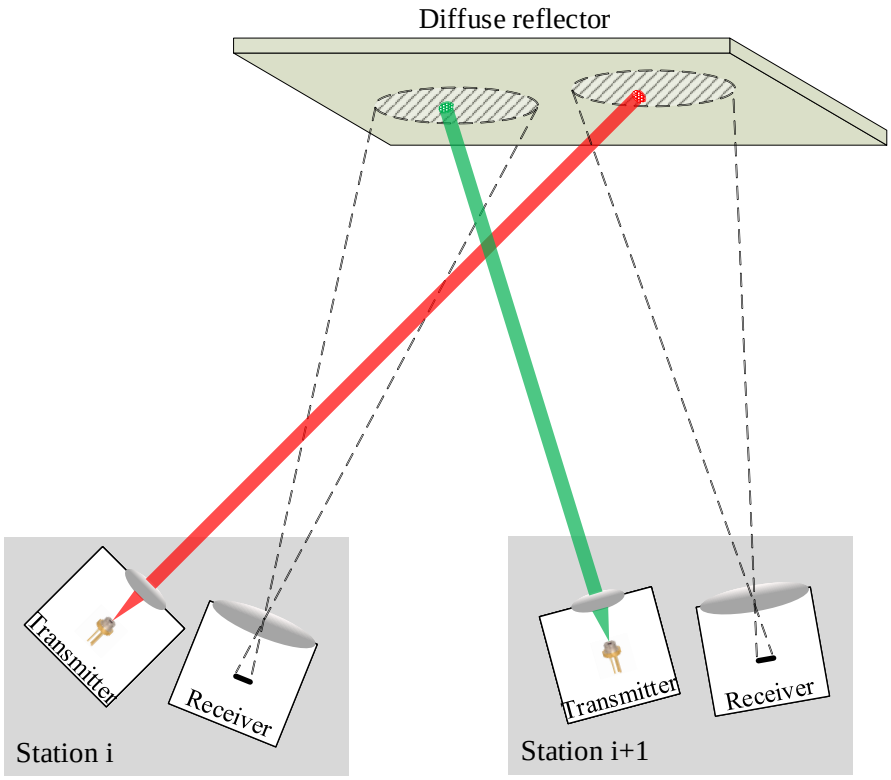

Figure 4.3 A pair of communicating FSO stations share a DR to establish a full-duplex DL-NLOS-FSOC.

to establish an optical link. The receiver that projects its projection onto a DR may find the DR occupied by an unintended transmitter. In this case, the receiver checks the destination medium access control (MAC) address of the data packets carried by the projected light on the diffusing surface and steers towards the next closest DR if the data packets are not intended for it. This process may continue until the receiver finds the right DR with the projection of its intended transmitter.

4.2 Results and Discussion

In this section, we provide the numerical analysis of the receiver power as a function of the distance between a DR and a vehicular/mobile station, which is performed in MATLAB®. Moreover, we discuss the adaptive control of the projection area of the receiver on a diffusing surface, the handover procedure for mobile receivers, and portable DRs.

We evaluate two ground-to-vehicle communication scenarios, comprising a stationary transmitter (i.e., a ground station) transmits and a mobile receiver (i.e., a car) receives. The car moves perpendicularly (i.e., 90 degrees) or longitudinally (i.e., along the plane of the DR) away from the DR, as Figure 4.4(a) shows. In the perpendicular-displacement scenario, the communication DR-receiver distance increases whereas the reflectance angle, θ_R, does not change as the receiver moves away from the DR. In the longitudinal-displacement scenario θ_R increases as the DR-receiver distance increases.

In the proposed DL-NLOS-FSOC system, we aim to provide a BER of 10^{-9} between a pair of communicating stations to achieve 1 Gbps. A BER of 10^{-9} is guaranteed with an SNR greater than or equal to 15.56 dB, according to equations (4.8) and (4.9). The number of photons per bit required to satisfy this SNR is calculated as greater than or equal to 57 for a receiver responsivity and quantum efficiency of 0.8 and 0.64 A/W, respectively, according to equations (4.6) and (4.7).

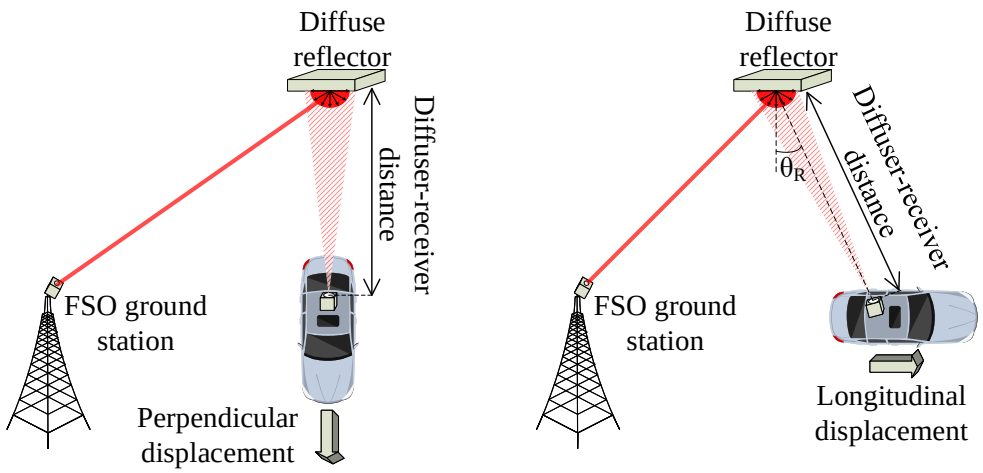

(a) Perpendicular displacement (b) Longitudinal displacement

Figure 4.4 Perpendicular and longitudinal displacements of a moving car.

The minimum required received power to satisfy a BER of 10^{-9} is -51.36 dBm, according to equation (4.5). Table 4.2 shows the parameters used in the evaluations.

The adopted laser diode in out proposal transmits a wavelength of 1550 nm. This is a well-studied wavelength for FSOC with the following advantages: 1) It falls in one of the atmospheric windows where the atmospheric attenuation is low.
2) High quality transmitter and detector components that use a 1550-nm wavelength are available in the market and they are capable of transmitting high power (i.e., more than 500 mW) and high data rates (i.e., more than 2.5 Gbps). 3) Lasers that use a wavelength of 1550 nm can transmit 50 to 65 times the transmission power of the lasers transmitting at 780 to 850 nm for the same eye safety classification [40, 85]. 4) Solar spectral irradiance at the wavelength of 1550 nm is lower than the other frequencies that are commonly used in FSOC systems, such as 850 and 1310 nm [124]. Therefore, FSOC systems that use 1550 nm as the transmission wavelength are less affected by the sun light as compared to other FSOC systems that use lower

Table 4.2 Evaluation Parameters for DL-NLOS-FSOC System

Parameter	**Symbol**	**Value**	**Unit**
Wavelength	λ	1550	nm
Transmission power	P_{tx}	[50, 200]	mW
Photodiode responsivity	S	0.8	A/W
Quantum efficiency	η	0.64	A/W
Energy of a photon at 1550 nm	hv	0.79989	eV
Data rate	B	1	Gbps
Reflectance	R	1	-
Surface area of the laser diode	A_{LD}	negligible	cm^2
Surface area of the photodiode	A_{PD}	5e-6	cm^2
Projected spot size of the transmitter	S_T	negligible	cm^2
Projection area of the receiver	S_R	variable	cm^2
Aperture area of the transmitting lens	A_T	10	cm^2
Aperture area of the receiving lens	A_R	95	cm^2

wavelengths than 1550 nm. 5) Sensitive HgCdTe APDs are available for 1550-nm wavelength [120, 89, 119].

4.2.1 Impact of the Communication Distance on the Received Power, SNR, and BER

Figure 4.5 shows the received power of the proposed DL-NLOS-FSOC system for a receiver moving perpendicularly away from a perfect Lambertian DR. The transmission power ranges from 50 to 200 mW, with a step size of 50 mW. In this evaluation, the ground station (i.e., the transmitter), located 100 meters away from the DR, transmits a narrow laser beam towards the DR. Owing to the use of a narrow beam, the distance between the transmitter and the DR does not affect the received power, even when the distance becomes tens of km [79]. In our experiments, we evaluate DR-receiver distances from 1 to 300 m, with a step-size variation of 5 m. The height of the DR from the ground is 100 m. According to the results in Figure 4.5, the maximum communication distances that provide a data rate of 1 Gbps are 141, 201, 251, and 286 m for transmission power of 50, 100, 150, and 200 mW, respectively.

Similarly, Figure 4.6 shows the received power of the proposed DL-NLOS-FSOC system in a scenario where a receiver moves longitudinally away from a DR. The calculated maximum communication distances in this figure are 127, 160, 183, and 201 m for the transmission power of 50, 100, 150, and 200 mW, respectively. These results correspond to a decrease of 21.78% in the average communication distance as compared to those in the perpendicular-displacement of the vehicle. This decrease is caused by the increase in the DR-receiver distance and the increase of the reflectance angle. The results in Figures 4.5 and 4.6 reveal that the average DR-receiver distance

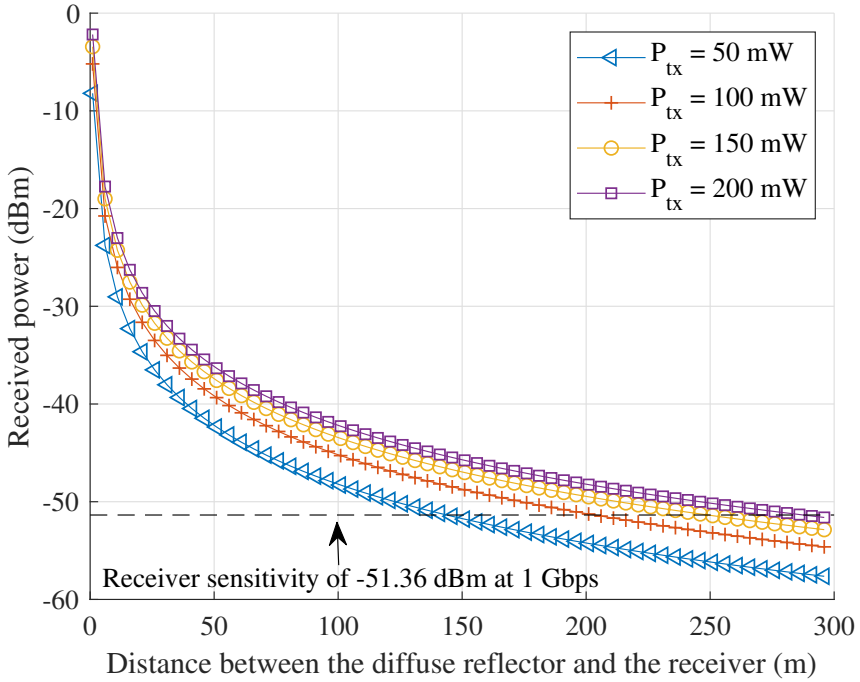

Figure 4.5 Received power as receiver car moves away from the DR under perpendicular displacements.

may be increased by around 20% if the receiving vehicle aims to receive the diffusely-reflected light from a DR with a minimum θ_R as the vehicle travels.

Figure 4.7 shows the SNR of the proposed DL-NLOS-FSOC system as the perpendicular-displacement of the vehicle varies. The transmission power ranges from 50 to 200 mW, with a step size of 50 mW. The DR-receiver distance varies from 100 to 300 m, with a step size of 5 m. We omit the corresponding results to the DR-receiver distances of 1 to 100 m to increase the readability of the results in the range of 100 to 300 m. The results in this figure reveal that the proposed communication system satisfies an SNR of 15.56 dB at the communication distances of up to 141, 201, 251, and 286 m for the transmission power of 50, 100, 150, and 200 mW, respectively. These results are consistent with the results given in Figure 4.5.

Figure 4.8 shows the SNR of the proposed DL-NLOS-FSOC system as the longitudinal-displacement of the receiver varies for the transmission power of 50 to

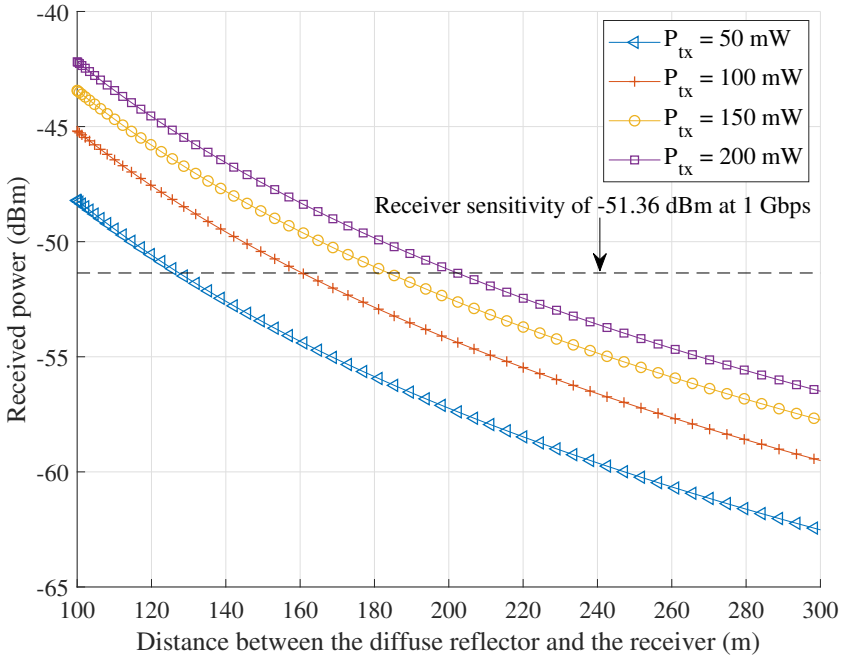

Figure 4.6 Received power as receiver car moves away from the DR under longitudinal displacements.

200 mW, with a step size of 50 mW. The DR-receiver distance varies from 100 to 300 m, with a step size of 5 m. The maximum communication distances that satisfy a minimum SNR of 15.56 are 128, 161, 184, and 203 m for 50, 100, 150, and 200 mW, respectively. The results in Figure 4.8 are also consistent with the results in 4.6.

Figures 4.9 and 4.10 show the corresponding BER of the proposed DL-NLOS-FSOC system for the perpendicular and longitudinal displacement of the receiver, respectively. The transmission power varies from 50 to 200 mW, with a step size of 50 mW. These results show that the proposed DL-NLOS-FSOC system can provide an error-free 1-Gbps optical link for a DR-receiver distance of up to 220 and 162 m in average, as the mobile receiver moves perpendicularly and longitudinally, respectively.

Figures 4.11 and 4.12 show the BER of the proposed DL-NLOS-FSOC system as the perpendicular and longitudinal DR-receiver distances changes under different transmission data rates, respectively. The transmission power is 100 mW. The results

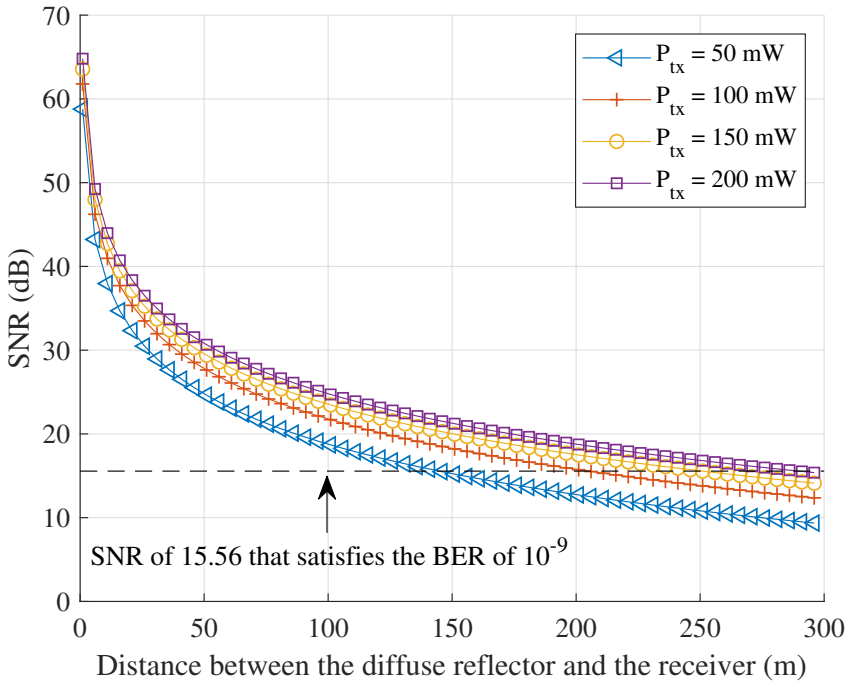

Figure 4.7 SNR as the distance between a DR and a receiver car varies when the receiver perpendicularly moves away from the DR.

in these figures show that the maximum communication distances yielding a BER of 10^{-9} are 201, 215, 289, and 374 m for perpendicular displacement and 160, 166, 202, and 240 m for longitudinal displacement as the corresponding transmission data rates are 1, 0.9, 0.5, and 0.3 Gbps, respectively. These results reveal that an adaptive data-rate scheme may be used to further increase the maximum communication distance of the proposed DL-NLOS-FSOC system by decreasing the transmission data rate as the DR-receiver distance increases.

4.2.2 Adaptive Control of the Projection Area of the Receiver on the Diffuse Reflector

The radius of the receiver's projection on the diffusing surface can be adjusted by varying the distance between the photodiode and the focusing lens at the receiver. The main goal of controlling the radius of the receiver's projection is to ensure the transmitted beam is completely within the FOV of the receiver as the distance

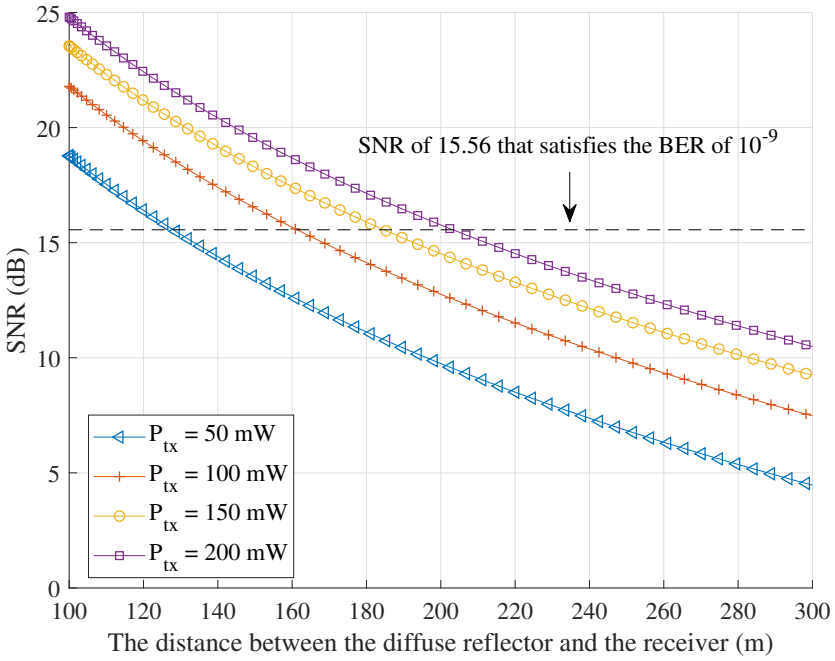

Figure 4.8 SNR as the distance between a DR and a receiver car varies when the receiver longitudinally moves away from the DR.

between the DR and the receiver varies. Note that the received power is maximized if the projections of the transmitted beam and the photodiode fully overlap. Moreover, the surface area of the receiver's projection is selected according to the surface area of the employed DR to avoid of creating a projection surface area that is larger than the surface area of the DR.

The focusing lens at the receiver follows the thin-lens equation if the projection of the photodiode is perfectly focused. The thin-lens equation is given by [63]:

$$\frac{1}{f_R} = \frac{1}{D_R} + \frac{1}{d_R} \tag{4.10}$$

The radius of the receiver's projection on a diffusing surface can be calculated by using equations (4.2) and (4.10) for given f_R and D_R. Specifically, as the distance

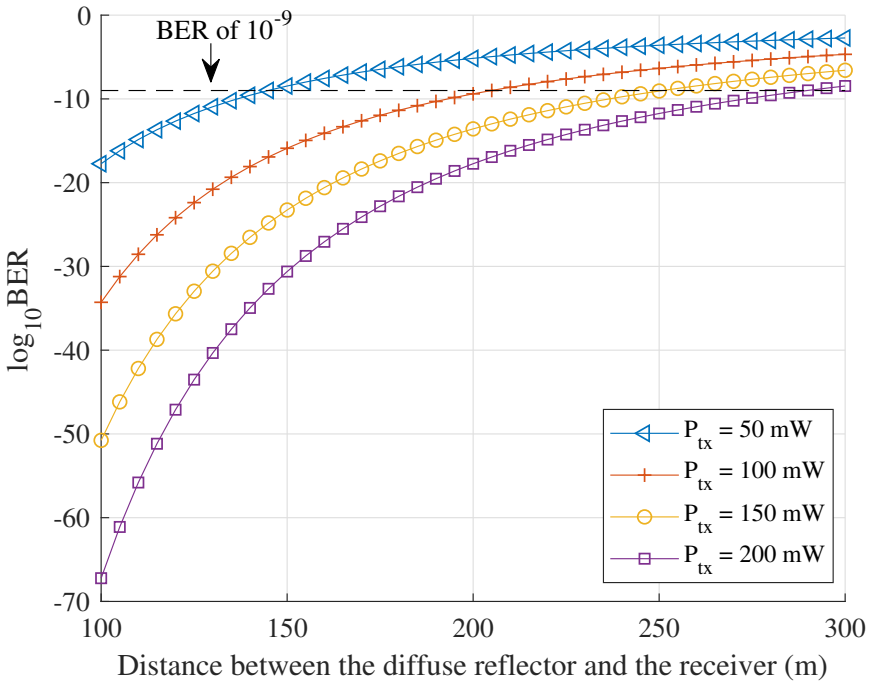

Figure 4.9 BER as the distance between a DR and a receiver car varies when the receiver perpendicularly moves away from the DR.

between the receiving lens and the photodiode decreases, the radius of the receiver's projection on the diffusing surface increases, and vice versa.

A motorized lens that uses a motor to control the distance between the focusing lens and the photodiode, such as the one used in motorized beam expanders [70], may be employed to adjust the radius of the receiver's projection according to the distance between the DR and the focusing lens. Section 3.1.4 gives more detail about the selection of beam expanders.

4.2.3 Handover

In a ground-to-mobile FSOC scenario, a handover mechanism may use the GPS coordinates of a transmitter and mobile receiver to select the best possible DR(s) to project and receive the transmitted beam as the receiver travels. Figure 4.13 shows an overview of a ground-to-mobile DL-NLOS-FSOC system just after a handover is performed as the receiver car travels from the field of regard of a source DR to

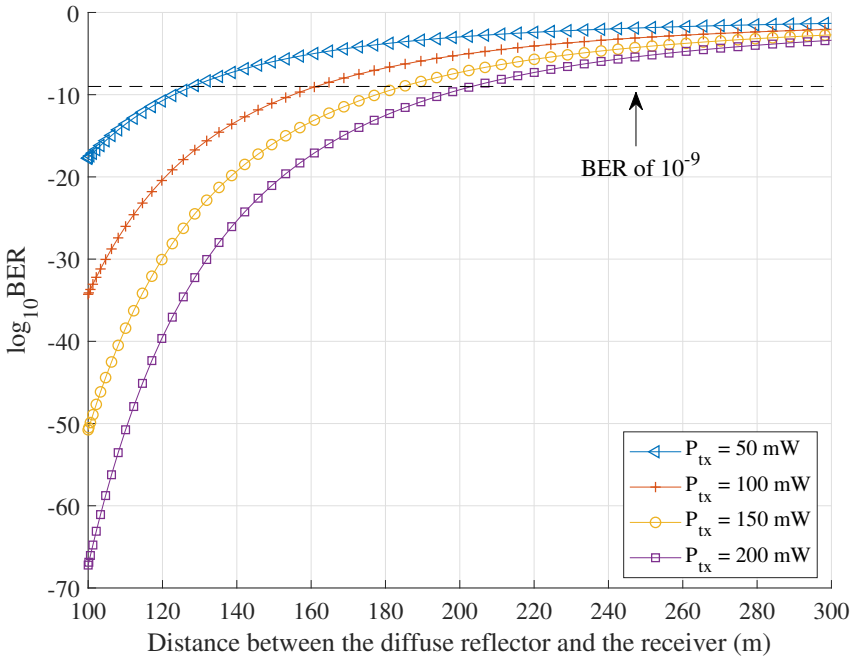

Figure 4.10 BER as the distance between a DR and a receiver car varies when the receiver longitudinally moves away from the DR.

the field of regard of a target DR, where both diffusing surfaces are illuminated by the same ground station. At the time the receiver enters the field of regard of the target DR the receiver steers and points its receiving aperture towards the target DR to perform the handover using the GSP coordinates of the source and target DRs, and itself. Any possible interruption of the data stream during a handover may be alleviated by using a data buffering technique not to experience any degradation in the quality-of-experience for interactive applications [87].

4.2.4 Portable Diffuse Reflectors

The DRs employed in the proposed DL-NLOS-FSOC system may not be attached to a stationary structure, such as a building, bridge, tower, interior wall of a tunnel, traffic sign, traffic light, or a street light. Drones may be also used to carry the DRs to be located anywhere they are needed. For instance, in case of a disaster that may

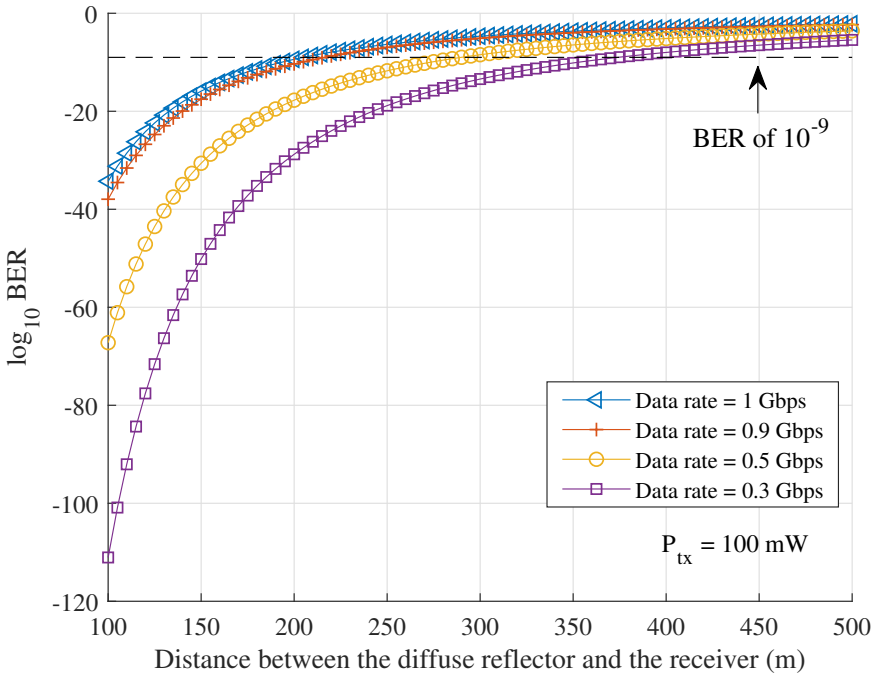

Figure 4.11 BER for different data rates as the distance between a DR and a receiver car changes under perpendicular displacement.

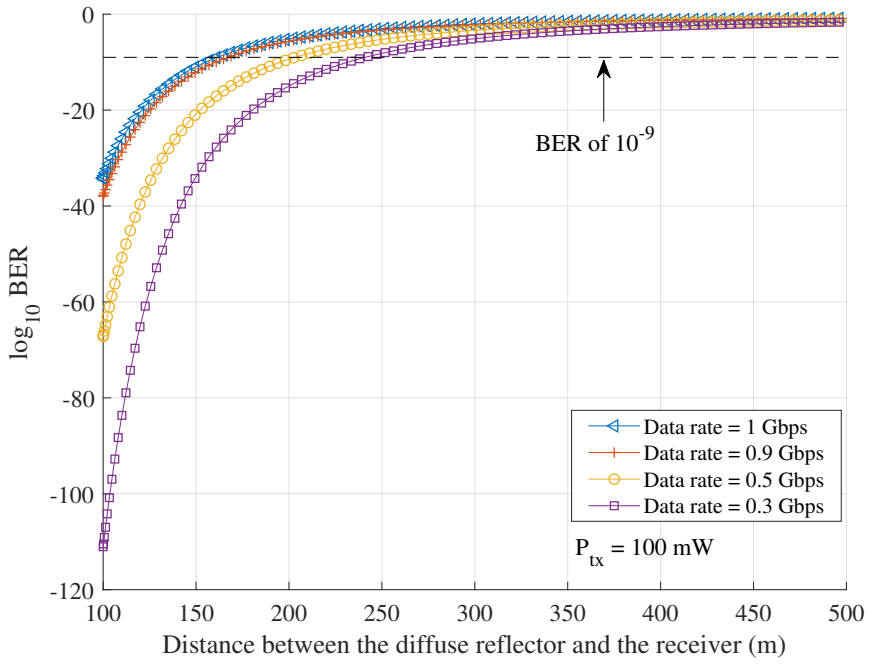

Figure 4.12 BER for different data rates as the distance between a DR and a receiver car changes under longitudinal displacement.

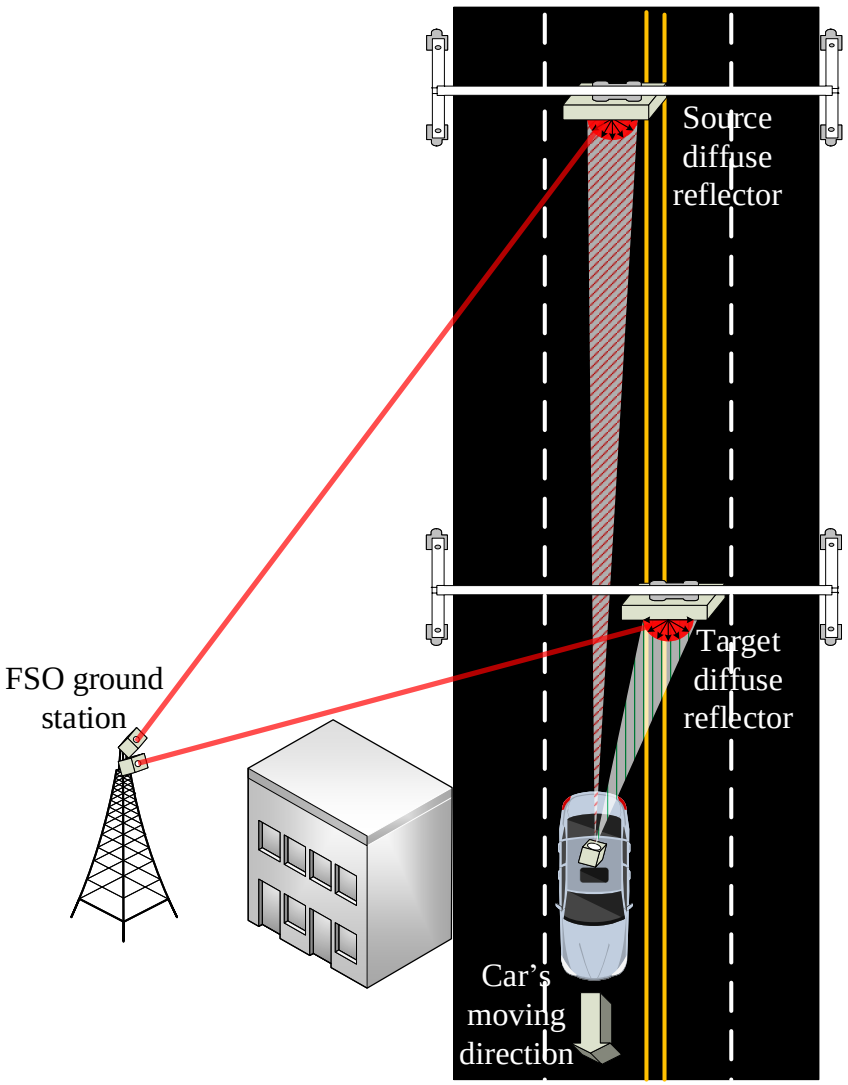

Figure 4.13 Handover being performed as the receiver car travels from the covered area of the source DR to the covered area of target DR.

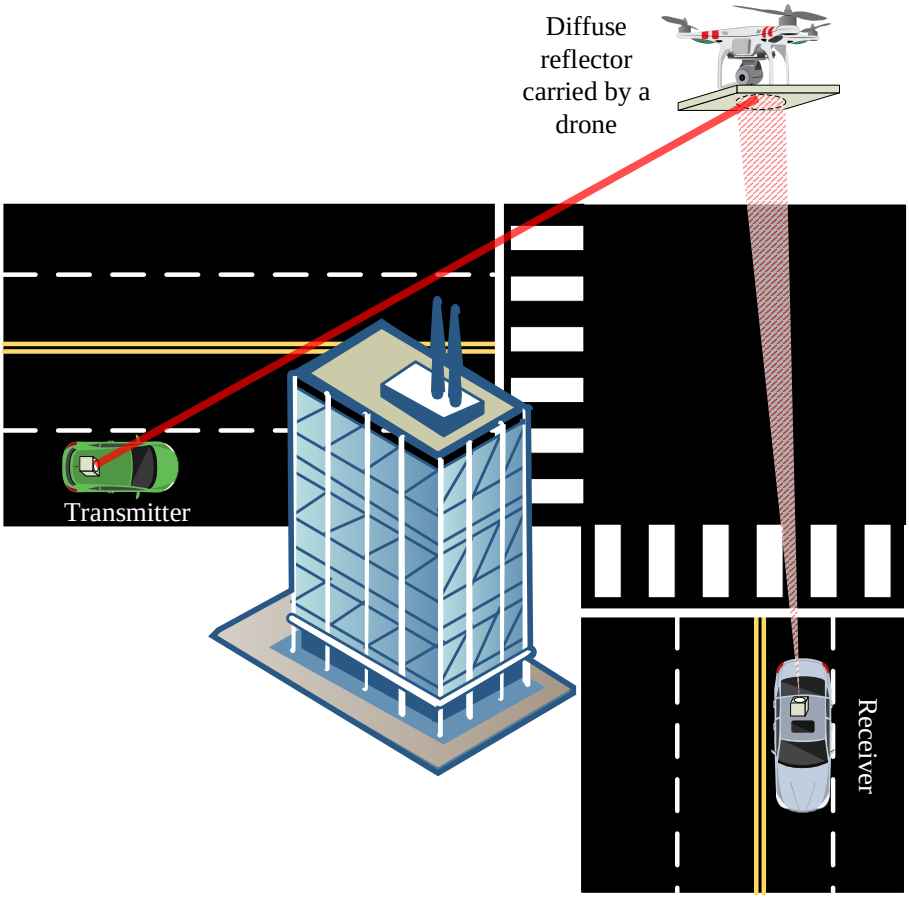

Figure 4.14 Portable DR carried by a drone in a V2V communication scenario.

destroy or damage the structures where the DRs attached to diffuse-reflector-carrying drones may be temporarily replace the damaged DR(s) to recover the interrupted communication. Moreover, a diffuse-reflector-carrying drone may track a receiver up to the maximum communication distance of the corresponding transmitter to eliminate the handover need of the receiver tracked by the drone.

4.3 Chapter Summary

In this chapter, we propose a novel DL-NLOS-FSOC system for vehicular networking. The proposed communications system uses DRs that can be attached to almost any

surface or even carried by drones to establish a high-speed (i.e., $\geq$ 1 Gbps) optical link between a transmitter and receiver without requiring LOS between a transmitter and receiver. The DRs are passive and inert materials, which simplify the design of the proposed DL-NLOS-FSOC system. A transmitter in the proposed communications system may use a narrow laser beam to minimize the geometric loss of transmitter-DR distance and considerably extend the communications range. Wide beams may also be used in special scenarios. We adopted a sensitive HgCdTe APD in our system and set a BER of 10^{-9} for an optical received power greater than or equal to -51.36 dBm. Our results show that high data rates can be achieved for a few hundred meters. For example, a 1-Gbps optical link can be achieved for a DR-to-receiver distance of 200 m and a transmitting power of 100 mW, and up to 300 m with 200 mW, including a wide covered area.

CHAPTER 5

CONCLUSIONS AND FUTURE WORK

In this dissertation, high-speed data communications systems for vehicular networks using FSOC are discussed. Three different FSOC systems that provide high-data rates ($\geq$ 1 Gbps) to vehicles are proposed to tackle the inherent different challenges in mobile FSOC.

In the first chapter, an introduction and mobility-specific challenges to FSOC were presented.

In second chapter, narrow and wide beams for FSOC in the context of ground-to-train HST communications were investigated. These beam modalities were compared, and their advantages and disadvantages were unveiled. The covered distance, steering speed, steering arc, covered area, and the impact of vibration for each angle were estimated. Considering the presented results, a divergence-angle range to enable a contact time larger than or equal to the worst-case handover time was proposed for HST communications. The impact of vibration was also examined. Our results show that the proposed range of divergence angles guarantees that the received power is larger than the receiver sensitivity threshold with the maximum vertical vibration amplitude smaller than or equal to 50 mm.

In the third chapter of the dissertation, an adaptive beam that adapts its divergence angle according to the receiver aperture diameter and the communication distance was presented. This approach improves the received power and eases the alignment between the communicating terminals as compared to a fixed-divergence beam in an FSOC system for HSTs. Our results show that the proposed adaptive beam outperforms a fixed-divergence beam that uses a divergence angle of 1 mrad by an average received-power difference of approximately 33 dB. Moreover, the adaptive

beam approach increases the maximum communication distance of an FSOC system for HSTs with an average of 742 m over a fixed-beam approach by guaranteeing a BER of $10^{-}9$ for different visibility values ranging from 0.1 to 1 km. Moreover, a new placement of ground transceivers above the track (above the train passage) is proposed that provides an optimum alignment with the train movement. The proposed transceiver placement decreases deviation of the beam between the transceiver on the train and a base station, which in turn increases the received power by 3.8 dB in average over the base station layout that places the base stations next to track.

In the fourth chapter, a novel diffused-light non-line-of-sight FSOC system for providing 1-Gbps Internet access to vehicles was proposed. The proposed communications system uses diffuse reflectors to establish a high-speed (i.e., $\geq$ 1 Gbps) optical link between a transmitter and receiver without requiring LOS between the transmitter and receiver. The DRs do not use any electric nor mechanical parts, which simplifies the design of the proposed DL-NLOS-FSOC system. Each transmitter in the proposed communications system uses a narrow laser beam that minimizes the geometric loss of transmitter-DR distance, which considerably extends the total communication range of the proposed communications system. Ultra-sensitive HgCdTe APDs adopted here sets a BER of 10^{-9} for an optical received power greater than or equal to -51.36 dBm. Our results show that a 1-Gbps optical link can be achieved with an average DR-to-receiver distance of 220 meters for varying transmit powers of 50 to 200 mW while guaranteeing such data rate.

5.1 Contributions

The contributions of this dissertation are summarized as follows:

1. It compares different beam modalities and reveals a viable range of divergence angles to realize an FSOC system for HSTs, for the first time. The revealed range of divergence angles mitigates the impairing effect of train-induced vibration while guaranteeing high data rates (i.e., $\geq$ 1 Gbps) for an HST. The

divergence angles in the proposed range meet the theoretical maximum steering speed of an FSM, and lowers the complexity of an FSOC system.

2. It proposes an adaptive-divergence beam in an FSOC system for HSTs, which improves the received power, signal-to-noise ratio, and the bit error rate as compared to a

   fixed-divergence beam. The proposed adaptive-divergence approach adapts the beam divergence angle of the transmitted beam to achieve a footprint of the diameter of the receiver aperture and minimize the geometric loss of the optical link for a given communication distance between a transmitter-receiver pair.

3. It proposes a new ground station placement in an FSOC system for HSTs to place the ground stations right above the passage of an HST to achieve an efficient alignment between the ground stations and the mobile FSO stations on the train. This new placement improve the received power by decreasing the lateral distance between the train and the ground transceivers, and makes the ground transceivers parallel to the track.

4. It proposes a novel outdoor DL-NLOS-FSOC system that does not require a direct LOS between the communicating parties for vehicular networks. The proposed communications system allows the receivers to receive a transmitted beam regardless of the angle of view, which eliminates the fine alignment requirement in mobile FSOC systems.

5.2 Future Work

1. Decreasing the handover time for vehicular networks or eliminating it completely with the support of cloud computing.

2. Developing a drone-based mobile FSOC system with adaptive data-rate for varying weather conditions to optimize the received power, communication distance, SNR, and BER.

BIBLIOGRAPHY

[1] Active optics / fast tip-tilt piezo steering mirrors, PI Motion Positioning. [Online]. Available: https://goo.gl/350XQj. Last Access Date: 9/19/2018.

[2] AIRE X-STREAM FSO (ultra low latency laser bridge), LightPointe Inc. [Online]. Available: http://goo.gl/WEQe7L. Last Access Date: 9/19/2018.

[3] Airebridge LX hybrid laser-radio, LightPointe Inc. [Online]. Available: https://goo.gl/i7RX8m. Last Access Date: 9/19/2018.

[4] Compound semiconductor photosensors, Hamamatsu Corp. [Online]. Available: https://goo.gl/w65E3q. Last Access Date: 9/19/2018.

[5] Fast Steering Mirror and Controller/Driver (FSM-300 Series), Newport Corp. [Online]. Available: https://goo.gl/MmVjHX. Last Access Date: 9/19/2018.

[6] Fast Steering Mirrors (FSM) overview, Applied Technology Associates (ATA). [Online]. Available: https://goo.gl/8Su2F7. Last Access Date: 9/19/2018.

[7] Fiber media converters, Perle Inc. [Online]. Available: https://goo.gl/EcKWvq. Last Access Date: 9/19/2018.

[8] Fiber optic network optical wavelength transmission bands, The Fiber Optic Association. [Online]. Available: https://goo.gl/MK1m32. Last Access Date: 9/19/2018.

[9] Fiber-to-fiber media converter overview, Omnitron Systems. [Online]. Available: https://goo.gl/05AfQR. Last Access Date: 9/19/2018.

[10] Fundamentals of power and energy measurement, CVI Melles Griot. [Online]. Available: https://goo.gl/EDCDms. Last Access Date: 9/19/2018.

[11] InGaAs photodiodes with preamp, ROSA type, G12072-54, Hamamatsu Corp. [Online]. Available: https://goo.gl/fXWr2q. Last Access Date: 9/19/2018.

[12] Large area Si PIN photodiodes, S3204/S3584 series, Hamamatsu Corp. [Online]. Available: https://goo.gl/Tg7UIo. Last Access Date: 9/19/2018.

[13] Optical and IC selector guide, Semtech. [Online]. Available: https://goo.gl/TMiiAW. Last Access Date: 9/19/2018.

[14] Optical components, Finisar Corp. [Online]. Available: https://goo.gl/MRL0jG. Last Access Date: 9/19/2018.

[15] Optical fiber communications, RP Photonics. [Online]. Available: https://goo.gl/ACvTZi. Last Access Date: 9/19/2018.

[16] Optiwave, Optical Communication System Design, OptiSystem. [Online]. Available: https://goo.gl/MhwjyX. Last Access Date: 9/19/2018.

[17] Si photodiodes, Hamamatsu Corp. [Online]. Available: https://goo.gl/d5cKEP. Last Access Date: 9/19/2018.

[18] Singlemode - Multimode Converter, Fiberbit Technology Co. Ltd. [Online]. Available: https://goo.gl/Kfpaz9. Last Access Date: 9/19/2018.

[19] The datasheet for S12023 series Si APD, Hamamatsu Corp. [Online]. Available: https://goo.gl/TcNF8k. Last Access Date: 9/19/2018.

[20] Moderate resolution atmospheric transmission (MODTRAN). [Online]. Available: https://goo.gl/9ZANk4, 2017. Last Access Date: 9/19/2018.

[21] Large PCX condenser lenses, Edmund Optics Inc. [Online]. Available: https://goo.gl/enCd3D, 2018. Last Access Date: 9/19/2018.

[22] Light-reflecting ceramic, Accuflect. [Online]. Available: https://accuratus.com/accuflprods.html, 2018. Last Access Date: 11/7/2018.

[23] Motorized tunable beam expanders (MOTEX), Altechna Inc. [Online]. Available: https://goo.gl/qNYC6T, 2018. Last Access Date: 9/19/2018.

[24] N-BK7 diffuse reflectors, protected gold coating, Thorlabs. [Online]. Available: https://goo.gl/4ZM2w6, 2018. Last Access Date: 11/7/2018.

[25] Optics: How to build a beam expander, Newport Inc. [Online]. Available: https://goo.gl/erZbJu, 2018. Last Access Date: 9/19/2018.

[26] Photodiode characteristics and applications, OSI Optoelectronics. [Online]. Available: https://goo.gl/RGqZjq, 2018. Last Access Date: 11/7/2018.

[27] Thorlabs - NIR bandpass and laser line filters: 700 - 1650 nm center wavelength. [Online]. Available: https://goo.gl/eg3EWQ, 2018. Last Access Date: 11/7/2018.

[28] Zenith polymer reflectance standards, Sphere Optics. [Online]. Available: https://goo.gl/qGmgxy, 2018. Last Access Date: 11/7/2018.

[29] National Highway Traffic Safety Administration et al. Federal motor vehicle safety standards; V2V communications. *Federal Register*, 82(8):3854–4019, 2017.

[30] G. P. Agrawal. "Optical Communication Systems OPT428". *Institute of Optics, University of Rochester, Rochester, NY*, 2007.

[31] M. Aguado, O. Onandi, P. S. Agustin, M. Higuero, and E. J. Taquet. "WiMax on rails". *IEEE Vehicular Technology Magazine*, 3(3):47–56, Sept 2008.

[32] I. Ahmad and D. Habibi. "A novel mobile WiMAX solution for higher throughput". In *2008 16th IEEE International Conference on Networks*, pages 1–5, Dec 2008.

[33] J. Akella, C. Liu, D. Partyka, M. Yuksel, S. Kalyanaraman, and P. Dutta. "Building blocks for mobile free-space-optical networks". In *Wireless and Optical Communications Networks, 2005. WOCN 2005. Second IFIP International Conference on*, pages 164–168. IEEE, 2005.

[34] J. Alda. "Laser and gaussian beam propagation and transformation". *Encyclopedia of Optical Engineering*, 2013:999–1013, 2003.

[35] A. G. Alkholidi and K. S. Altowij. "Free space optical communications—theory and practices". In *Contemporary Issues in Wireless Communications*. INTECH Open Access Publisher, 2014.

[36] G. Karagiannisand O. Altintas, E. Ekici, G. Heijenk, B. Jarupan, K. Lin, and T. Weil. "Vehicular networking: A survey and tutorial on requirements, architectures, challenges, standards and solutions". *IEEE Communications Surveys and Tutorials*, 13(4):584–616, 2011.

[37] L. C. Andrews and R. L. Phillips. *Laser Beam Propagation Through Random Media*, volume 152. Bellingham, WA: SPIE Press, 2005.

[38] T. Arita and F. Teraoka. "Providing a high-speed train with a broadband NEMO environment: a report of a field test using a train in service". In *Proceedings of the Sixth Asian Internet Engineering Conference*, pages 64–71. ACM, 2010.

[39] S. Arnon and D. Kedar. "Non-line-of-sight underwater optical wireless communication network". *Journal of the Optical Society of America A*, 26(3):530–539, 2009.

[40] S. Bloom, E. Korevaar, J. Schuster, and H. Willebrand. "Understanding the performance of free-space optics [invited]". *Journal of Optical Networking*, 2(6):178–200, 2003.

[41] D. K. Borah, A. C. Boucouvalas, C. C. Davis, S. Hranilovic, and K. Yiannopoulos. "A review of communication-oriented optical wireless systems". *EURASIP Journal on Wireless Communications and Networking*, 2012(1):1–28, 2012.

[42] D. K. Borah and D. G. Voelz. "Pointing error effects on free-space optical communication links in the presence of atmospheric turbulence". *Journal of Lightwave Technology*, 27(18):3965–3973, 2009.

[43] O. Bouchet. *Wireless Optical Communications*. London, UK: John Wiley and Sons, 2013.

[44] A. Boudkhil and B. Soudini. "Analysis of fundamental photodetection noises and evaluation of pin and apd photodiodes performances using an optical high debit transmission chain simulated by optisystem". *International Journal of Computer Applications*, 115(18), 2015.

[45] B. Bova. *The Story of Light*. Naperville, IL: Sourcebooks, Inc., 2002.

[46] G. A. Cap, H. H. Refai, and J. J. Sluss Jr. "Optical tracking and auto-alignment transceiver system". *Aerospace and Electronic Systems Magazine, IEEE*, 25(9):26–34, 2010.

[47] T. Cevik and S. Yilmaz. "An overview of visible light communication systems,". *arXiv preprint arXiv:1512.03568*, abs/1512.03568, 2015.

[48] V. W. S. Chan. "Free-space optical communications". *Journal of Lightwave Technology*, 24(12):4750–4762, 2006.

[49] G.-Y. Huand C.-Y. Chen and Z.-Q. Chen. "Free-space optical communication using visible light". *Journal of Zhejiang University-SCIENCE A*, 8(2):186–191, 2007.

[50] J. Conti. "High speeds at high speed". *Engineering and Technology*, 4(15):69–71, 2009.

[51] S. Dhahbi, A. Abbas-Turki, S. Hayat, and A. El Moudni. "Study of the high-speed trains positioning system: European signaling system ERTMS/ETCS". In *Logistics (LOGISTIQUA), 2011 4th International Conference on*, pages 468–473. IEEE, 2011.

[52] M. Dickinson. University Laser Safety Manual (ULSM), University of Manchester. [Online]. Available: https://goo.gl/SX7AkU, 2002. Last Access Date: 9/19/2018.

[53] B. L. Edwards. "NASA's current activities in free space optical communications". In *International Conference on Space Optics*, volume 7, page 10, 2014.

[54] M. A. Elshimy and S. Hranilovic. "Non-line-of-sight single-scatter propagation model for noncoplanar geometries". *Journal of the Optical Society of America A*, 28(3):420–428, 2011.

[55] A. A. Farid and S. Hranilovic. "Outage capacity optimization for free-space optical links with pointing errors". *Journal of Lightwave Technology*, 25(7):1702–1710, 2007.

[56] S. Fathi-Kazerooni, Y. Kaymak, R. Rojas-Cessa, J. Feng, N. Ansari, M. Zhou, and T. Zhang. "Optimal positioning of ground base stations in free-space optical communications for high-speed trains". *IEEE Transactions on Intelligent Transportation Systems*, 19(6):1940–1949, June 2018.

[57] D. T. Fokum and V. S. Frost. "A survey on methods for broadband internet access on trains". *IEEE Communications Surveys and Tutorials*, 12(2):171–185, 2010.

[58] L. Gasca. "From O to L: The future of optical-wavelength bands". [Online]. Available: http://goo.gl/F8GBQq, 2008. Last Access Date: 9/19/2018.

[59] F. R. Gfeller and U. Bapst. "Wireless in-house data communication via diffuse infrared radiation". *Proceedings of the IEEE*, 67(11):1474–1486, 1979.

[60] Z. Ghassemlooy and W. O. Popoola. *Terrestrial Free-Space Optical Communications*. London, UK: INTECH Open Access Publisher, 2010.

[61] B. Glushko, D. Kin, and A. Shar. "Gigabit optical wireless communication system for personal area networking". *Optical Memory and Neural Networks*, 22(2):73–80, 2013.

[62] P. F. Goldsmith, Institute of Electrical, Electronics Engineers, Microwave Theory, and Techniques Society. *Quasioptical Systems: Gaussian Beam Quasioptical Propagation and Applications*. New York, NY: IEEE Press, 1998.

[63] J. W. Goodman. *Introduction to Fourier Optics*. New York, NY: W. H. Freeman and Company, 2017.

[64] C. M. Goral, K. E. Torrance, D. P. Greenberg, and B. Battaile. "Modeling the interaction of light between diffuse surfaces". In *ACM SIGGRAPH Computer Graphics*, volume 18, pages 213–222. ACM, 1984.

[65] J. Goya, L. Zamora-Cadenas, S. Arrizabalaga, A. Brazález, J. Meléndez, and J. Mendizabal. "Advanced train location simulator (ATLAS) for developing, testing and validating on-board railway location systems". *European Transport Research Review*, 7(3):24, 2015.

[66] I. S. Gradshteyn and L. M. Ryzhik. *Table of Integrals, Series, and Products*. Waltham, MA: Academic Press, 2014.

[67] G. Chen H. Ding, B. M. Sadler A. K. Majumdar, and Z. Xu. "Modeling of non-line-of-sight ultraviolet scattering channels for communication". *IEEE journal on selected areas in communications*, 27(9), 2009.

[68] J. He, R. A. Norwood, M. Brandt-Pearce, I. B. Djordjevic, M. Cvijetic, S. Subramaniam, R. Himmelhuber, C. Reynolds, P. Blanche, B. Lynn, et al. "A survey on recent advances in optical communications". *Computers and Electrical Engineering*, 40(1):216–240, 2014.

[69] K. Hemani and K. Georges. "Free space optical communication: Challenges and mitigation techniques". *arXiv preprint arXiv:1506.04836*, abs/1506.04836, 2015.

[70] K. H. Heng, N. Liu, Y. He, W. D. Zhong, and T. H. Cheng. "Adaptive beam divergence for inter-UAV free space optical communications". In *2008 IEEE PhotonicsGlobal@Singapore*, pages 1–4, Dec 2008.

[71] H. Henniger and O. Wilfert. "An introduction to free-space optical communications". *Radioengineering*, 19(2), 2010.

[72] T.-Z. Ho, S. Trisno, A. Desai, J. Llorca, S. D. Milner, and C. C. Davis. "Performance and analysis of reconfigurable hybrid FSO/RF wireless networks". In *Lasers and Applications in Science and Engineering*, pages 119–130. International Society for Optics and Photonics, 2005.

[73] M. Ijaz, Z. Ghassemlooy, J. Pesek, O. Fiser, H. Le Minh, and Edward E. Bentley. "Modeling of fog and smoke attenuation in free space optical communications link under controlled laboratory conditions". *Journal of Lightwave Technology*, 31(11):1720–1726, 2013.

[74] M. Janecek and W. W. Moses. "Optical reflectance measurements for commonly used reflectors". *IEEE Transactions on Nuclear Science*, 55(4):2432–2437, 2008.

[75] J. M. Kahn and J. R. Barry. "Wireless infrared communications". *Proceedings of the IEEE*, 85(2):265–298, 1997.

[76] G. K. Karagiannidis and A. S. Lioumpas. "An improved approximation for the Gaussian Q-function". *IEEE Communications Letters*, 11(8), 2007.

[77] S. V. Kartalopoulos. *Free Space Optical Networks for Ultra-Broad Band Services*. Hoboken, NJ: John Wiley and Sons, 2011.

[78] Harsimranjit Kaur and Gaurav Soni. Performance analysis of free space optical communication link using different modulation and wavelength. *Journal of Scientific Research and Reports*, 6(3):201–209, 2015.

[79] Y. Kaymak, R. Rojas-Cessa, J. Feng, N. Ansari, and M. Zhou. "On divergence-angle efficiency of a laser beam in free-space optical communications for high-speed trains". *IEEE Transactions on Vehicular Technology*, 66(9):7677–7687, Sept 2017.

[80] Y. Kaymak, R. Rojas-Cessa, J. Feng, N. Ansari, M. Zhou, and T. Zhang. "A survey on acquisition, tracking, and pointing mechanisms for mobile free-space optical communications". *IEEE Communications Surveys and Tutorials*, 20(2):1104–1123, 2018.

[81] R. H. Kern and U. Kugel. "Pointing, acquisition and tracking (PAT) subsystems and components for optical space communication systems". In *1989 Intl Congress on Optical Science and Engineering*, pages 97–107. International Society for Optics and Photonics, 1989.

[82] M. A. Khalighi and M. Uysal. "Survey on free space optical communication: A communication theory perspective". *IEEE Communications Surveys and Tutorials*, 16(4):2231–2258, 2014.

[83] M. A. Khalighi, F. Xu, Y. Jaafar, and S. Bourennane. "Double-laser differential signaling for reducing the effect of background radiation in free-space optical systems". *Journal of Optical Communications and Networking*, 3(2):145–154, 2011.

[84] D. Killinger. "Free space optics for laser communication through the air". *Optics and Photonics News*, 13(10):36–42, 2002.

[85] I. I. Kim, B. McArthur, and E. J. Korevaar. "Comparison of laser beam propagation at 785 nm and 1550 nm in fog and haze for optical wireless communications". In *Optical Wireless Communications III*, volume 4214, pages 26–38. International Society for Optics and Photonics, 2001.

[86] M.-H. Kim, M. F. Schubert, Q. Dai, J. K. Kim, E. F. Schubert, J. Piprek, and Y. Park. "Origin of efficiency droop in gan-based light-emitting diodes". *Applied Physics Letters*, 91(18):183507, 2007.

[87] R. Koodli. "Fast handovers for mobile IPv6". RFC 4068, 2005.

[88] H. Kotake, S. Haruyama, and M. Nakagawa. "A new ground-to-train communication system using free-space optics technology". *IEEJ Transactions on Industry Applications*, 128(4):523–528, 2008.

[89] M. A. Krainak, G. Yang, X. Sun, W. Lu, S. Merritt, and J. Beck. "Novel photon-counting detectors for free-space communication". In *Free-Space Laser Communication and Atmospheric Propagation XXVIII*, volume 9739, page 97390T. International Society for Optics and Photonics, 2016.

[90] P. W. Kruse, L. D. McGlauchlin, and R. B. McQuistan. *Elements of Infrared Technology: Generation, Transmission and Detection*. 1962.

[91] J. H. Lambert. *Photometria Sive de Mensura et Gradibus Luminis, Colorum et Umbrae*. Leipzig: Germany, Klett, 1760.

[92] S. G. Lambert and W. L. Casey. *Laser Communications in Space*. Norwood, MA: Artech House, 1995.

[93] X. Liu. "Free-space optics optimization models for building sway and atmospheric interference using variable wavelength". *IEEE Transactions on Communications*, 57(2):492–498, 2009.

[94] P. LoPresti, H. Refai, J. Sluss, and I. Varela-Cuadrado. "Adaptive divergence and power for improving connectivity in free-space optical mobile networks". *Applied Optics*, 45(25):6591–6597, 2006.

[95] W. Luo, R. Zhang, and X. Fang. A CoMP soft handover scheme for lte systems in high speed railway. *EURASIP Journal on Wireless Communications and Networking*, 2012(1):1–9, 2012.

[96] M. Brandt-Pearce M. Noshad and S. G. Wilson. "NLOS UV communications using M-ary spectral-amplitude-coding". *IEEE Transactions on Communications*, 61(4):1544–1553, 2013.

[97] R. N. Mahalati and J. M. Kahn. "Effect of fog on free-space optical links employing imaging receivers". *Optics Express*, 20(2):1649–1661, 2012.

[98] A. K. Majumdar. *Advanced Free Space Optics (FSO): A Systems Approach*, volume 186. New York City, NY: Springer, 2014.

[99] A. K. Majumdar and J. C. Ricklin. *Free-Space Laser Communications: Principles and Advances*, volume 2. New York, NY: Springer Science and Business Media, 2010.

[100] H. Manor and S. Arnon. "Performance of an optical wireless communication system as a function of wavelength". *Applied Optics*, 42(21):4285–4294, 2003.

[101] MATLAB. *version 8.3.0.532 (R2014a)*. The MathWorks Inc., Natick, MA, 2014.

[102] H. Le Minh, Z. Ghassemlooy, D. O'Brien, and G. Faulkner. "Indoor gigabit optical wireless communications: Challenges and possibilities". In *12th International Conference on Transparent Optical Networks*, pages 1–6, June 2010.

[103] H. Le Minh, D. O'Brien, and G. Faulkner. "A gigabit/s indoor optical wireless system for home access networks". In *Communication Systems Networks and Digital Signal Processing (CSNDSP), 2010 7th International Symposium on*, pages 532–536. IEEE, July 2010.

[104] K. Mori, M. Terada, K. Nakamura, R. Murakami, K. Kaneko, F. Teraoka, D. Yamaguchi, and S. Haruyama. "Fast handover mechanism for high data rate ground-to-train free-space optical communication system". In *Globecom Workshops (GC Wkshps), 2014*, pages 499–504. IEEE, 2014.

[105] F. Nakajima, M. Nada, and T. Yoshimatsu. "High-speed avalanche photodiode and high-sensitivity receiver optical subassembly for 100-gb/s ethernet". *Journal of Lightwave Technology*, 34(2):243–248, 2016.

[106] V. V. Nikulin, J. Sofka, and R. M. Khandekar. "Effect of the sampling rate of the tracking system on free-space laser communications". *Optical Engineering*, 47(3):036003–036003, 2008.

[107] D. C. O'Brien, G. Faulkner, M. H. Le, O. Bouchet, M. El Tabach, M. Wolf, J. W. Walewski, S. Randel, S. Nerreter, M. Franke, et al. "Gigabit optical wireless for a home access network". In *Personal, Indoor and Mobile Radio Communications, 2009 IEEE 20th International Symposium on*, pages 1–5. IEEE, 2009.

[108] C. W. Oh, F. M. Huijskens, Z. Cao, E. Tangdiongga, and A. M. J. Koonen. "Toward multi-gbps indoor optical wireless multicasting system employing passive diffractive optics". *Optics Letters*, 39(9):2622–2625, 2014.

[109] C. W. Oh, E. Tangdiongga, and A. M. J. Koonen. "Steerable pencil beams for multi-gbps indoor optical wireless communication". *Optics Letters*, 39(18):5427–5430, 2014.

[110] G. Ollivier, R. Bullock, Y. Jing, J. Sondhri, N. Zhou, and World Bank Beijing. Chinese high-speed: an evaluation of traffic. [Online]. Available: https://goo.gl/43Lq9f, February 2015. Last Access Date: 9/19/2018.

[111] D. C. O'Brien, M. Katz, P. Wang, K. Kalliojarvi, S. Arnon, M. Matsumoto, R. J. Green, and S. Jivkova. "Short-range optical wireless communications". In *Wireless World Research Forum*, pages 1–22, 2005.

[112] R. Paudel, Z. Ghassemlooy, H. Le-Minh, and S. Rajbhandari. "Modelling of free space optical link for ground-to-train communications using a Gaussian source". *Optoelectronics, IET*, 7(1):1–8, 2013.

[113] R. Paudel, Z. Ghassemlooy, H. Le-Minh, S. Rajbhandari, and B. Livingstone. "Investigation of FSO ground-to-train communications in a laboratory environment". In *2011 Second Asian Himalayas International Conference on Internet (AH-ICI)*. IEEE, 2011.

[114] R. Paudel, H. Le Minh, Z. Ghassemlooy, M. Iaz, and S. Rajbhandari. "High speed train communications systems using free space optics". In *The Institution of Engineering and Technology Annual Report*. The Institution of Engineering and Technology, 2010.

[115] A. A. Portillo, G. G. Ortiz, and C. Racho. "Fine pointing control for optical communications". In *2001 IEEE Aerospace Conference Proceedings (Cat. No.01TH8542)*, pages 3/1541–3/1550 vol.3. IEEE, March 2001.

[116] X. Qian, H. Wu, and J. Meng. "A dual-antenna and mobile relay station based handover in distributed antenna system for high-speed railway". In *Innovative Mobile and Internet Services in Ubiquitous Computing (IMIS), 2013 Seventh International Conference on*, pages 585–590. IEEE, 2013.

[117] J. Ready. *"Optical Detectors and Human Vision"*. Hoboken, NJ: John Wiley and Sons, 1991.

[118] J. Rodríguez-Piñeiro, M. Lerch, J. A. García-Naya, S. Caban, M. Rupp, and L. Castedo. "Emulating extreme velocities of mobile LTE receivers in the downlink". *EURASIP Journal on Wireless Communications and Networking*, 2015(1):106, 2015.

[119] J. Rothman, P. Bleuet, L. Andre, Q. Abadie, G. Bordot, S. Bisotto, G. Audoit, J.-A. Nicolas, B. Dupont, J.-P. Rostand, et al. "HgCdTe APDs for free space optical communications". In *Free-Space Laser Communication and Atmospheric Propagation XXX*, volume 10524, page 1052411. International Society for Optics and Photonics, 2018.

[120] J. Rothman, G. Lasfargues, and J. Abergel. "HgCdTe APDs for free space optical communications". In *Unmanned/Unattended Sensors and Sensor Networks XI; and Advanced Free-Space Optical Communication Techniques and Applications*, volume 9647, page 96470N. International Society for Optics and Photonics, 2015.

[121] J. Rzasa, M. C. Ertem, and C. C. Davis. "Pointing, acquisition, and tracking considerations for mobile directional wireless communications systems". In *SPIE Optical Engineering + Applications*, pages 88740C–88740C. International Society for Optics and Photonics, 2013.

[122] A. Sniady and J. Soler. "LTE for railways: impact on performance of ETCS railway signaling". *Vehicular Technology Magazine, IEEE*, 9(2):69–77, 2014.

[123] D. Thompson. *Railway Noise and Vibration: Mechanisms, Modelling and Means of Control*. Oxford, UK: Elsevier, 2008.

[124] G. Thuillier, M. Hersé, T. Foujols, W. Peetermans, D. Gillotay, P. C. Simon, H. Mandel, et al. "The solar spectral irradiance from 200 to 2400 nm as measured by the SOLSPEC spectrometer from the ATLAS and EURECA missions". *Solar Physics*, 214(1):1–22, 2003.

[125] S. Trisno. *"Design and analysis of advanced free space optical communication systems"*. PhD thesis, Univ. of Maryland, College Park, MD, April 2006. Available: http://hdl.handle.net/1903/3400.

[126] H. Urabe, S. Haruyama, T. Shogenji, S. Ishikawa, M. Hiruta, F. Teraoka, T. Arita, H. Matsubara, and S. Nakagawa. "High data rate ground-to-train free-space optical communication system". *Optical Engineering*, 51(3):031204–1, 2012.

[127] B. H. Walke, S. Mangold, and L. Berlemann. *IEEE 802 Wireless Systems: Protocols, Multi-hop Mesh/Relaying, Performance and Spectrum Coexistence*. West Sussex, UK: John Wiley and Sons, 2007.

[128] C.-X. Wang, F. Haider, X. Gao, X.-H. You, Y. Yang, D. Yuan, H. Aggoune, H. Haas, S. Fletcher, and E. Hepsaydir. "Cellular architecture and key technologies for 5G wireless communication networks". *IEEE Communications Magazine*, 52(2):122–130, 2014.

[129] G. M. Williams, M. A. Compton, and A. S. Huntington. "High-speed photon counting with linear-mode APD receivers". In *Advanced Photon Counting Techniques III*, volume 7320, page 732012. International Society for Optics and Photonics, 2009.

[130] M. Yoshikawa, A. Murakami, J. Sakurai, H. Nakayama, and T. Nakamura. "High power VCSEL devices for free space optical communications". In *Electronic Components and Technology Conference, 2005. Proceedings. 55th*, pages 1353–1358. IEEE, 2005.

[131] T. Yuge and S. Sasaki. "Train radio system using leaky coaxial cable". In *Vehicular Technology Conference, 1984. 34th IEEE*, volume 34, pages 43–48. IEEE, 1984.

[132] G. Yun and M. Kavehrad. "Indoor infrared wireless communications using spot diffusing and fly-eye receivers". *Canadian Journal of Electrical and Computer Engineering*, 18(4):151–157, 1993.

[133] W. Zhai, Z. He, and X. Song. "Prediction of high-speed train induced ground vibration based on train-track-ground system model". *Earthquake Engineering and Engineering Vibration*, 9(4):545–554, 2010.

[134] D. Zhou, P. G. LoPresti, and H. H. Refai. "Enlargement of beam coverage in FSO mobile network". *Journal of Lightwave Technology*, 29(10):1583–1589, 2011.

[135] Y. Zhou and B. Ai. "Handover schemes and algorithms of high-speed mobile environment: A survey". *Computer Communications*, 47:1–15, 2014.

[136] L. Zhu, F. R. Yu, and B. Ning. "A seamless handoff scheme for train-ground communication systems in CBTC". In *Vehicular Technology Conference Fall (VTC 2010-Fall), 2010 IEEE 72nd*, pages 1–5. IEEE, 2010.